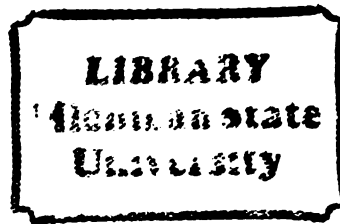




THESIS



This is to certify that the

dissertation entitled

Application of the Green's Function  
Monte Carlo Method to Hamiltonian  
Lattice Field Theories  
presented by

David William Heys

has been accepted towards fulfillment  
of the requirements for

Ph. D. degree in Physics

*David R. Stump*

Major professor

David R. Stump

Date July 17, 1964



RETURNING MATERIALS:  
Place in book drop to  
remove this checkout from  
your record. FINES will  
be charged if book is  
returned after the date  
stamped below.

--	--	--

APPLICATION OF THE GREEN'S FUNCTION MONTE CARLO METHOD  
TO HAMILTONIAN LATTICE FIELD THEORIES

by

David William Heys

A DISSERTATION

Submitted to  
Michigan State University  
in partial fulfillment of the requirements  
for the degree of

DOCTOR OF PHILOSOPHY

Department of Physics and Astronomy

1984

32209/6

ABSTRACT

APPLICATION OF THE GREEN'S FUNCTION MONTE CARLO METHOD  
TO HAMILTONIAN LATTICE FIELD THEORIES

by

David William Heys

The Green's function Monte Carlo (GFMC) method is adapted for application to Hamiltonian lattice gauge theories, and is applied to the SU(2) and U(1) models. The method is a Monte Carlo method for finding the ground state of a quantum mechanical system with many degrees of freedom, by iteration of an integral equation of which the ground state is an eigenstate. An interesting aspect of the method is the use of an importance sampling technique that makes use of variational wave functions to reduce fluctuations and accelerate convergence of GFMC estimates of various quantities. The calculations have been restricted, by the availability of computer time, to estimates of simple quantities, the ground state energy per plaquette and the mean plaquette field, on a small lattice (3 x 3 x 3). There is no difficulty, subject to the availability of computer time, in computing other quantities or in using larger lattices. The results are interpreted in terms of the phase structure of the two groups; the SU(2) model exists in a single quark confining phase for all values of the coupling constant whereas the U(1) model in 3+1 dimensions undergoes a phase transition from a confining

phase at strong coupling ( $g^2 \rightarrow \infty$ ) to a non-confining phase at weak coupling ( $g^2 \rightarrow 0$ ).

The method is not restricted to gauge theories and is also applied to the Hamiltonian XY model in 1+1 dimensions. The results obtained on this model are interpreted with regard to the Kosterlitz-Thouless phase transition.

## ACKNOWLEDGEMENTS

I would like to thank Dr. D.R. Stump for introducing me to lattice gauge theories and for suggesting this particular research topic. His guidance and encouragement have certainly been invaluable in helping to bring this work to fruition.

I am also indebted to Dr. W.W. Repko with whom I have had a number of interesting and enlightening conversations on various subjects.

My colleagues and friends A. Abbasabadi, E. Garboczi, H. He and M. Thomsen have been a great help in making my stay at Michigan State a pleasant one for which I will always be grateful. Conversations with them, not necessarily concerning physics, have always been stimulating.

Very special thanks are due my wife, Susan, whose constant support and encouragement, though not often acknowledged, are truly appreciated. Her patience and understanding, especially during the writing of this manuscript, have been nothing less than amazing.

Finally, I would like to thank Dr. B.H. Wildenthal for his assistance in bringing me to Michigan State and for his support during the first few months here.

## TABLE OF CONTENTS

List of Figures .....	v
Chapter 1: Introduction .....	1
Chapter 2: The Green's function Monte Carlo method .....	5
2.1 Introduction .....	5
2.2 Algorithm 1: Unweighted ensemble .....	10
2.3 Algorithm 2: Weighted ensemble .....	13
2.4 Importance sampling .....	17
Chapter 3: The SU(2) lattice gauge theory in 3+1 dimensions .....	26
3.1 Definition of the model .....	26
3.2 Variational calculation .....	29
3.3 GFMC calculation .....	38
Chapter 4: The U(1) lattice gauge theory in 3+1 dimensions .....	45
4.1 Definition of the model .....	45
4.2 Variational calculation .....	47
4.3 GFMC calculation .....	52

Chapter 5: n-space formulation of the U(1) lattice gauge theory .....	60
5.1 The n-space equations .....	60
5.2 Variational calculations .....	63
5.2.1 Disordered wave function .....	63
5.2.2 Gaussian wave function .....	65
5.2.3 Variational results .....	66
5.3 GFMC calculations .....	71
Chapter 6: The Hamiltonian XY model .....	77
Chapter 7: Summary and conclusions .....	85
Appendix A: Green's function Monte Carlo calculations on the SU(2) and U(1) lattice gauge theories .....	88
Appendix B: Application of the Green's function Monte Carlo method to the compact Abelian lattice gauge theory .....	128
List of References .....	140

## LIST OF FIGURES

Figure 1: Variational estimates of (a) the magnetic energy, and (b) the electric energy versus the variational parameter $\beta$ for the SU(2) theory .....	33
Figure 2: Variational estimate of the ground state energy per plaquette versus $\lambda$ for the SU(2) theory .....	35
Figure 3: Variational estimate of the mean plaquette field versus $\lambda$ for the SU(2) theory .....	37
Figure 4: GFMC estimate of the ground state energy per plaquette versus $\lambda$ for the SU(2) theory .....	42
Figure 5: GFMC estimate of the mean plaquette field versus $\lambda$ for the SU(2) theory .....	43
Figure 6: Variational estimates of (a) the magnetic energy, and (b) the electric energy versus the variational parameter $\beta$ for the U(1) theory .....	49
Figure 7: Variational estimate of the ground state energy per plaquette versus $\lambda$ for the U(1) theory .....	50
Figure 8: Variational estimate of the mean plaquette field versus $\lambda$ for the U(1) theory .....	52
Figure 9: GFMC estimate of the ground state energy per plaquette versus $\lambda$ for the U(1) theory .....	55
Figure 10: GFMC estimate of the mean plaquette field versus $\lambda$ for the U(1) theory .....	58
Figure 11: Variational estimates of the ground state energy per plaquette versus $\lambda$ for the n-space formulation of the U(1) theory .....	67
Figure 12: $a/a_n$ versus $\lambda$ for the variational wave function $\phi_2[n]$ .....	69
Figure 13: Variational estimates of the mean plaquette field versus $\lambda$ for the n-space formulation of the U(1) theory .....	70

Figure 14: GFMC estimates of the ground state energy per plaquette versus $\lambda$ for the n-space formulation of the U(1) theory .....	72
Figure 15: GFMC estimate of the mean plaquette field versus $\lambda$ computed using the trial wave function $\phi_2[n]$ for importance sampling .....	74
Figure 16: GFMC estimate of the mean plaquette field versus $\lambda$ computed using the trial wave function $\phi_1[n]$ for importance sampling .....	76
Figure B1: GFMC estimate of the expectation value of $1-\cos B(p)$ for the two dimensional U(1) theory using the harmonic wave function $\phi_2$ for importance sampling .....	138
Figure B2: GFMC estimate of the expectation value of $1-\cos B(p)$ for the two dimensional U(1) theory using the uncorrelated wave function $\psi_1$ for importance sampling .....	139

## CHAPTER 1

### Introduction

The candidate theory of strong interaction physics is quantum chromodynamics (QCD), a gauge theory based on the non-abelian group  $SU(3)$ . Due to the remarkable property of asymptotic freedom [1] possessed by non-abelian gauge theories, short distance phenomena in QCD can be adequately understood in terms of perturbation theory. However, a number of important strong-coupling phenomena, such as the meson and baryon masses and quark confinement, can not be treated in this way since the perturbation series is not convergent for strong coupling. Lattice gauge theories were invented to study such non-perturbative aspects of gauge theories.

In a lattice theory the space-time continuum is replaced by a lattice of discrete points at which the various matter fields of the theory are defined. The inverse lattice spacing provides a natural ultraviolet cut off, so that renormalization effects are finite and numerical calculations can be performed with no divergent results. Of

course, in order to make contact with the real world, the cut off must eventually be removed, i.e., the lattice spacing must be taken to zero so that the continuum theory is recovered.

There are two complementary formulations of lattice gauge theories. In Wilson's approach [2] the Feynman path-integral of the theory, which in the continuum is a functional integral, is replaced by a lattice approximation involving only ordinary multiple integrals. In this formulation both space and time coordinates are treated as discrete. On the other hand, in the Hamiltonian formulation of Kogut and Susskind [3] time remains continuous and one deals with a lattice version of the Hamiltonian of the theory. The two formulations can be shown to be equivalent by means of the transfer matrix [4].

Both versions of the theory have been the subject of intense study in recent years using a variety of techniques: perturbation expansions [5], the renormalization group [6], mean field theory [7], the variational principle [8-10], and Monte Carlo methods [11]. An excellent review of the current status of lattice gauge theories may be found in Ref.[12]. More elementary reviews covering lattice gauge theory basics are Refs.[13,14]. The Monte Carlo calculations, which so far have only been applied to the Euclidean path integral formulation, have provided by far the most exciting results to date. Such calculations have given us evidence of confinement in  $SU(2)$  and  $SU(3)$  gauge theories [15-17], chiral symmetry breaking in QCD [18,19], numerical evidence for quark deconfinement at finite temperature along with rough estimates of the deconfinement temperature [20], and some

crude but promising estimates of glueball, meson and baryon masses [18,21,22].

It is natural, then, to try to develop a Monte Carlo method for Hamiltonian lattice gauge theories in the hope that the above calculations can be checked in a completely independent way. This work is a first step toward that goal.

The particular Monte Carlo method used here is the Green's function Monte Carlo (GFMC) method. This is a numerical technique for studying properties of the ground state of quantum systems with many degrees of freedom. It was originally developed for application to quantum many-body problems [23-25]. In this work the method is adapted for application to lattice gauge theories.

Perhaps the most interesting aspect of the GFMC method is an importance sampling technique. This technique makes use of an approximation of the ground state wave function, usually derived from a variational calculation, to bias the Monte Carlo procedure; this reduces the fluctuations associated with stochastic sampling and also accelerates the convergence of Monte Carlo estimates of various quantities. In principle the final results are independent of the particular importance function used, though in practice it should closely approximate the ground state. By observing how a particular variational wave function behaves as an importance function it is possible to determine how well it resembles the ground state. In this way one can learn something about the structure of the ground state wave

function. In contrast the path-integral Monte Carlo method provides only numerical results, and does not easily yield any information regarding the structure of the ground state. The possibility of obtaining analytic information from the Monte Carlo calculation provides one of the strongest motivations for this work.

## CHAPTER 2

### The Green's function Monte Carlo method

#### 2.1 Introduction

Consider the Hamiltonian

$$H = H_0 - \lambda H_1 \tag{2.1}$$

where  $H_0$  and  $H_1$  are positive definite operators and  $\lambda$  is a positive coupling parameter. Furthermore assume that  $H_0$  has a zero eigenvalue. (This can always be arranged by simply adding a suitable constant to the Hamiltonian.) The restriction to positive definite operators is not an essential feature of the GFMC method and, in fact, some of the most fruitful applications of the method have been to systems involving non-positive definite operators [24]. In all the applications to be discussed here the operators  $H_0$  and  $H_1$  are positive definite and so we need not consider the more complicated general case. The interested

reader should consult Ref.[25] for more information pertaining to the use of non-positive definite operators.

The first step of the GFMC method is to write the eigenvalue equation

$$H|\psi\rangle = E|\psi\rangle \quad (2.2)$$

as an integral equation. To this end rewrite Eq.(2.2) as

$$(H_0 - E)|\psi\rangle = \lambda H_1 |\psi\rangle \quad (2.3)$$

and now consider  $E$  to be the known quantity and  $\lambda$  to be the desired eigenvalue. This is the reverse of the usual situation in which the coupling parameter  $\lambda$  is known and the energy  $E$  is the unknown eigenvalue. Clearly the eigensolutions are the same regardless of which variable is used as the eigenvalue, as are all observables of the system. Now introduce a set of basis states  $\{|x\rangle\}$  where the label  $x$  represents all the parameters needed to uniquely specify a state. Two different basis sets immediately suggest themselves: the eigenstates of  $H_0$ , and the eigenstates of  $H_1$ .

Consider the case in which  $|x\rangle$  is an eigenstate of  $H_1$ , i.e.,

$$H_1 |x\rangle = H_1(x) |x\rangle \quad (2.4)$$

Introducing the Green's function operator  $G$  as the inverse of  $(H_0 - E)$ , i.e.,

$$(H_0 - E)G = 1, \quad (2.5)$$

we may rewrite the eigenvalue equation Eq.(2.3) as

$$\psi(x) = \lambda \int dx' G(x,x') H_1(x') \psi(x') \quad (2.6)$$

where

$$\psi(x) = \langle x | \psi \rangle$$

and

$$G(x,x') = \langle x | G | x' \rangle .$$

Clearly, in order for the Green's function to exist the operator  $(H_0 - E)$  must be non-singular, i.e. must have no zero eigenvalues. This is obviously true for  $E < 0$ , since the smallest eigenvalue of  $H_0$  is zero. It should be remembered that, in general,  $x$  represents a large number of parameters, some of which may be discrete, so that the integral in Eq.(2.6) must be thought of as a sum over all values of the discrete parameters and an integral over the domains of all the continuous parameters. We will continue to use this simple notation.

A different integral equation may be obtained by using as the basis set  $\{|x\rangle\}$  the set of eigenstates of  $H_0$ , i.e.,

$$H_0 |x\rangle = H_0(x) |x\rangle . \quad (2.7)$$

In this case, Eq.(2.3) may be written, with obvious notation, as

$$[H_0 - E]\psi(x) = \lambda \int dx' H_1(x,x') \psi(x') . \quad (2.8)$$

Defining a new function  $\chi(x)$  as



$$\chi(\mathbf{x}) = [H_0(\mathbf{x}) - E]\psi(\mathbf{x}) , \quad (2.9)$$

Eq.(2.8) becomes

$$\chi(\mathbf{x}) = \lambda \int d\mathbf{x}' H_1(\mathbf{x}, \mathbf{x}') \frac{1}{[H_0(\mathbf{x}') - E]} \chi(\mathbf{x}') . \quad (2.10)$$

It is seen that the integral equations Eq.(2.6) and Eq.(2.10) are both of the same form:

$$F(\mathbf{x}) = \lambda \int d\mathbf{x}' K(\mathbf{x}, \mathbf{x}') V(\mathbf{x}') F(\mathbf{x}') . \quad (2.11)$$

The form of the functions  $F(\mathbf{x})$  and  $V(\mathbf{x})$  and the kernel  $K(\mathbf{x}, \mathbf{x}')$  depends on whether  $|\mathbf{x}\rangle$  is an eigenstate of  $H_0$  or of  $H_1$ .

It is easy to show that the sequence of functions  $\{F^{(r)}(\mathbf{x})\}$  defined iteratively by

$$F^{(r+1)}(\mathbf{x}) = \lambda^{(r)} \int d\mathbf{x}' K(\mathbf{x}, \mathbf{x}') V(\mathbf{x}') F^{(r)}(\mathbf{x}') , \quad (2.12)$$

where  $\lambda^{(r)}$  is an arbitrary parameter which may change from one iteration to the next, converges to the ground-state eigenfunction of Eq.(2.11). Suppose that  $F_n(\mathbf{x})$  is an eigensolution of Eq.(2.11) with corresponding eigenvalue  $\lambda_n$ , (recall that  $\lambda$  is now the eigenvalue), i.e.,

$$F_n(\mathbf{x}) = \lambda_n \int d\mathbf{x}' K(\mathbf{x}, \mathbf{x}') V(\mathbf{x}') F_n(\mathbf{x}') . \quad (2.13)$$

Since  $\{F_n(\mathbf{x})\}$  is assumed to be a complete set, we may write

$$F^{(0)}(\mathbf{x}) = \sum_n c_n F_n(\mathbf{x}) \quad (2.14)$$

so that

$$F^{(1)}(\mathbf{x}) = \sum_n \frac{\lambda^{(0)}}{\lambda_n} c_n F_n(\mathbf{x}) \quad (2.15)$$

and

$$F^{(r)}(\mathbf{x}) = \sum_n \frac{\prod_{i=0}^{r-1} \lambda^{(i)}}{\lambda_n^r} c_n F_n(\mathbf{x}) \quad (2.16)$$

where the product runs over  $i$  from 0 to  $(r-1)$ . If the eigenvalues are ordered such that  $0 < \lambda_0 < \lambda_1 < \dots$  then as  $r \rightarrow \infty$  the sum on the right hand side of Eq.(2.16) will be dominated by the  $n=0$  term, so that up to a normalization constant

$$\lim_{r \rightarrow \infty} F^{(r)}(\mathbf{x}) = F_0(\mathbf{x}) \quad (2.17)$$

where  $F_0(\mathbf{x})$  is the ground-state eigenfunction of the Hamiltonian. In practice, the integrals involved in the iteration of Eq.(2.11) are multidimensional and can not be performed exactly. The GFMC algorithm provides a means to carry out the iteration stochastically so that after many Monte Carlo iterations one obtains an ensemble of basis configurations sampled randomly from the probability density  $F_0(\mathbf{x})$ . (We assume that the eigenfunctions  $F_n(\mathbf{x})$  satisfy the normalization condition  $\int F_n(\mathbf{x}) d\mathbf{x} = 1$ .)

A discussion of how to calculate interesting quantities such as the eigenvalue  $\lambda_0$  and ground-state expectation values will be deferred until the next section where the concept of importance sampling will be introduced. Here we content ourselves with a detailed description of the basic Monte Carlo procedure. Two algorithms will be described one

of which utilizes an ensemble of unweighted configurations and another which utilizes an ensemble of weighted configurations. Each one has its advantages over the other: the first algorithm is more straightforward to implement whereas the second algorithm, though being more complicated than the first, is for that very reason of wider applicability.

In what follows it will be assumed that  $K(x, x')$  and  $F_0(x)$  are both positive functions. It should also be realized that the function  $V(x)$  is automatically positive because the operators  $H_0$  and  $H_1$  are positive definite and because we restrict our attention to  $E < 0$ .

## 2.2 Algorithm 1: Unweighted ensemble

Write the kernel appearing in Eq.(2.11) in the form

$$K(x, x') = k(x, x') Z(x') \quad (2.18)$$

where the function  $k(x, x')$  is normalized such that

$$\int k(x, x') dx = 1 \quad (2.19)$$

for all  $x'$ . This is always possible in principle by letting

$$Z(x') = \int K(x, x') dx \quad (2.20)$$

but in practice this decomposition may not be the most convenient because the integral in Eq.(2.20) may not be tractable.

Suppose that  $E^{(r)} = \{x_\sigma; \sigma=1,2,\dots,N^{(r)}\}$  is an ensemble of points in parameter space, representing a set of basis states, sampled randomly from the probability density function  $F^{(r)}(x) / \int F^{(r)}(x)dx$ , i.e., the expected number of points of the ensemble lying in the range of parameter space between  $x$  and  $x+dx$  is  $N^{(r)}F^{(r)}(x) / \int F^{(r)}(x)dx$ . For each point  $x_\sigma$  of  $E^{(r)}$  a number  $\nu_\sigma$ , called the braching number, is chosen randomly in such a way that the expected value of  $\nu_\sigma$  is given by

$$\langle \nu_\sigma \rangle = \lambda^{(r)} Z(x_\sigma) V(x_\sigma) \quad . \quad (2.21)$$

This can be done in any number of ways, the simplest of which is to set

$$\nu_\sigma = \text{integral part} [ \langle \nu_\sigma \rangle + \xi ] \quad (2.22)$$

where  $\xi$  is a uniform random deviate in the interval (0,1). If  $r$  is the largest integer for which  $r < \langle \nu_\sigma \rangle$  then the probability that  $\nu_\sigma=r$  is clearly given by

$$p(\nu_\sigma=r) = r + 1 - \langle \nu_\sigma \rangle \quad (2.23)$$

and the probability that  $\nu_\sigma=r+1$  is

$$p(\nu_\sigma=r+1) = \langle \nu_\sigma \rangle - r \quad . \quad (2.24)$$

The expected value of  $\nu_\sigma$  is therefore

$$r(r+1-\langle \nu_\sigma \rangle) + (r+1)(\langle \nu_\sigma \rangle-r) = \langle \nu_\sigma \rangle$$

as required. Note that the possibility  $\nu_\sigma=0$  is allowed.

Now, randomly select  $\nu_\sigma$  new points from the conditional probability density  $k(\mathbf{x}, \mathbf{x}_\sigma)$ . The details of the sampling procedure depend on the functional form of  $k(\mathbf{x}, \mathbf{x}')$  and no general method can be given.

The new points chosen in this way constitute the  $(r+1)$ st ensemble  $E^{(r+1)}$ . The expected number of points  $\rho(\mathbf{x})d\mathbf{x}$  of  $E^{(r+1)}$  lying in the region of parameter space between  $\mathbf{x}$  and  $\mathbf{x}+d\mathbf{x}$  is clearly

$$\begin{aligned} \rho(\mathbf{x})d\mathbf{x} &= \sum_{\sigma} d\mathbf{x} k(\mathbf{x}, \mathbf{x}_\sigma) \nu_\sigma \\ &= \sum_{\sigma} d\mathbf{x} k(\mathbf{x}, \mathbf{x}_\sigma) \lambda^{(r)} Z(\mathbf{x}_\sigma) V(\mathbf{x}_\sigma) \quad . \\ &= d\mathbf{x} \lambda^{(r)} \sum_{\sigma} K(\mathbf{x}, \mathbf{x}_\sigma) V(\mathbf{x}_\sigma) \end{aligned} \quad (2.25)$$

which in the mean may be written as

$$\rho(\mathbf{x})d\mathbf{x} = d\mathbf{x} \lambda^{(r)} \int d\mathbf{x}' K(\mathbf{x}, \mathbf{x}') V(\mathbf{x}') \frac{N^{(r)} F^{(r)}(\mathbf{x}')}{\int F^{(r)}(\mathbf{x})d\mathbf{x}} \quad (2.26)$$

Using Eq.(2.13) it is seen that the right hand side of Eq.(2.26) is proportional to  $F^{(r+1)}(\mathbf{x})$ , specifically

$$\rho(\mathbf{x})d\mathbf{x} = \frac{N^{(r)} F^{(r+1)}(\mathbf{x})}{\int F^{(r)}(\mathbf{x})d\mathbf{x}} d\mathbf{x} \quad . \quad (2.27)$$

The ensemble  $E^{(r+1)}$  may, therefore, be considered to be randomly sampled from the probability density function  $F^{(r+1)}(\mathbf{x})/\int F^{(r+1)}(\mathbf{x})d\mathbf{x}$ .

### 2.3 Algorithm 2: Weighted ensemble

As in algorithm 1, introduce a function  $k(x, x')$  normalized as in Eq.(2.19) but this time write the kernel  $K(x, x')$  in the slightly more general form

$$K(x, x') = k(x, x') Z(x, x') \quad . \quad (2.28)$$

Note that the function  $Z(x, x')$  may depend on  $x$  as well as on  $x'$  so that this algorithm is somewhat more generally applicable than algorithm 1.

Suppose that  $E^{(r)} = \{(x_\sigma^{(r)}, w_\sigma^{(r)}; \sigma=1, 2, \dots, N)\}$  is an ensemble of weighted points in parameter space and define the function  $F^{(r)}(x)$  by

$$F^{(r)}(x) = \langle \sum_{\sigma} \delta(x - x_\sigma^{(r)}) w_\sigma^{(r)} \rangle \quad , \quad (2.29)$$

where the angle brackets denote the expected value. For each point  $x_\sigma^{(r)}$ , a new point  $x_\sigma^{(r+1)}$  is chosen randomly from the conditional probability density function  $k(x_\sigma^{(r+1)}, x_\sigma^{(r)})$  and this new point is given weight

$$w_\sigma^{(r+1)} = \lambda^{(r)} w_\sigma^{(r)} Z(x_\sigma^{(r+1)}, x_\sigma^{(r)}) V(x_\sigma^{(r)}) \quad . \quad (2.30)$$

The weighted points generated in this way constitute the  $(r+1)$ st ensemble  $E^{(r+1)}$ . Notice that the number of points in the ensemble is constant.

Clearly

$$\langle \sum_{\sigma} \delta(x - x_\sigma^{(r+1)}) w_\sigma^{(r+1)} \rangle = \langle \sum_{\sigma} k(x, x_\sigma^{(r)}) w_\sigma^{(r)} \lambda^{(r)} Z(x, x_\sigma^{(r)}) V(x_\sigma^{(r)}) \rangle$$

$$\begin{aligned}
&= \lambda^{(r)} \int dx' k(x, x') Z(x, x') V(x') < \sum_{\sigma} \delta(x' - x_{\sigma}^{(r)}) w_{\sigma}^{(r)} > \\
&= \lambda^{(r)} \int dx' K(x, x') V(x') F^{(r)}(x') \\
&= F^{(r+1)}(x) \tag{2.31}
\end{aligned}$$

We see from Eq.(2.31) that the algorithm described above does indeed generate a sequence of functions  $\{F^{(r)}(x)\}$  related by Eq.(2.12) and so provides a means of iterating Eq.(2.11). However, it should be pointed out that this algorithm does not work in practice. The reason for this is that after only a few Monte Carlo iterations the weights of a very small number of points become much larger than those of all the other points together and the ensemble is effectively reduced to a statistically insignificant size; in the worst possible case the ensemble is dominated by a single point.

Fortunately, there is a simple solution to this problem — a technique known as splitting or branching. As the name suggests, this involves splitting a point  $x_{\sigma}$  with "large" weight  $w_{\sigma}$  into  $\nu_{\sigma}$  new points identical to  $x_{\sigma}$  but each having a smaller weight  $w_{\sigma}/\nu_{\sigma}$ . The precise way in which this is done will be described shortly. Clearly the definition of  $F^{(r)}(x)$  in Eq.(2.29) remains unchanged by this modification of the ensemble. Of course, in carrying out this branching procedure, the ensemble size increases and continues to do so as the Monte Carlo iteration proceeds. If this growth went unchecked, the ensemble would quickly reach an unmanageable size, and so it is necessary to truncate the ensemble in some way. This may be done by eliminating a sufficient number of points with "small" weights from the ensemble in such a way as

to preserve Eq.(2.29). To achieve this, the truncation must be done stochastically, so that, for example, if  $p$  is the probability that a particular point  $x_o$  be eliminated from the ensemble, i.e. be given zero weight, then with probability  $(1-p)$  that point will survive the truncation but with increased weight  $w'$ , the numbers  $p$  and  $w'$  being chosen in such a way that

$$(1-p)w' = w_o . \quad (2.32)$$

In principle, the branching number  $\nu_o$  appearing in the splitting procedure, and the probability of elimination  $p$ , are arbitrary. However, in practice it is important that all the weights be of comparable magnitude, within a factor of about four of each other. It is also useful to not simply prevent the ensemble size from becoming too large, but to keep it approximately constant. If this is done then reliable estimates of program execution time can be made which would not be possible if the ensemble size fluctuated wildly. With these two points in mind, the following implementation of the branching and truncation procedure is particularly useful.

For a given point  $x_o$ , the branching number  $\nu_o$  is randomly chosen in such a way that the expected value is

$$\langle \nu_o \rangle = N w_o / \sum_o w_o , \quad (2.33)$$

where  $N$  is the desired ensemble size. As shown in the discussion following Eq.(2.21) this may be most simply done by setting

$$\nu_o = \text{integral part } [\langle \nu_o \rangle + \xi] , \quad (2.34)$$

where  $\xi$  is a uniform random deviate in the interval (0,1). Note that, as in algorithm 1, the possibility  $\nu_o = 0$  is allowed. If  $\langle \nu_o \rangle \geq 1$  the point is split into  $\nu_o$  identical points each with weight  $w_o/\nu_o$ . This has the effect of splitting points with large weight, i.e. greater than  $\Sigma w_o/N$ , into a number of points with weights less than  $2\Sigma w_o/N$ . If  $\langle \nu_o \rangle < 1$  then if  $\nu_o = 0$  the point is eliminated from the ensemble, but if  $\nu_o = 1$  the point survives and its weight is increased to  $\Sigma w_o/N$ . It is easy to see that this branching and truncation procedure maintains the ensemble size at approximately  $N$ , and also forces all weights to be approximately equal.

In practice the factor  $Z(x, x')$  is usually approximately equal to 1, so that in calculating  $w_o^{(r+1)}$  from  $w_o^{(r)}$  by Eq.(2.30) the factor  $\lambda^{(r)}v(x_o^{(r)})$  plays a dominant role. The following practical Monte Carlo algorithm then proves useful.

- (1) Multiply the weights by the corresponding factor  $\lambda^{(r)}v(x_o^{(r)})$ .
- (2) Carry out the branching and truncation procedure.
- (3) Generate the points  $\{x_o^{(r+1)}\}$  from  $\{x_o^{(r)}\}$  using the conditional probability density  $k(x_o^{(r+1)}, x_o^{(r)})$ .
- (4) Multiply the weights by the corresponding factor  $Z(x_o^{(r+1)}, x_o^{(r)})$ .

The reason for this rather strange order of events is that the factor  $\lambda^{(r)}v(x_o^{(r)})$  causes the greatest change to the weights, so by first multiplying the weights by this factor and then performing the branching and truncation of the ensemble immediately afterwards, but before generating the new points  $\{x_o^{(r+1)}\}$ , one ensures that the weights

of the points in the final ensemble will be approximately equal. This would not be the case if the steps outlined above were carried out in the perhaps more obvious order (2),(3),(1),(4), where steps (1) and (4) would be combined into a single step.

#### 2.4 Importance sampling

So far two algorithms have been described for carrying out the iteration indicated by Eq.(2.12) and it has been shown that  $F^{(r)}(x) \rightarrow F_0(x)$ , the lowest lying eigenfunction of Eq.(2.11), as  $r \rightarrow \infty$ . To be of any practical value there must be some way to compute quantities such as the eigenvalue  $\lambda_0$  and ground-state expectation values.

The precise details of such calculations depend on which algorithm one is using to implement the GFMC method. Since the situation is somewhat more complicated for algorithm 2 than for algorithm 1, we will focus our attention on that case. Corresponding results for algorithm 1 are easily derived. The eigenvalue  $\lambda_0$  may be estimated in a very straightforward way. For large  $r$ ,  $F^{(r)}(x) = aF_0(x)$  where  $a$  is some proportionality constant, so that, using Eq.(2.13), Eq.(2.12) becomes

$$F^{(r+1)}(x) = \frac{\lambda^{(r)}}{\lambda_0} F^{(r)}(x) \quad . \quad (2.35)$$

If this equation is integrated over all parameter space then one obtains the simple result

$$\lambda_0 = \lambda^{(r)} \frac{\langle w_{\text{tot}}^{(r)} \rangle}{\langle w_{\text{tot}}^{(r+1)} \rangle}, \quad (2.36)$$

where

$$w_{\text{tot}}^{(r)} = \sum_{\sigma} w_{\sigma}^{(r)}, \quad (2.37)$$

and we have used the defining equation Eq.(2.29) for  $F^{(r)}(x)$ . Since the expected values are not known, Eq.(2.36) suggests the following Monte Carlo estimator for  $\lambda_0$ :

$$\lambda_0^{(\text{est})} = \lambda^{(r)} \frac{w_{\text{tot}}^{(r)}}{w_{\text{tot}}^{(r+1)}}. \quad (2.38)$$

This estimate, known as the growth estimate because it is computed from the growth of the total weight of the ensemble from one iteration to the next, suffers from three sources of error:

- (1) Convergence error due to the fact that Eq.(2.36) is valid only in the limit  $r \rightarrow \infty$ .
- (2) Random sampling error due to the stochastic nature of the GFMC method.
- (3) Systematic error due to replacing the ratio of expected values in Eq.(2.36) by the ratio of the values themselves in Eq.(2.38).

In principle the convergence error is not a significant problem since by simply waiting until the quantity  $\lambda_0^{(\text{est})}$  settles down to fluctuate about some constant value this error can be eliminated. In practice, however, one may have to carry out many thousands of

iterations before  $\lambda_0^{(est)}$  converges.

Similarly, the random sampling error may, in principle, be reduced by increasing the ensemble size, but in practice it may be that in order to reduce the fluctuations to an acceptable level, an unmanageably large ensemble is required. This turns out to be the case in all calculations of practical interest.

The third source of error, the systematic error, can not be estimated but can at least be bounded by making use of the theorem

$$\min(a_j/b_j) \leq \frac{\sum a_j}{\sum b_j} \leq \max(a_j/b_j) \quad . \quad (2.39)$$

Specifically

$$\min(W_{tot}^{(r)}/W_{tot}^{(r+1)}) \leq \frac{\langle W_{tot}^{(r)} \rangle}{\langle W_{tot}^{(r+1)} \rangle} \leq \max(W_{tot}^{(r)}/W_{tot}^{(r+1)}) \quad (2.40)$$

so that if the random error can be reduced then the systematic error will also be reduced.

All of these sources of error may be greatly reduced by means of a technique called importance sampling. In this technique, a function, called the importance function, is used to bias the diffusion of points in parameter space in favor of regions where the importance function is largest. If the importance function is suitably chosen, this biasing causes points to cluster in regions where the eigenfunction  $F_0(x)$  is large, and so the ensembles generated by the Monte Carlo procedure

provide much better representations of  $F_0(x)$  than if no importance sampling is used.

To see how to implement this technique first multiply Eq.(2.11) by a function, the importance function,  $F_I(x)$ . Then the new function  $P(x)$  defined by

$$P(x) = F_I(x)F(x) \quad (2.41)$$

satisfies the equation

$$P(x) = \lambda \int dx' \frac{F_I(x) K(x,x')}{F_I(x)} V(x') P(x') \quad , \quad (2.42)$$

which is of the same form as Eq.(2.11) but with  $F(x)$  replaced by  $P(x)$  and  $K(x,x')$  replaced by

$$K_I(x,x') = \frac{F_I(x) K(x,x')}{F_I(x)} \quad . \quad (2.43)$$

This means that the two algorithms presented earlier may still be used to iterate Eq.(2.42). Furthermore, the eigenfunctions of Eq.(2.42) are clearly simply

$$P_n(x) = F_I(x)F_m(x) \quad (2.44)$$

with corresponding eigenvalues  $\lambda_0$  and iteration of Eq.(2.42) converges to  $P_0(x)$ . Suppose we let

$$F_I(x) = V(x)F_0(x) \quad . \quad (2.45)$$

Of course this is not possible in practice since the eigenfunction is

not known. Iteration of Eq.(2.41) generates a sequence of functions  $\{P^{(r)}(\mathbf{x})\}$  defined by

$$P^{(r+1)}(\mathbf{x}) = \lambda^{(r)} \int d\mathbf{x}' K_I(\mathbf{x}, \mathbf{x}') V(\mathbf{x}') P^{(r)}(\mathbf{x}) . \quad (2.46)$$

Now

$$\begin{aligned} \int d\mathbf{x} K_I(\mathbf{x}, \mathbf{x}') &= \int d\mathbf{x} \frac{F_0(\mathbf{x})V(\mathbf{x})K(\mathbf{x}, \mathbf{x}')}{F_0(\mathbf{x}') V(\mathbf{x}')} \\ &= \frac{1}{\lambda_0 V(\mathbf{x}')} , \end{aligned} \quad (2.47)$$

where we have used the fact that

$$K(\mathbf{x}, \mathbf{x}') = K(\mathbf{x}', \mathbf{x}) \quad (2.48)$$

and Eq.(2.13). Integrating Eq.(2.46) over the variables  $\mathbf{x}$  and using the result Eq.(2.47) one obtains

$$\int P^{(r+1)}(\mathbf{x})d\mathbf{x} = \frac{\lambda^{(r)}}{\lambda_0} \int P^{(r)}(\mathbf{x})d\mathbf{x} , \quad (2.49)$$

so that

$$\lambda_0 = \lambda^{(r)} \frac{\langle W_{\text{tot}}^{(r)} \rangle}{\langle W_{\text{tot}}^{(r+1)} \rangle} \quad (2.50)$$

for all  $r$ , i.e., there is no convergence error. The Monte Carlo estimator Eq.(2.38) still suffers from random sampling error and systematic error but because the distribution of points in parameter space is biased, the random error and hence, because of Eq.(2.40), the systematic error may both be expected to be greatly reduced.

In practice the importance function is chosen to be

$$F_I(x) = F_T(x)V(x) \quad (2.51)$$

where  $F_T(x)$  is a function optimized by the variational principle, which should resemble as closely as possible the eigenfunction  $F_0(x)$ . With this choice of importance function it is reasonable to expect the estimator  $\lambda_0^{(est)}$  to converge much faster than when no importance sampling is used, and also that the statistical fluctuations of  $\lambda_0^{(est)}$  will be much smaller. This is in fact the case.

A better estimator, known as the variational estimator for reasons which will soon become apparent, which does not suffer from any kind of error when the optimum choice of importance function  $F_I(x)=V(x)F_0(x)$  is used may be derived from the eigenvalue equation Eq.(2.3) for the ground-state  $|\psi\rangle$  of the Hamiltonian,

$$(H_0-E)|\psi_0\rangle = \lambda_0 H_1 |\psi_0\rangle \quad (2.52)$$

Suppose for the moment  $|x\rangle$  is an eigenstate of  $H_0$ . With this choice of basis one has

$$F_I(x) = \psi_T(x)[H_0(x)-E] \quad (2.53)$$

and

$$P_0(x) = \psi_T(x)[H_0(x)-E]\psi_0(x) \quad (2.54)$$

where  $\psi_T(x)$  is a variational wave function which should approximate  $\psi_0(x)$ . From Eq.(2.52) it is clear that

$$\lambda_0^{-1} = \frac{\int dx dx' \psi_T(x) H_1(x, x') \psi_0(x')}{\int dx \psi_T(x) [H_0(x) - E] \psi_0(x)} \quad (2.55)$$

which, using Eq.(2.54) leads to the Monte Carlo estimator

$$(\lambda_0^{(est)})^{-1} = \frac{1}{W_{tot}^{(r)}} \sum_{\sigma} w_{\sigma} \frac{\int dx \psi_T(x) H_1(x, x_{\sigma})}{\psi_T(x_{\sigma}) [H_0(x_{\sigma}) - E]} \quad (2.56)$$

The corresponding estimator when  $|x\rangle$  is an eigenstate of  $H_1$  is

$$\lambda_0^{(est)} = \frac{1}{W_{tot}^{(r)}} \sum_{\sigma} \frac{w_{\sigma}}{H_1(x_{\sigma}) \psi_T(x_{\sigma})} \int dx \psi_T(x) [H_0(x, x_{\sigma}) - E \delta(x - x_{\sigma})] \quad (2.57)$$

If  $\psi_T(x) = \psi_0(x)$ , corresponding to the choice  $F_I(x) = V(x)F_0(x)$  discussed earlier, then

$$(\lambda_0^{(est)})^{-1} = \lambda_0^{-1} \quad (2.58)$$

with no error of any kind. It is found that the variational estimator has much smaller fluctuations than the growth estimator and so this is the one that will be used in the applications to be described later.

The technique of importance sampling also provides a very simple means of estimating ground-state expectation values. Again for the moment suppose that  $|x\rangle$  is an eigenstate of  $H_0$  and write

$$\psi_T(x) = \psi_0(x) + \epsilon \eta(x) \quad (2.59)$$

where all functions are normalized and  $\epsilon$  is small if  $\psi_T(x)$  is a good variational wave function. Then, it is easy to show that for any operator  $A$



$$\frac{\langle \psi_0 | A | \psi_0 \rangle}{\langle \psi_0 | \psi_0 \rangle} = 2 \frac{\langle \psi_T | A | \psi_0 \rangle}{\langle \psi_T | \psi_0 \rangle} - \frac{\langle \psi_T | A | \psi_T \rangle}{\langle \psi_T | \psi_T \rangle} \quad (2.60)$$

to order  $\epsilon^2$ . The quantity on the left is the desired expectation value, and the second term on the right is the expectation value of A in the variational state  $|\psi_T\rangle$ . The first term on the right, known as the mixed expectation value, may be estimated from a Monte Carlo calculation as

$$\frac{\langle \psi_T | A | \psi_0 \rangle}{\langle \psi_T | \psi_0 \rangle} \approx \sum_{\sigma} \frac{A(\mathbf{x}_\sigma)}{[H_0(\mathbf{x}_\sigma) - E]} \bigg/ \sum_{\sigma} \frac{1}{[H_0(\mathbf{x}_\sigma) - E]} \quad (2.61)$$

The corresponding result when  $|x\rangle$  is an eigenstate of  $H_1$  is

$$\frac{\langle \psi_T | A | \psi_0 \rangle}{\langle \psi_T | \psi_0 \rangle} \approx \sum_{\sigma} \frac{A(\mathbf{x}_\sigma)}{H_1(\mathbf{x}_\sigma)} \bigg/ \sum_{\sigma} \frac{1}{H_1(\mathbf{x}_\sigma)} \quad (2.62)$$

The symbol  $\approx$  in these last two equations indicates that the estimate has a systematic error associated, as usual, with replacing the ratio of two expected values with the ratio of the valued themselves. But, again the systematic error is bounded by the statistical fluctuations of the estimate so that if the fluctuations are small so is the systematic error. In any case, in quoting results, allowance may be made of the systematic error by simply increasing the error bars of the various quantities by a factor of  $\sqrt{2}$ .

We see, then, that the quantities appearing on the right hand side of Eq.(2.60) may be calculated and so one may in this way obtain estimates of various expectation values. Of course, such estimates are only reliable if the variational expectation value and the mixed

expectation value are not very different, i.e. if  $\epsilon$  in Eq.(2.59) is small, since otherwise the  $O(\epsilon^2)$  terms will make a significant (perhaps dominant) contribution. It would be much better if there were some way to compute expectation values which did not rely on the accuracy of the variational wave function  $\psi_T(x)$ . Such a method does exist [25] but is very demanding on computer resources if any precision is to be achieved and will not be considered further.

## CHAPTER 3

### The SU(2) lattice gauge theory in 3+1 dimensions

#### 3.1 Definition of the model

The Hamiltonian of a lattice gauge theory with a unitary gauge group is

$$H = \sum_{\ell, a} E_a^2(\ell) + \frac{\lambda}{d} \sum_p [ d - \frac{1}{2} \text{Tr}(U_p + U_p^\dagger) ] , \quad (3.1)$$

where  $d$  is the dimension of the particular group representation being used, the plaquette variables  $U_p$  are defined in terms of the group elements  $U(\ell)$  residing on the links of the lattice as

$$U_p = U(\ell_1)U(\ell_2)U^\dagger(\ell_3)U^\dagger(\ell_4) , \quad (3.2)$$

where  $\ell_1, \ell_2, \ell_3, \ell_4$  are the links defining plaquette  $p$ , and the electric field operators  $E_a(\ell)$  are defined by the commutation relations

$$[E_a(\ell), U(\ell')] = -T_a U(\ell) \delta(\ell, \ell') , \quad (3.3)$$

where  $T_a$  is a generator of the representation.

In this chapter we shall concentrate on the  $SU(2)$  lattice gauge theory, in particular we shall consider the fundamental representation for which  $d=2$  and  $\text{Tr}(U_p^\dagger) = \text{Tr}(U_p)$ . The Hamiltonian may then be written as

$$H = \sum_{\ell, a} E_a^2(\ell) + \lambda \sum_p \Phi(p) , \quad (3.4)$$

where the gauge invariant plaquette variable  $\Phi(p)$  is defined by

$$\Phi(p) = 1 - \frac{1}{2} \text{Tr}(U_p) . \quad (3.5)$$

The parameter  $\lambda$  is related to the conventional coupling constant  $g$  by

$$\lambda = 8/g^4 . \quad (3.6)$$

The group element  $U(\ell)$  may be parametrized in a number of ways. For example, in terms of the three component gauge field  $A_a(\ell)$  ( $a = 1, 2, 3$ ),

$$U(\ell) = \exp[ \frac{1}{2} i \sigma_a A_a(\ell) ] , \quad (3.7)$$

where  $\sigma_a$  is a Pauli matrix. Another useful parametrization is

$$U(\ell) = a_0(\ell) + i \vec{\sigma} \cdot \vec{a}(\ell) , \quad (3.8)$$

where  $\vec{a}$  is a 3-vector and

$$a_0^2 + \vec{a}^2 = 1 . \quad (3.9)$$

The (real) numbers  $a_\mu$  ( $\mu = 0, 1, 2, 3$ ) all lie in the domain  $(-1, 1)$  and may

be thought of as the components of a Euclidean 4-vector. Then Eqs.(3.8) and (3.9) indicate that there is a one-to-one correspondence between the elements of  $SU(2)$  and the points in the space  $S_3$ , the three dimensional surface of a four dimensional sphere. In fact the connection lies much deeper; the geometry of the  $SU(2)$  group manifold is identical with that of  $S_3$ , i.e., the two spaces are isomorphic. We will not prove this assertion here but point out an important implication: the invariant group integration measure is simply the volume element in the space  $S_3$ . This may be seen most easily by introducing a third parametrization of the group element  $U(\ell)$  in terms of three angular variables  $\psi(\ell), \theta(\ell), \phi(\ell)$  with domains  $(0, \pi), (0, \pi), (0, 2\pi)$  respectively. These variables are just the spherical coordinates in four dimensions. In terms of these variables,

$$U(\ell) = \cos\psi(\ell) + i\vec{\sigma}\cdot\vec{n}(\ell)\sin\psi(\ell) , \quad (3.10)$$

where  $\vec{n}$  is a unit 3-vector with polar angles  $(\theta, \phi)$ , i.e.,

$$\vec{n} = (\sin\theta\cos\phi, \sin\theta\sin\phi, \cos\theta) . \quad (3.11)$$

Using standard techniques [26] the invariant measure of the group may be found to be

$$d\Omega = \frac{\sin^2\psi \sin\theta \, d\psi \, d\theta \, d\phi}{2\pi^2} , \quad (3.12)$$

which is the volume element in  $S_3$  with the total volume normalized to unity. This means that if  $f(g)$  is some function defined on the group and  $f_p(\psi, \theta, \phi)$  is the corresponding function on the parameter space  $S_3$ , then

$$\int d\Omega f(g) = \int f_p(\psi, \theta, \phi) \frac{\sin^2 \psi \sin \theta d\psi d\theta d\phi}{2\pi^2} . \quad (3.13)$$

This result is important for the numerical calculations to be described shortly where one needs to know how to carry out group integrations in the parameter space.

### 3.2 Variational calculation

The simplest gauge invariant wave function is of the form

$$\psi_T[A] = \prod_p u(\Phi(p)) , \quad (3.14)$$

where  $u$  is an arbitrary function of the plaquette variable  $\Phi(p)$ . This wave function is disordered in the sense that there are no explicit correlations between the variables  $\Phi(p)$  on different plaquettes. For small values of  $\lambda$  the Hamiltonian is dominated by the electric energy term  $\sum E_a^2(\ell)$ . This is a sum of single link operators and so for small  $\lambda$  the link variables  $U(\ell)$  will be completely uncorrelated. Then, the plaquette variables will also be uncorrelated and so for small  $\lambda$  one should expect the wave function given in Eq.(3.14) to be a good representation of the exact vacuum state.

In the present calculations we do not attempt to optimize the functional form of  $u(\Phi(p))$  but simply use

$$u(\Phi(p)) = \exp [ -2\beta\Phi(p) ] , \quad (3.15)$$

where  $\beta$  is a variational parameter chosen to minimize the energy

$$E_0 = \frac{\int d\Omega \psi_T[A] H \psi_T[A]}{\int d\Omega \psi_T^2[A]} . \quad (3.16)$$

This is a sum of two terms: the magnetic energy given by

$$\lambda E_{\text{mag}} = \frac{\lambda \int d\Omega \psi_T^2[A] \sum_{\mathbf{p}} \Phi(\mathbf{p})}{\int d\Omega \psi_T^2[A]} , \quad (3.17)$$

and the electric energy, which, using the hermitian character of  $E_a(\ell)$ , may be written as

$$E_{\text{el}} = \frac{\int d\Omega \psi_T^2[A] \sum_{\ell, a} \{\psi_T^{-1}[A] E_a(\ell) \psi_T[A]\}^2}{\int d\Omega \psi_T^2[A]} . \quad (3.18)$$

If the quantities  $E_{\text{mag}}$  and  $E_{\text{el}}$  defined above could be evaluated analytically as functions of the variational parameter  $\beta$ , it would be a straightforward matter to minimize the energy  $E_0$  with respect to  $\beta$  for any given value of the coupling parameter  $\lambda$ . Unfortunately, analytic expressions can only be derived in the two limits  $\beta \rightarrow 0$  and  $\beta \rightarrow \infty$ . For small  $\beta$  one may use the so called Euclidean strong coupling expansions [27], similar to high temperature expansions used in statistical mechanics, to evaluate the integrals. The results of such a calculation are:

$$E_{\text{mag}}/N_p = 1 - \beta + 2\beta^3/3 + O(\beta^5) , \quad (3.19)$$

$$E_{\text{el}}/N_p = 3\beta^2 - 2\beta^4 + O(\beta^6) ,$$

where  $N_p$  is the number of plaquettes in the lattice. For large  $\beta$  the wave function is sharply peaked in the region of configuration space

where all the group elements  $U(\ell)$  are close to the identity, i.e.,  $A_a(\ell) \rightarrow 0$ . Then, with negligible error in the limit, the range of integration of the field variables  $A_a(\ell)$  may be extended to  $(-\infty, \infty)$ , and the integrals in Eqs.(3.17) and (3.18) become straightforward gaussian integrals which can be easily evaluated. Then, one finds that for  $\beta \rightarrow \infty$ ,

$$E_{\text{mag}}/N_P = \frac{1}{4\beta} + O(\beta^{-2}) , \quad (3.20)$$

$$E_{\text{el}}/N_P = 3\beta - \frac{3}{4} + O(\beta^{-1}) .$$

Of course, one really needs to compute these quantities for intermediate values of  $\beta$ . To do this a Monte Carlo method is used. The limiting expressions given in Eqs.(3.19) and (3.20) then provide useful checks on the accuracy of the Monte Carlo results. In this particular calculation, Creutz's heat bath algorithm, described in detail in Ref.[15], is used to generate an ensemble of field configurations  $\{A^{(r)}; r=1,2,\dots,N\}$  from the probability density  $\psi_T^2[A]/\int d\Omega \psi_T^2[A]$ . Then, any expectation value of the form

$$\langle O \rangle = \frac{\int d\Omega \psi_T^2[A] O[A]}{\int d\Omega \psi_T^2[A]} \quad (3.21)$$

may be computed as the expected value of the ensemble average of  $O[A]$ , i.e.,

$$\langle O \rangle = \left\langle \frac{\sum_r O[A^{(r)}]}{N} \right\rangle \quad (3.22)$$

where the angle brackets on the right hand side denote the expected

value which may be estimated as the average over many different ensembles. Using this method,  $E_{\text{mag}}$  and  $E_{\text{el}}$  are computed for many different values of  $\beta$  and the resulting data are fitted, by means of a least squares analysis, to the specific functional forms

$$E_{\text{mag}}^{(\text{fit})} = \exp [ f_{\text{m}}(\beta) ] , \quad (3.23)$$

$$E_{\text{el}}^{(\text{fit})} = f_{\text{e}}(\beta) ,$$

where  $f_{\text{m}}(\beta)$  and  $f_{\text{e}}(\beta)$  are polynomials in  $\beta$  of sufficient degree to give good fits to the data. The  $\chi^2$ -test, with a significance level of 5%, is used to judge the goodness of fit.

The particular functional forms in Eq.(3.23) are chosen, largely by trial and error, to give good fits with as few adjustable parameters as possible. For  $0 \leq \beta \leq 1.2$ , which is the region of interest, with 65 data points,  $f_{\text{m}}(\beta)$  must be of degree 5 and  $f_{\text{e}}(\beta)$  must be of degree 6 in order to pass the  $\chi^2$ -test.

Figure 1 shows graphs of  $E_{\text{mag}}/N_{\text{p}}$  and  $E_{\text{el}}/N_{\text{p}}$  as functions of  $\beta$ . The points are Monte Carlo results and the solid lines are the fitted functions defined in Eq.(3.23). Only a sample of the Monte Carlo results are plotted. The dashed lines are the large- and small- $\beta$  limits given by Eqs.(3.19) and (3.20). The fits are clearly very good as is the agreement between the Monte Carlo results and the two limiting curves.

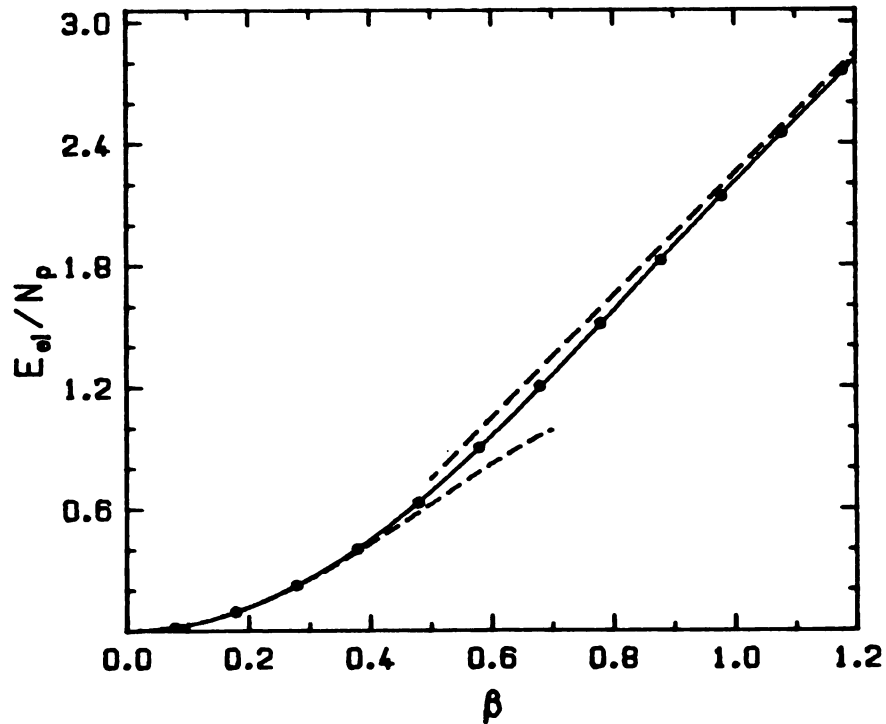
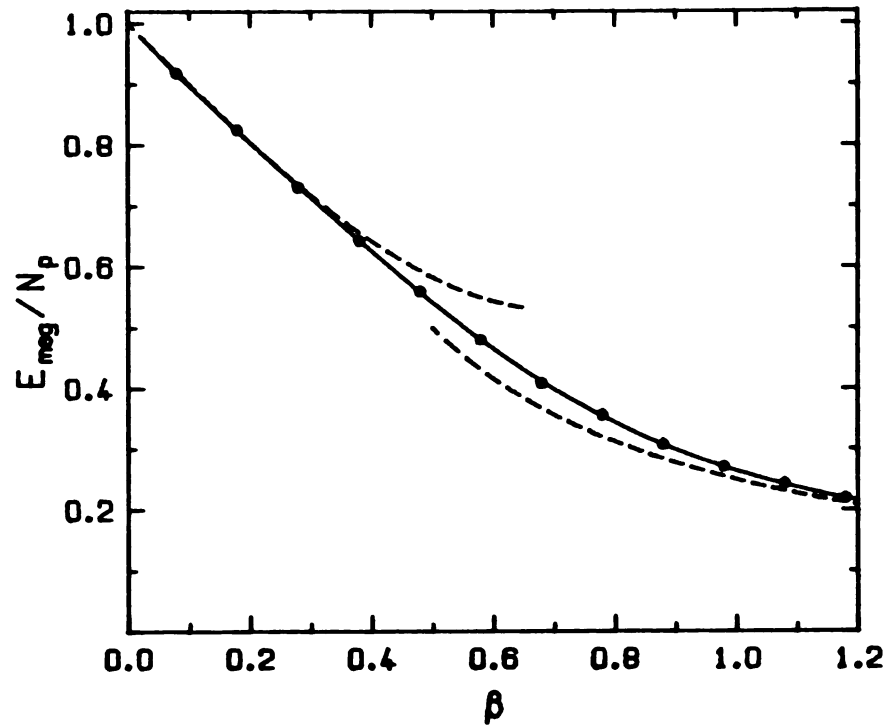


Figure 1: Variational estimates of (a) the magnetic energy, and (b) the electric energy versus the variational parameter  $\beta$  for the SU(2) theory.

In Figure 2 the variational estimate of the ground-state energy per plaquette as a function of  $\lambda$  is compared to the large- $\lambda$  and small- $\lambda$  limits computed in perturbation theory:

$$E_0/N_p \approx \lambda - \frac{\lambda^2}{12} + \frac{11}{14976} \lambda^4 + O(\lambda^6) \quad \text{as } \lambda \rightarrow 0, \quad (3.24)$$

$$E_0/N_p \approx c(n)(2\lambda)^{1/2} + O(1) \quad \text{as } \lambda \rightarrow \infty,$$

for an  $n \times n \times n$  lattice; the constant  $c(n)$  is weakly dependent on  $n$ , e.g.,

$$c(3) = 1.181, \quad c(\infty) = 1.194. \quad (3.25)$$

The constant term in the large- $\lambda$  limit derives from the four-field coupling of the fields in the small field approximation of the theory and at the present time has not been calculated.

The agreement between the variational results and the small- $\lambda$  limit comes as no great surprise since, as mentioned earlier, the variational wave function is expected to be a good approximation of the exact ground state wave function for small  $\lambda$ . Also the apparent disagreement between the variational results and the large- $\lambda$  limit is not meaningful since a constant term is yet to be added to the perturbation theory result. The agreement may then improve or worsen and one does not know, a priori, which it will be.

For this reason, perhaps a more interesting quantity to look at is  $E_{\text{mag}}/N_p = \langle \Phi(p) \rangle$ . For the exact ground state this is related to the energy  $E_0$  by

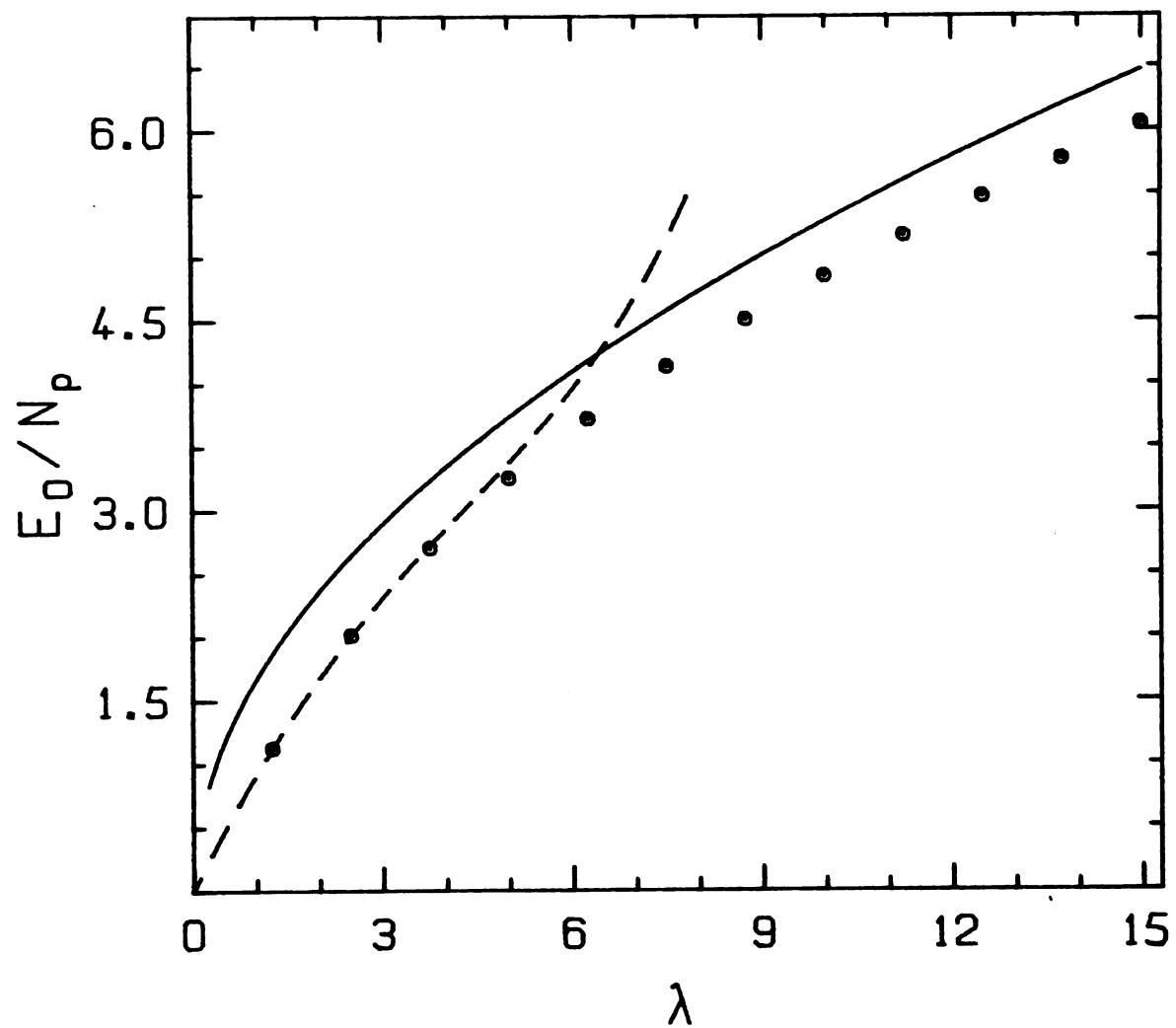


Figure 2: Variational estimate of the ground state energy per plaquette versus  $\lambda$  for the SU(2) theory.

$$\langle \phi(p) \rangle = \frac{1}{N_p} \frac{dE_0}{d\lambda} \quad (3.26)$$

so that the small- and large- $\lambda$  limits are:

$$\langle \phi(p) \rangle \approx 1 - \frac{\lambda}{6} + \frac{11}{3744} \lambda^3 + O(\lambda^5) \quad \text{as } \lambda \rightarrow 0, \quad (3.27)$$

$$\langle \phi(p) \rangle \approx c(n)(2\lambda)^{-1/2} + O(\lambda^{-1}) \quad \text{as } \lambda \rightarrow \infty.$$

These are plotted in Figure 3 along with the variational results. Again one sees excellent agreement between the variational results and the small- $\lambda$  perturbation theory result. However there is a slight discrepancy between the variational results and the large- $\lambda$  limit, the difference increasing somewhat as  $\lambda$  increases. This is an indication of the inadequacy of this uncorrelated variational wave function as a model of the vacuum state of the theory. Other quantities, such as the string tension and the excitation energy of the theory, provide much more sensitive tests of the accuracy of the variational wave function than the mean plaquette field  $\langle \phi(p) \rangle$  calculated here. Calculations of these quantities have been carried out [9,10] and clearly show the failure of the variational wave function to model the vacuum state of the theory at large- $\lambda$ . Those calculations, although of some interest, do not concern us here since we are mainly interested in the variational calculation as a means of providing an importance function for use in the GFMC calculations to be described in the next section.

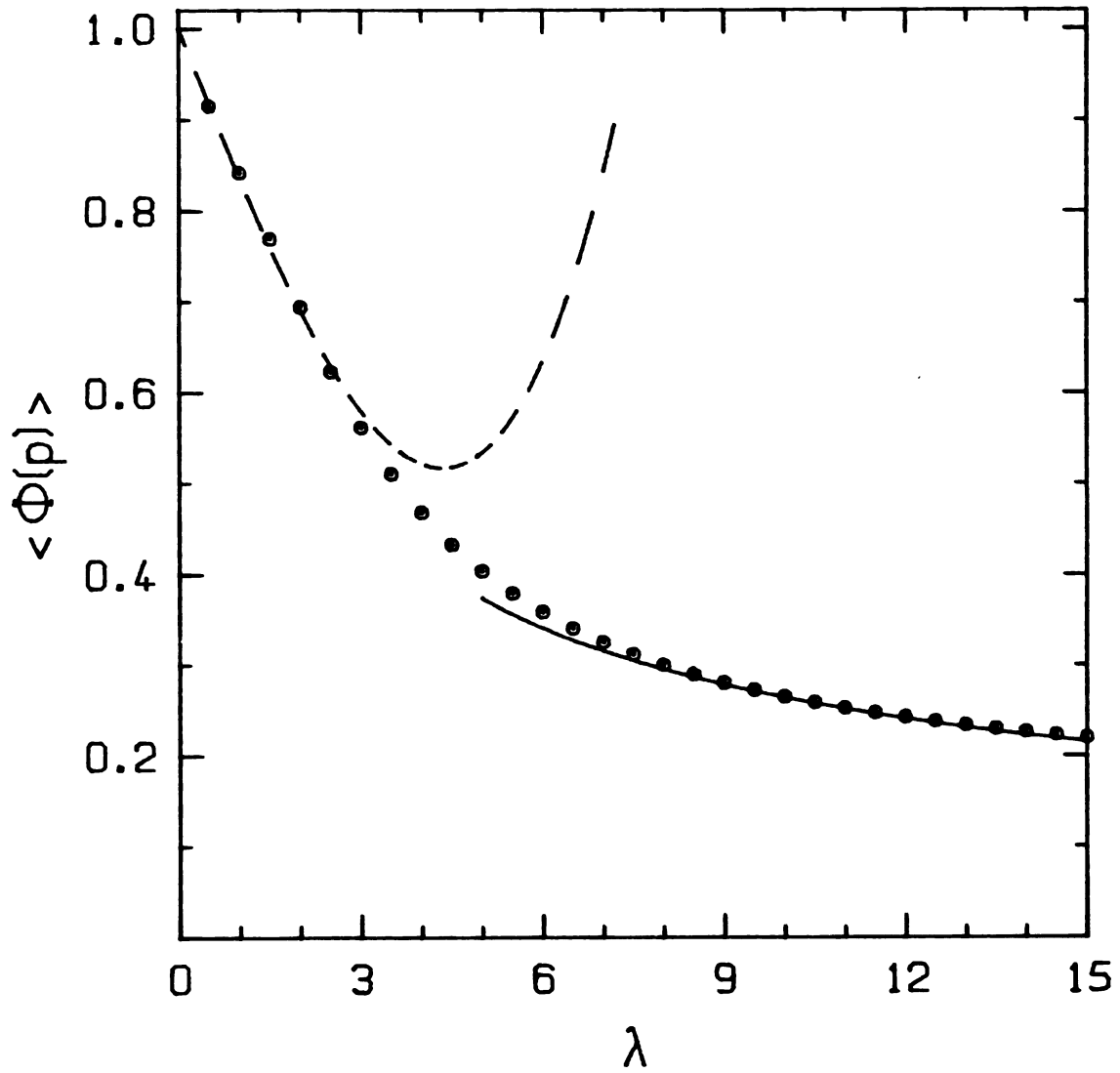


Figure 3: Variational estimate of the mean plaquette field versus  $\lambda$  for the SU(2) theory.

### 3.3 GFMC calculation

The Hamiltonian defined in Eq.(3.4) can not be used as it stands in a GFMC calculation because it is not of the form  $H_0 - \lambda H_1$  with  $H_0$  and  $H_1$  positive definite operators. However, a slightly modified Hamiltonian

$$H_{\text{GFMC}} = \sum_{\ell, a} E_a^2(\ell) - \lambda M \quad (3.28)$$

where

$$M = \sum_{\mathbf{p}} [ 1 + \frac{1}{3} \text{Tr}(U_{\mathbf{p}}) ] \quad (3.29)$$

is of the required form and the GFMC method, described in detail in chapter 2, may be used to compute various ground-state properties. Notice that  $H_{\text{GFMC}}$  differs from  $H$  only by a trivial constant term so that the eigenstates of the two Hamiltonians are identical.

As shown in chapter 2, the ground-state energy of  $H_{\text{GFMC}}$  is negative and so it is useful to write the eigenvalue equation as

$$H_{\text{GFMC}} |\psi\rangle = -Q^2 |\psi\rangle . \quad (3.30)$$

The connection between  $Q^2$  and  $E_0$ , the ground-state energy of  $H$ , is

$$E_0 = 2N_{\mathbf{p}} \lambda - Q^2 . \quad (3.31)$$

The non-normalizable basis  $\{|[A]\rangle\}$  is used, where a state in this basis is determined uniquely by the set of gauge fields  $A_a(\ell)$  (or, alternatively, the angle variables  $\psi(\ell), \theta(\ell), \phi(\ell)$ ) on all the links of the lattice. In this basis, the operator  $M$  defined in Eq.(3.29) is diagonal and the equation to be iterated by the GFMC algorithm is

(cf. Eq.(2.6))

$$\psi[A] = \lambda \int d\Omega' G[A,A'] M[A'] \psi[A'] , \quad (3.32)$$

where

$$G[A,A'] = \langle [A] | [ \sum_{\ell,a} E_a^2(\ell) + Q^2 ]^{-1} | [A'] \rangle . \quad (3.33)$$

The only aspect of the GFMC algorithm not covered in chapter 2 was the very crucial problem of how to sample field configurations from the (unnormalized) probability density  $G[A,A']$ . This matter is discussed at length in the paper reproduced in appendix A. Basically the idea is to write the Green's function as

$$G[A,A'] = \int_0^\infty dt \exp(-tQ^2) \langle [A] | \exp[-t\sum_a E_a^2(\ell)] | [A'] \rangle \quad (3.34)$$

and to use the function  $\exp(-tQ^2)$  to sample  $t$ , then, conditional on this choice, to use  $\langle [A] | \exp[-t\sum_a E_a^2(\ell)] | [A'] \rangle$  to sample field configurations  $[A]$ . The state  $|[A]\rangle$  may be written as a direct product of single link states  $|A(\ell)\rangle$  so that the matrix element appearing on the right hand side of Eq.(3.34) may be written as a product of single link matrix elements. Now since  $Q^2$  is typically large, the variable  $t$  will be small. In this limit it is possible to obtain an explicit expression for the matrix element. The result is

$$\langle A(\ell) | \exp[-tE_a^2(\ell)] | A'(\ell) \rangle \approx \frac{\exp[-(\delta s)^2/t]}{(\pi t)^{3/2}} , \quad (3.35)$$

where  $(\delta s)^2$  is the metric in the parameter space  $S_3$

$$(\delta s)^2 = (\delta\psi)^2 + \sin^2\psi(\delta\theta)^2 + \sin^2\psi\sin^2\theta(\delta\phi)^2 \quad (3.36)$$

$$\delta\psi = \psi' - \psi ; \delta\theta = \theta' - \theta ; \delta\phi = \phi' - \phi . \quad (3.37)$$

The problem of sampling  $G[A,A']$  then reduces to that of sampling the gaussian function  $\exp(-\delta s^2/t)$  for which several methods are available. Of course, there is a complication involved in the sampling of this gaussian due to the fact that the parameter space is curved. The precise details of the sampling procedure may be found in appendix A.

Before going on to discuss the results of the GFMC calculation, one further point should be noted. In order to obtain statistically significant results, it is essential to use some form of importance sampling in the manner described in Sec. 2.4. The details of how to carry out the sampling procedure in this case may again be found in appendix A.

All the calculations presented here were carried out on a 3 x 3 x 3 spatial lattice. An ensemble of approximately 100 configurations was used; the ensemble size changes slightly with each iteration. The results given are averages over 600 Monte Carlo iterations. The first few hundred iterations, during which convergence takes place, are discarded. To calculate the quantities presented here required approximately 3.5 hours of computation time for each value of  $Q^2$  considered (recall that  $Q^2$  rather than  $\lambda$  is the input parameter to the GFMC algorithm) on a CDC Cyber 750 computer at Michigan State University.

Figure 4 shows the ground-state energy per plaquette  $E_0/N_p$  as a function of the coupling parameter  $\lambda$ . The dashed curve is the variational bound obtained in the previous section and the crosses are GFMC results obtained using importance sampling based on the variational wave function  $\psi_T[A]$ . The GFMC points agree very well with the variational bound at small  $\lambda$ ; this is to be expected since the variational wave function is an accurate representation of the exact vacuum state for small  $\lambda$ . As  $\lambda$  increases the GFMC points begin to lie lower than the variational bound, the difference increasing with increasing  $\lambda$ . Again this is as expected; the variational wave function is known to become less accurate as a model of the ground state as  $\lambda$  increases and so the exact vacuum energy should be lower than the variational bound.

As in the previous section, a more interesting quantity to look at is the mean plaquette field  $\langle\phi(p)\rangle$ . This is shown in Figure 5. Again the dashed curve is the variational estimate and the crosses are GFMC estimates; these GFMC results were computed from the mixed expectation value, Eq.(2.62). The solid curves are the large- and small- $\lambda$  limits given by Eq.(3.27).

The GFMC points tend to lie below the variational curve for small- $\lambda$  and are inconsistent with the small- $\lambda$  perturbation theory curve. Ordinarily this would be taken as evidence that the variational wave function  $\psi_T[A]$ , used for importance sampling, is not a good representation of the vacuum state. However, in this case,  $\psi_T[A]$  is believed to accurately describe the exact ground state for small  $\lambda$  and

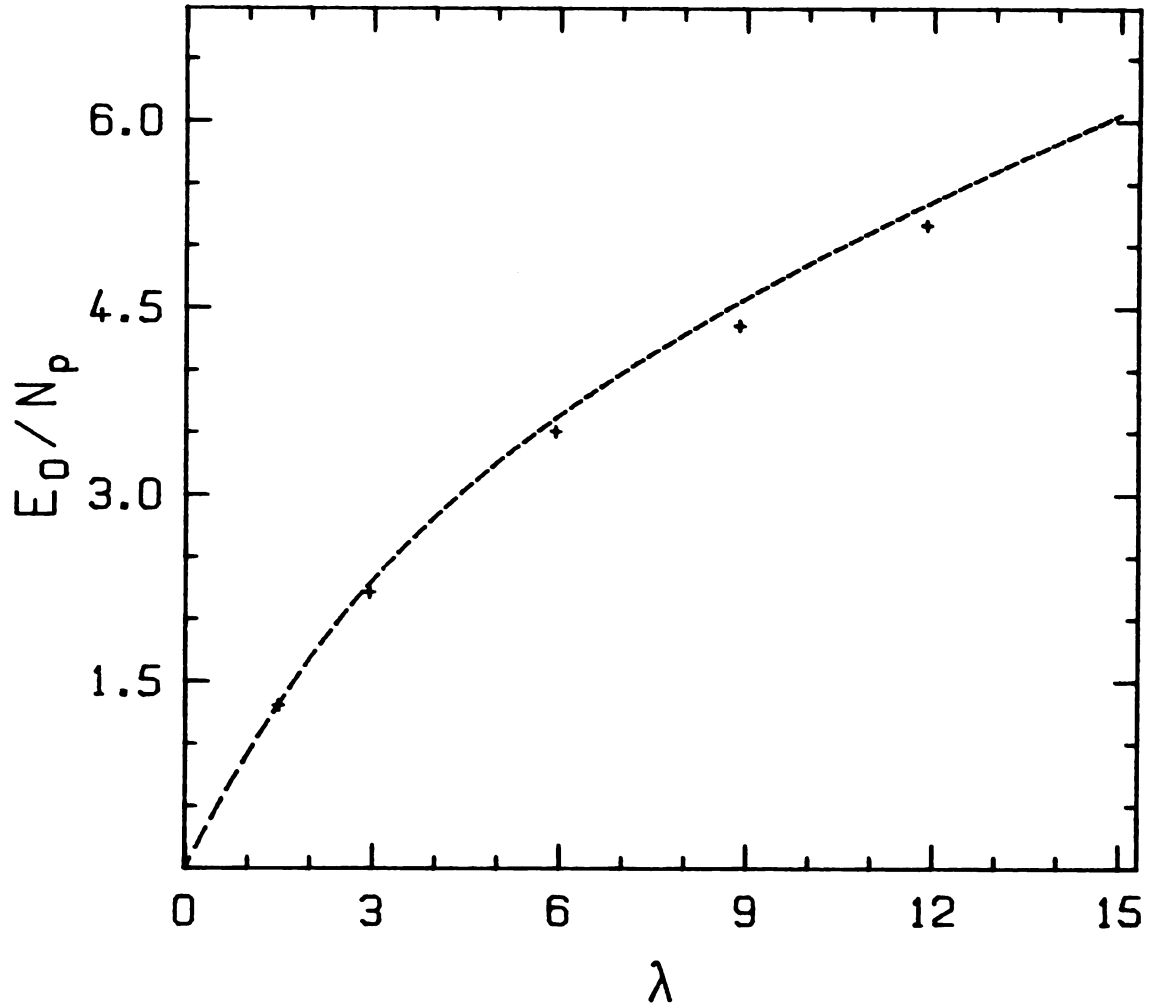


Figure 4: GFMC estimate of the ground state energy per plaquette versus  $\lambda$  for the SU(2) theory.

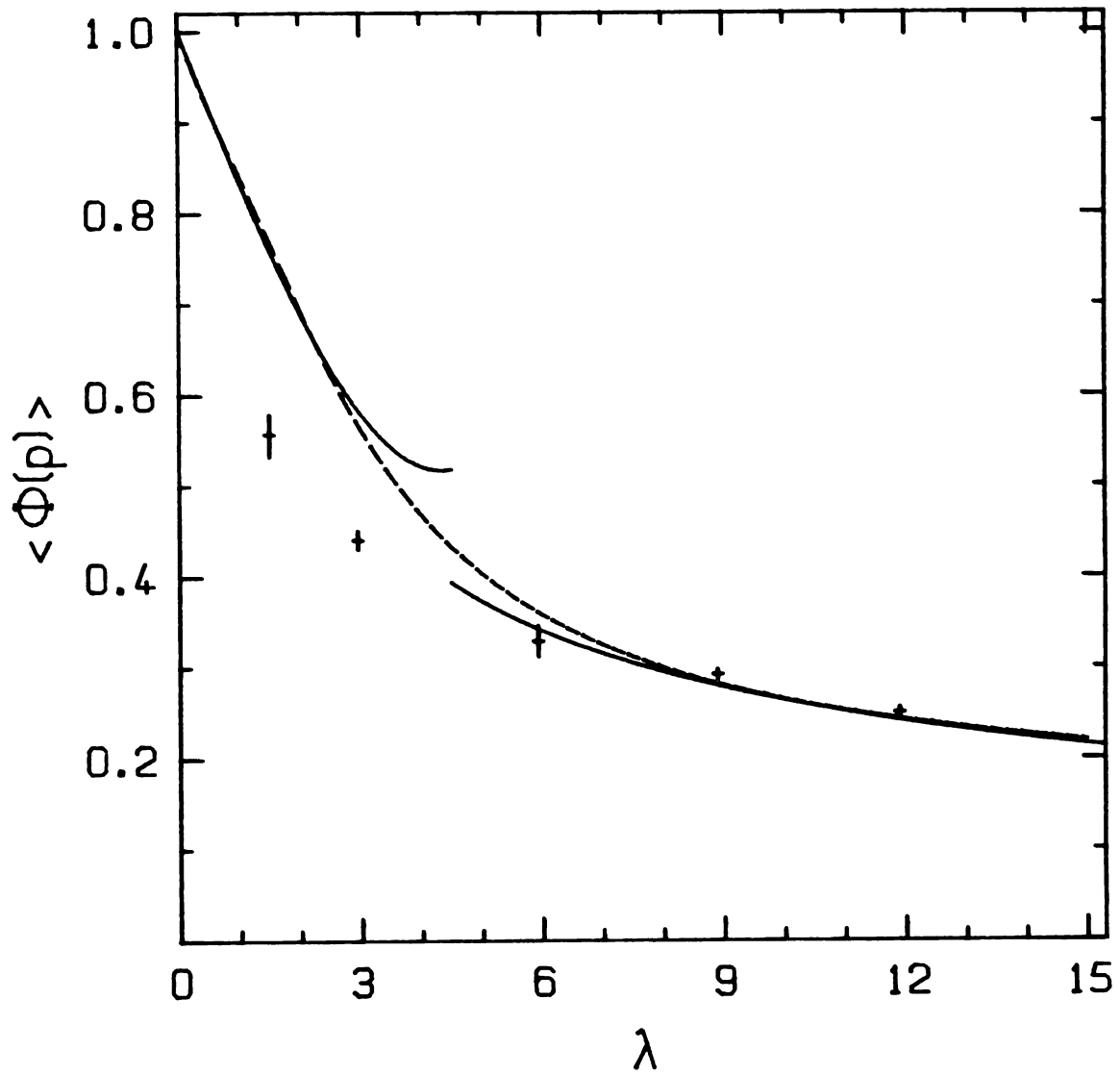


Figure 5: GFMC estimate of the mean plaquette field versus  $\lambda$  for the SU(2) theory.

to become increasingly worse as  $\lambda$  increases. The results on the energy per plaquette shown in Figure 4, where the GFMC points are in close agreement with the variational bound but begin to deviate as  $\lambda$  increases, are consistent with this view. The poor accuracy of the GFMC results for small  $\lambda$  in Figure 5 may be due to the failure of the small time step approximation used to calculate the matrix elements of  $\exp(-t\Sigma_a^2(\ell))$ . The time  $t$  is sampled from the probability density  $\exp(-tQ^2)$  and so is of order  $1/Q^2$ , which increases as  $\lambda$  decreases. The approximation will, therefore, be least valid for small  $\lambda$ . This explanation could be checked by subdividing every time step into intervals smaller than some fixed  $\delta t$ , and then observing how the results change as  $\delta t$  decreases. On the other hand, since the wave function is disordered for small  $\lambda$ , one might expect that errors in the sampling procedure would be unimportant. Another possible explanation of this discrepancy is that the calculation may not have been carried out for enough iterations to deduce a meaningful estimate of the uncertainty indicated by the error bars. Successive GFMC ensembles are highly correlated and fluctuations of measured quantities extend over many iterations, so it is possible that the 600 iterations used to compute the GFMC results are dominated by one very long fluctuation which causes the estimates to be too small. If this is correct it is not clear why the same problem does not occur for the larger values of  $\lambda$ . Clearly further investigation is needed to clarify the situation.

## CHAPTER 4

### The U(1) lattice gauge theory in 3+1 dimensions

#### 4.1 Definition of the model

In this chapter calculations on the U(1) lattice gauge theory will be described which parallel those on the SU(2) model discussed in the previous chapter. By studying this somewhat simpler model it may be possible to resolve some of the questions raised by the GFMC calculations on the SU(2) model. Also, Monte Carlo calculations in the Euclidean path-integral formulation of the theory have clearly demonstrated that the vacuum state of the U(1) model undergoes a second order phase transition in four dimensions from a charge confining phase at strong coupling ( $g^2 \rightarrow \infty$ ,  $\lambda \rightarrow 0$ ) to a non-confining phase at weak coupling ( $g^2 \rightarrow 0$ ,  $\lambda \rightarrow \infty$ ) [28], and it will be interesting to see if evidence of this transition shows up in the Hamiltonian formulation of the theory.

The elements of the group  $U(1)$  may be parametrized as

$$U = \exp(iA) \quad (4.1)$$

where the gauge field  $A$  lies in the domain  $(0, 2\pi)$ . With this parametrization the plaquette variable  $U_p$  may be written as

$$U_p = \exp[iB(p)] \quad (4.2)$$

where  $B(p)$  is the lattice curl of  $A$  at plaquette  $p$ :

$$B(p) = A(\ell_1) + A(\ell_2) - A(\ell_3) - A(\ell_4) . \quad (4.3)$$

The links  $\ell_1, \ell_2, \ell_3, \ell_4$ , define the plaquette  $p$ .

An explicit expression for the electric field operator  $E(\ell)$  may be obtained from the commutation relation (cf. Eq.(3.3))

$$[E(\ell), U(\ell')] = - U(\ell) \delta(\ell, \ell') , \quad (4.4)$$

and is found to be

$$E(\ell) = i \frac{\partial}{\partial A(\ell)} . \quad (4.5)$$

The Hamiltonian Eq.(3.1) may then be written as

$$H = - \sum_{\ell} \frac{\partial^2}{\partial A^2(\ell)} + \lambda \sum_p \Phi(p) , \quad (4.6)$$

where the gauge invariant plaquette field  $\Phi(p)$  is defined by

$$\Phi(p) = 1 - \cos B(p) , \quad (4.7)$$

and the constant  $\lambda$  is related to the conventional coupling constant  $g$  by

$$\lambda = 2/g^4 \quad (4.8)$$

The group manifold is one dimensional and the invariant measure is easily shown to be

$$d\Omega = \frac{dA}{2\pi} , \quad (4.9)$$

so that group integrations may be carried out in the parameter space by simply integrating over the gauge fields  $A(\ell)$ .

#### 4.2 Variational calculation

As in the previous chapter, we will use the disordered wave function

$$\psi [A] = \prod_p u(\phi(p)) , \quad (4.10)$$

with the specific choice

$$u(\phi(p)) = \exp[ -\frac{1}{2}\beta\phi(p) ] . \quad (4.11)$$

The factor of  $\frac{1}{2}$  in the exponent is chosen purely for aesthetic reasons. The calculation proceeds in precisely the same way as the SU(2) variational calculation, the only difference being in the choice of gauge group.

Figure 6 shows graphs of  $E_{\text{mag}}/N_p$  and  $E_{\text{el}}/N_p$  as functions of the variational parameter  $\beta$ . The points are a sample of the Monte Carlo variational estimates and the solid lines are the functions  $E_{\text{mag}}^{(\text{fit})}(\beta)$  and  $E_{\text{el}}^{(\text{fit})}(\beta)$ . The functional forms given in Eq.(3.23) again give good fits to the data with the least number of parameters: in the region  $0 \leq \beta \leq 1.8$  with 92 data points,  $f_m(\beta)$  is a polynomial of degree 7 and  $f_e(\beta)$  is one of degree 8. More parameters are needed in this case than in the SU(2) calculation because a larger range of  $\beta$  is covered and more data points are used. The dashed lines in Figure 6 are small- and large- $\beta$  limits derived from Euclidean strong coupling expansions and the Gaussian approximation respectively. The functions describing these curves are, for small  $\beta$ ,

$$E_{\text{mag}}/N_p = 1 - \beta/2 + \beta^3/16 + O(\beta^5) , \quad (4.12)$$

$$E_{\text{el}}/N_p = \beta^2/2 - \beta^4/16 + O(\beta^6) ,$$

and for large  $\beta$ ,

$$E_{\text{mag}}/N_p = \frac{1}{3\beta} + O(\beta^{-2}) , \quad (4.13)$$

$$E_{\text{el}}/N_p = \beta - 1/3 + O(\beta^{-1}) .$$

Figure 7 shows the variational estimate of the ground state energy per plaquette as a function of the coupling parameter  $\lambda$  and compares these results to the large- and small- $\lambda$  limits derived from perturbation theory:

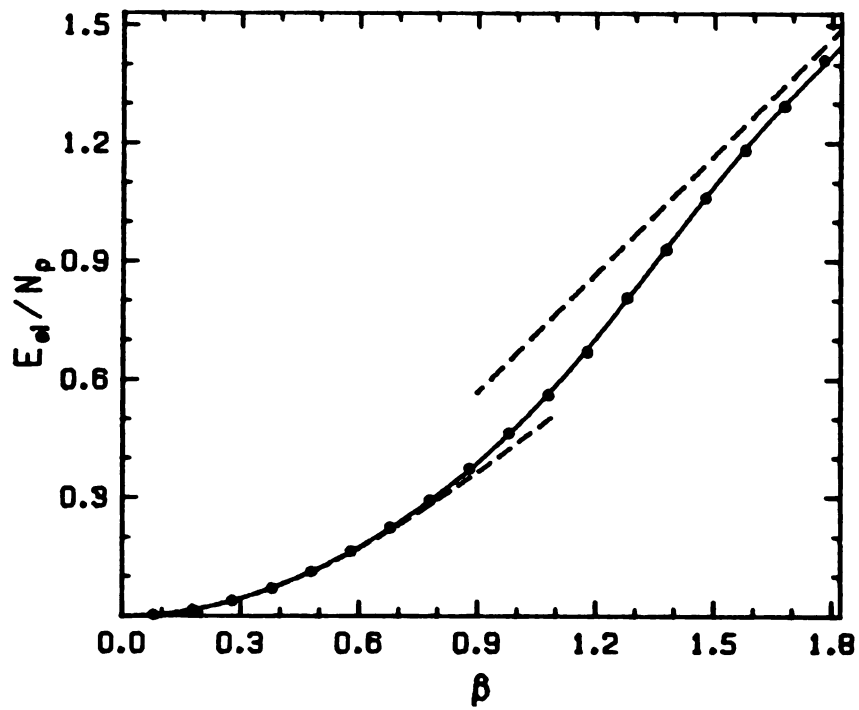
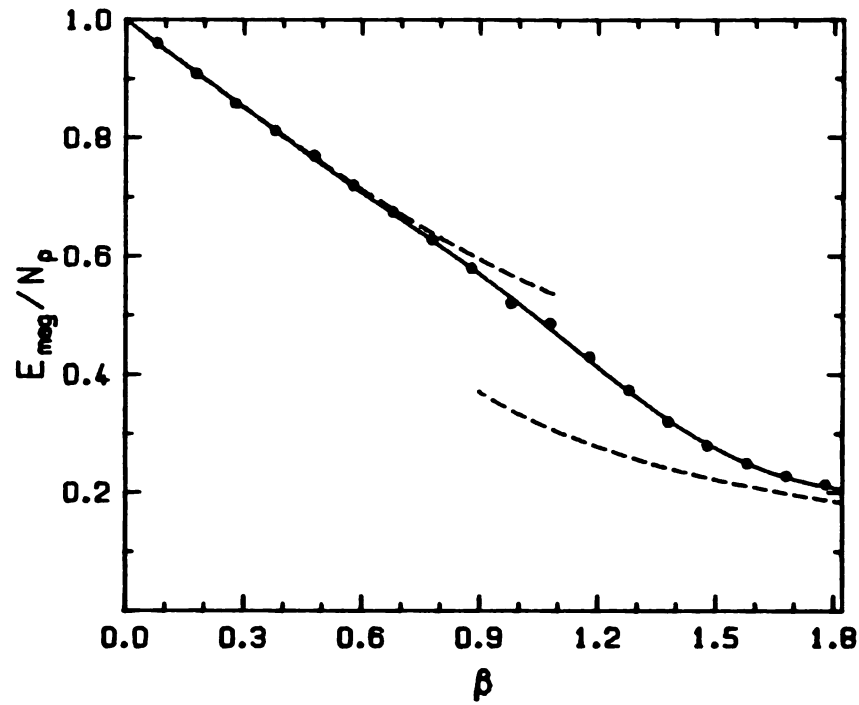


Figure 6: Variational estimates of (a) the magnetic energy, and (b) the electric energy versus the variational parameter  $\beta$  for the U(1) theory.

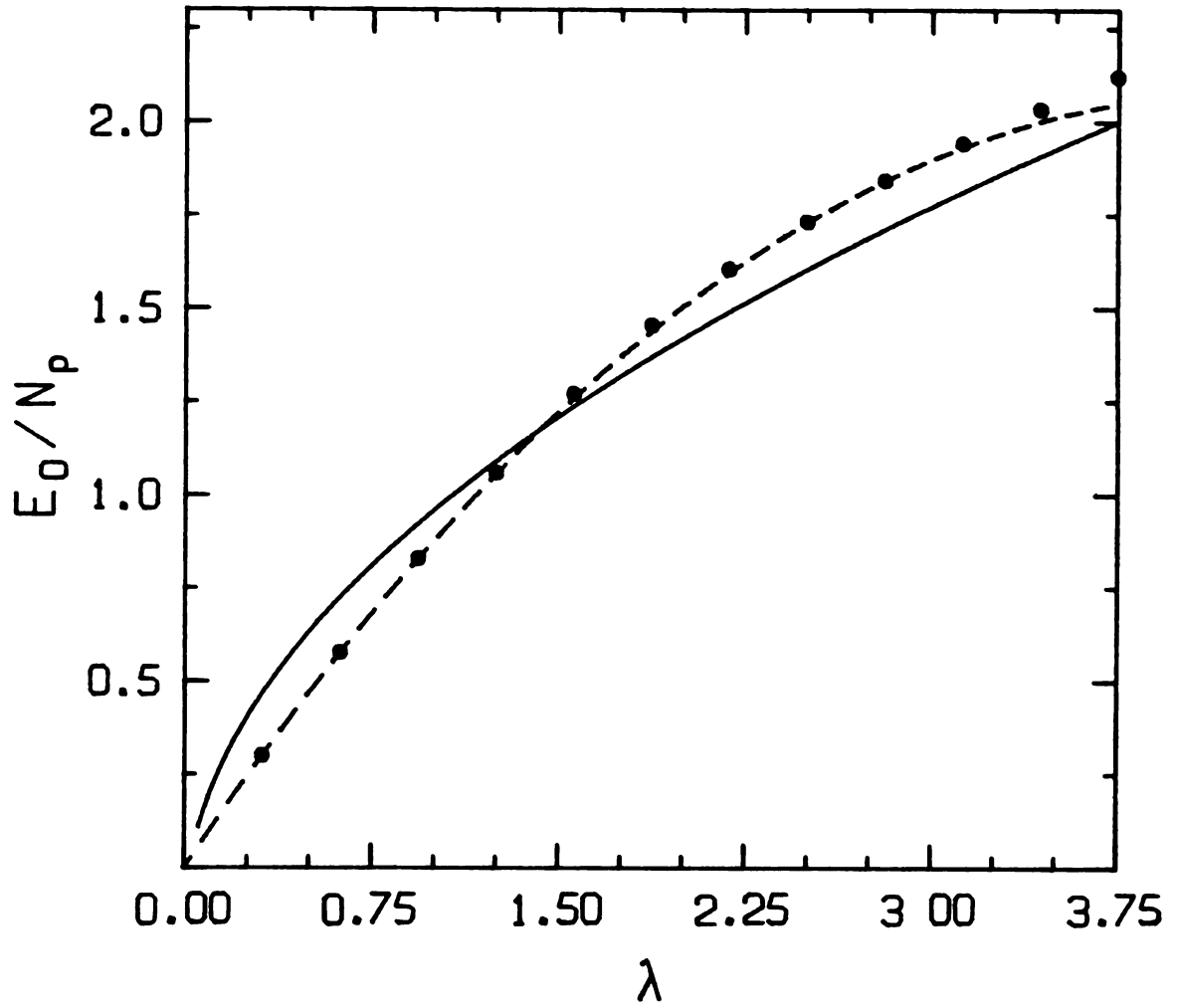


Figure 7: Variational estimate of the ground state energy per plaquette versus  $\lambda$  for the U(1) theory.

$$E_0/N_p \approx \lambda - \lambda^2/8 + 3\lambda^4/10240 + O(\lambda^6) \quad \text{as } \lambda \rightarrow 0, \quad (4.14)$$

$$E_0/N_p \approx d(n)(2\lambda)^{1/2} - d^2(n)/4 + O(\lambda^{-1/2}) \quad \text{as } \lambda \rightarrow \infty,$$

for an  $n \times n \times n$  lattice. As in the  $SU(2)$  large- $\lambda$  limit, the constant  $d(n)$  depends weakly on the lattice size, e.g.,

$$d(3) = 0.787, \quad d(\infty) = 0.796.$$

At small  $\lambda$  the variational estimates are in excellent agreement with perturbation theory as expected, but at large  $\lambda$  the variational estimates lie significantly higher than the perturbation theory result. This clearly indicates the inadequacy of the simple uncorrelated wave function Eq.(4.10) as a model of the vacuum state of the theory at large  $\lambda$ .

The same conclusion also follows from a consideration of the variational estimate of the mean plaquette field  $\langle \phi(p) \rangle$  as a function of  $\lambda$ . This is shown in Figure 8 along with the large- and small- $\lambda$  limits determined using Eq.(3.26):

$$\langle \phi(p) \rangle \approx 1 - \lambda/4 + 3\lambda^3/2560 + O(\lambda^5) \quad \text{as } \lambda \rightarrow 0, \quad (4.15)$$

$$\langle \phi(p) \rangle \approx d(n)/(2\lambda)^{1/2} + O(\lambda^{-3/2}) \quad \text{as } \lambda \rightarrow \infty.$$

### 4.3 GFMC calculation

The discussion of section 3.3 leading to Eq.(3.32) is applicable almost without change to the  $U(1)$  model, so that the equation to be

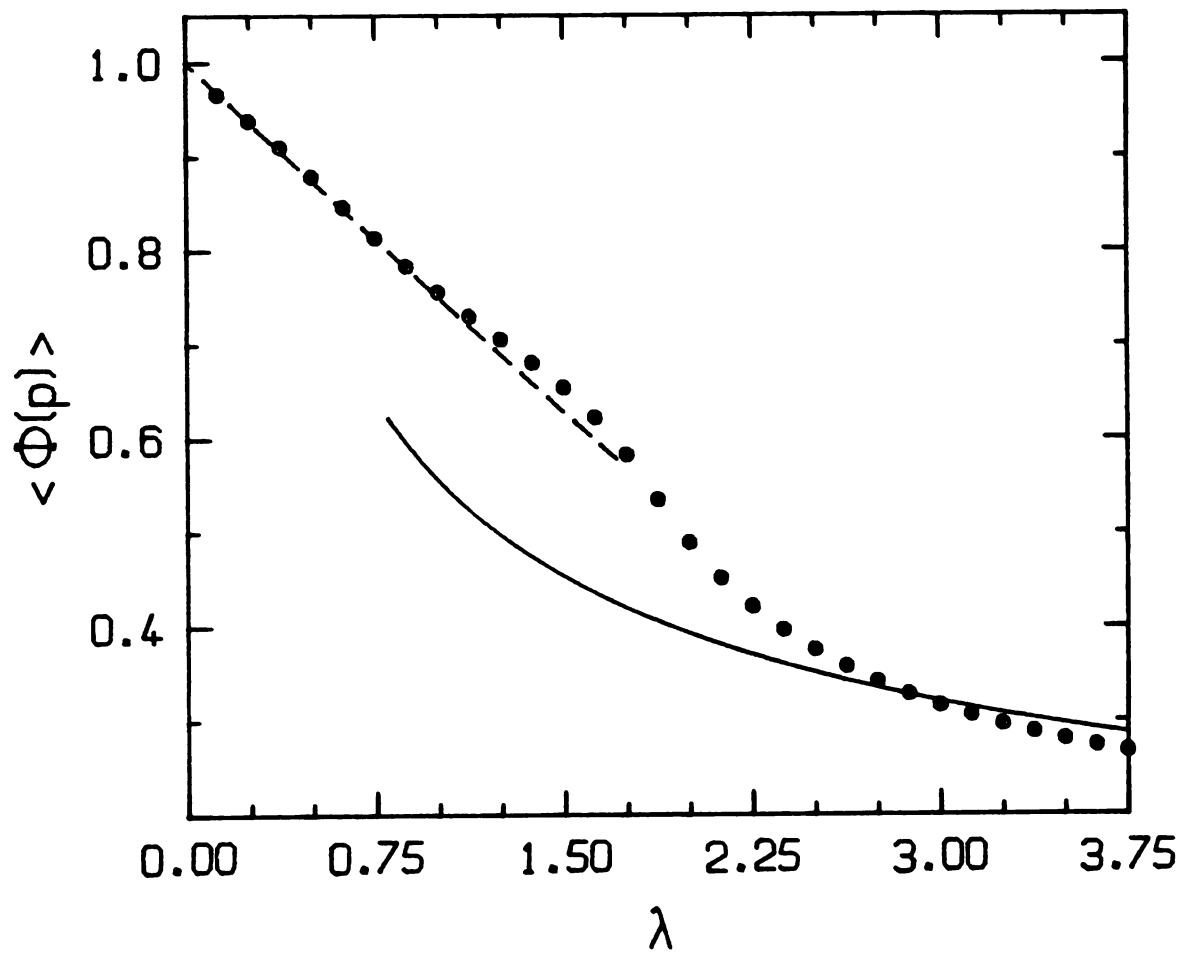


Figure 8: Variational estimate of the mean plaquette field versus  $\lambda$  for the U(1) theory.

iterated by the GFMC method is

$$\psi[A] = \int d\Omega G[A,A'] M[A'] \psi[A'] \quad (4.16)$$

where

$$M[A] = \sum_p [ 1 + \cos B(p) ] \quad (4.17)$$

and

$$G[A,A'] = \langle [A] | \left[ -\Sigma \frac{\partial^2}{\partial A^2(\ell)} + Q^2 \right]^{-1} | [A'] \rangle , \quad (4.18)$$

$$= \int dt \exp(-tQ^2) \langle [A] | \exp\left[t \Sigma \frac{\partial^2}{\partial A^2(\ell)}\right] | [A'] \rangle . \quad (4.19)$$

The state  $|[A]\rangle$  may be written as a direct product of single link states  $|A(\ell)\rangle$  so that the matrix element appearing in the integrand of Eq.(4.19) may be written as

$$\prod_{\ell} \langle A(\ell) | \exp\left[t \frac{\partial^2}{\partial A^2(\ell)}\right] | A'(\ell) \rangle . \quad (4.20)$$

In appendix A it is shown that in the small-t limit this single link matrix element may be written as

$$\langle A(\ell) | \exp\left[t \frac{\partial^2}{\partial A^2(\ell)}\right] | A'(\ell) \rangle \approx \frac{\exp[-(\delta A)^2/4t]}{(4\pi t)^{1/2}} . \quad (4.21)$$

The problem of sampling field configurations from the Green's function  $G[A,A']$  then reduces, as in the  $SU(2)$  case, to sampling a gaussian distribution. The precise details of the calculation,

including the use of importance sampling based on the variational wave function Eq.(4.11), may be found in appendix A.

As in the SU(2) case these calculations have been carried out on a  $3 \times 3 \times 3$  spatial lattice, with an ensemble size of approximately 100 configurations which changes slightly with each iteration. The results given are averages over 600 Monte Carlo iterations and required approximately 200 seconds of computation time for each value of  $Q^2$  considered.

Figure 9 shows the ground-state energy per plaquette  $E_0/N_p$  as a function of  $\lambda$ . The crosses are GFMC results and the dashed curve is the variational bound obtained in the previous section. The solid curve is the large- $\lambda$  perturbation theory result Eq.(4.14). At small  $\lambda$  the GFMC results agree with the variational bound but for larger values of  $\lambda$  the GFMC points lie significantly lower, clearly indicating that the uncorrelated wave function Eq.(4.11) is no longer a good model of the ground state at large  $\lambda$ . In fact for large  $\lambda$  the exact ground-state wave function can be derived. In that limit the energy is dominated by the magnetic energy and so the terms  $1 - \cos B(p)$  will be small, i.e.,  $B(p) \rightarrow 0$  as  $\lambda \rightarrow \infty$ . With this approximation, the Hamiltonian Eq.(4.6) is quadratic so that the ground-state wave function is a gaussian in the gauge fields  $A(\ell)$ :

$$\psi[A] = \exp \left[ -\frac{1}{2} a \sum_k A_k(\vec{x}) M_{kk}(\vec{x}, \vec{x}') A_k(\vec{x}') \right] \quad (4.22)$$

where

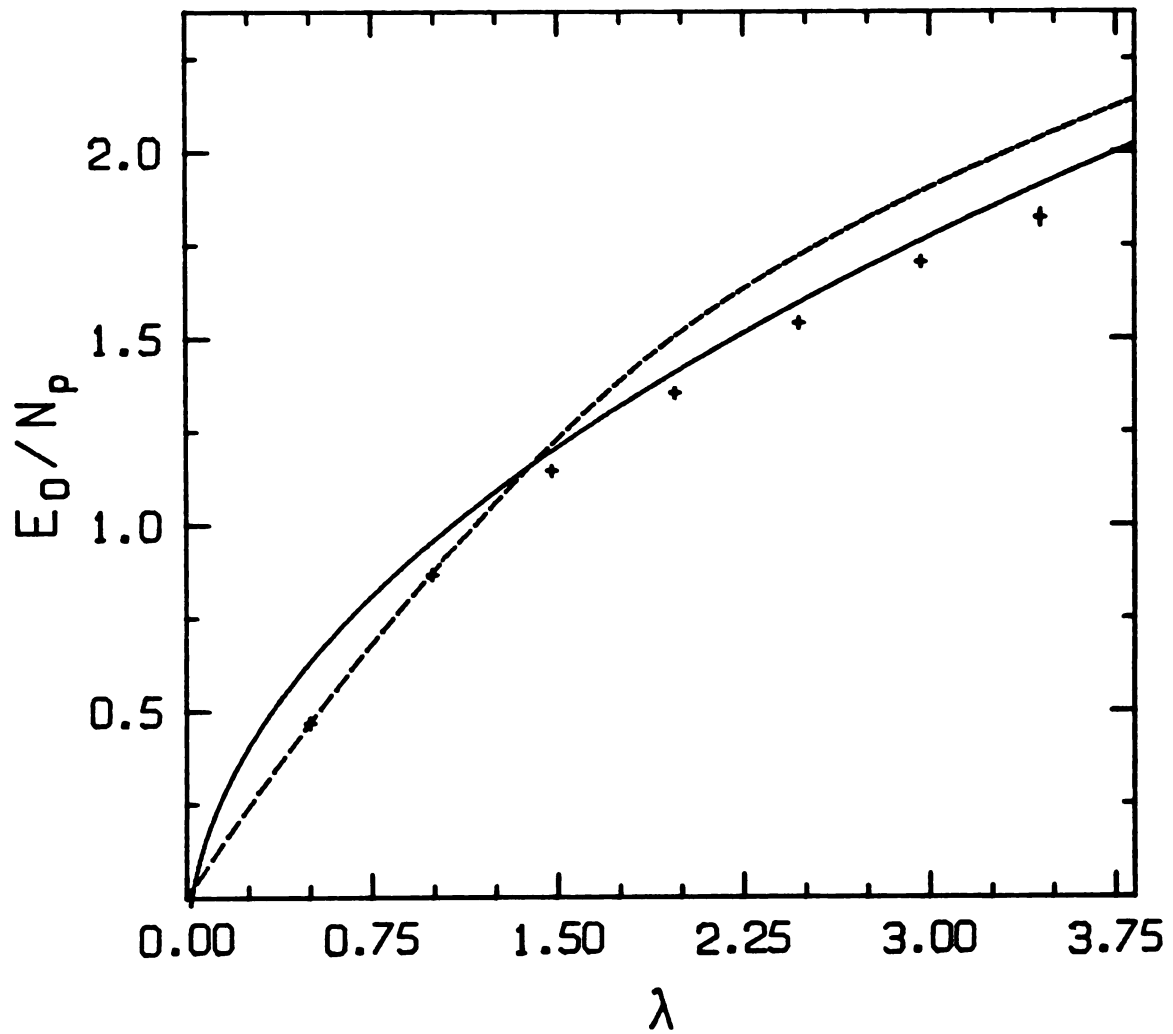


Figure 9: GPMC estimate of the ground state energy per plaquette versus  $\lambda$  for the U(1) theory.

$$a = (\lambda/2)^{1/2} , \quad (4.23a)$$

$$M_{kk'}(\vec{x}, \vec{x}') = \frac{1}{n^3} \sum_{\vec{q}} m_{kk'}(\vec{q}) \exp\left[ \frac{2\pi i}{n} \vec{q} \cdot (\vec{x} - \vec{x}') \right] , \quad (4.23b)$$

$$m_{kk'}(\vec{q}) = \frac{f^2(\vec{q}) \delta_{kk'} - f_k(\vec{q}) f_{k'}^*(\vec{q})}{f(\vec{q})} , \quad (4.23c)$$

$$f_k(\vec{q}) = 1 - \exp\left( \frac{2\pi i}{n} q_k \right) , \quad (4.23d)$$

$$f(\vec{q}) = \sum_k |f_k(\vec{q})|^2 , \quad (4.23e)$$

for an  $n \times n \times n$  lattice. The sum in Eq.(4.22) is over all  $\vec{x}, \vec{x}', k, k'$ . In these equations a link  $\ell$  is defined by two indices  $\vec{x}$  and  $k$ ; the link lies between the lattice sites at  $\vec{x}$  and  $\vec{x} + \vec{e}_k$  where  $\vec{e}_k$  is a unit vector. At large  $\lambda$  then, the ground-state wave function explicitly couples links which are widely spaced; this type of coupling is absent in the simple disordered wave function Eq.(4.11).

There appears to be an abrupt crossover point at  $\lambda \approx 1.2$  in Figure 9 where the GFMC results begin to deviate markedly from the variational bound. This may be taken as evidence, albeit inconclusive, of a phase transition at that point. For  $\lambda < 1.2$  the ground state of the theory resembles the disordered variational wave function as indicated by the close agreement between the variational results and the (in principle) exact GFMC results, but for  $\lambda > 1.2$  the disordered wave function is no longer accurate and the ground state is more closely represented by the gaussian wave function Eq.(4.22) with its explicit couplings between widely separated links.

It is interesting to compare this result to the corresponding result for the SU(2) model shown in Figure 4. In that case the deviation of the exact GFMC results from the variational curve simply increased very gradually as  $\lambda$  increased. This is consistent with the fact that there is no phase transition in the ground state of the SU(2) theory.

The GFMC results at large  $\lambda$  in Figure 9 appear to lie significantly lower than the large- $\lambda$  perturbation theory curve. It may be that by using a poor importance function one obtains inaccurate estimates of the energy with an ensemble as small as 100 configurations; the GFMC method relies heavily on the law of large numbers of probability theory and so it is conceivable that small ensembles result in inaccurate GFMC results. To study this systematically would require repeating the calculations for different ensemble sizes and observing how the results vary as the ensemble size increases. Such an undertaking would clearly be very demanding on computer time. Furthermore, it may be that if the importance function is too inaccurate the ensemble size necessary to obtain good results is unmanageably large. With these points in mind, the problem of ensemble size dependence of the GFMC results has been left for future investigation.

Figure 10 shows the mean plaquette field  $\langle\phi(p)\rangle$  as a function of  $\lambda$ . Again the crosses are GFMC results based on the mixed expectation value Eq.(2.62), the dashed curve is the variational estimate, and the solid curve is the large- $\lambda$  perturbation theory result Eq.(4.15). Notice again the abrupt deviation of the GFMC points from the variational curve at

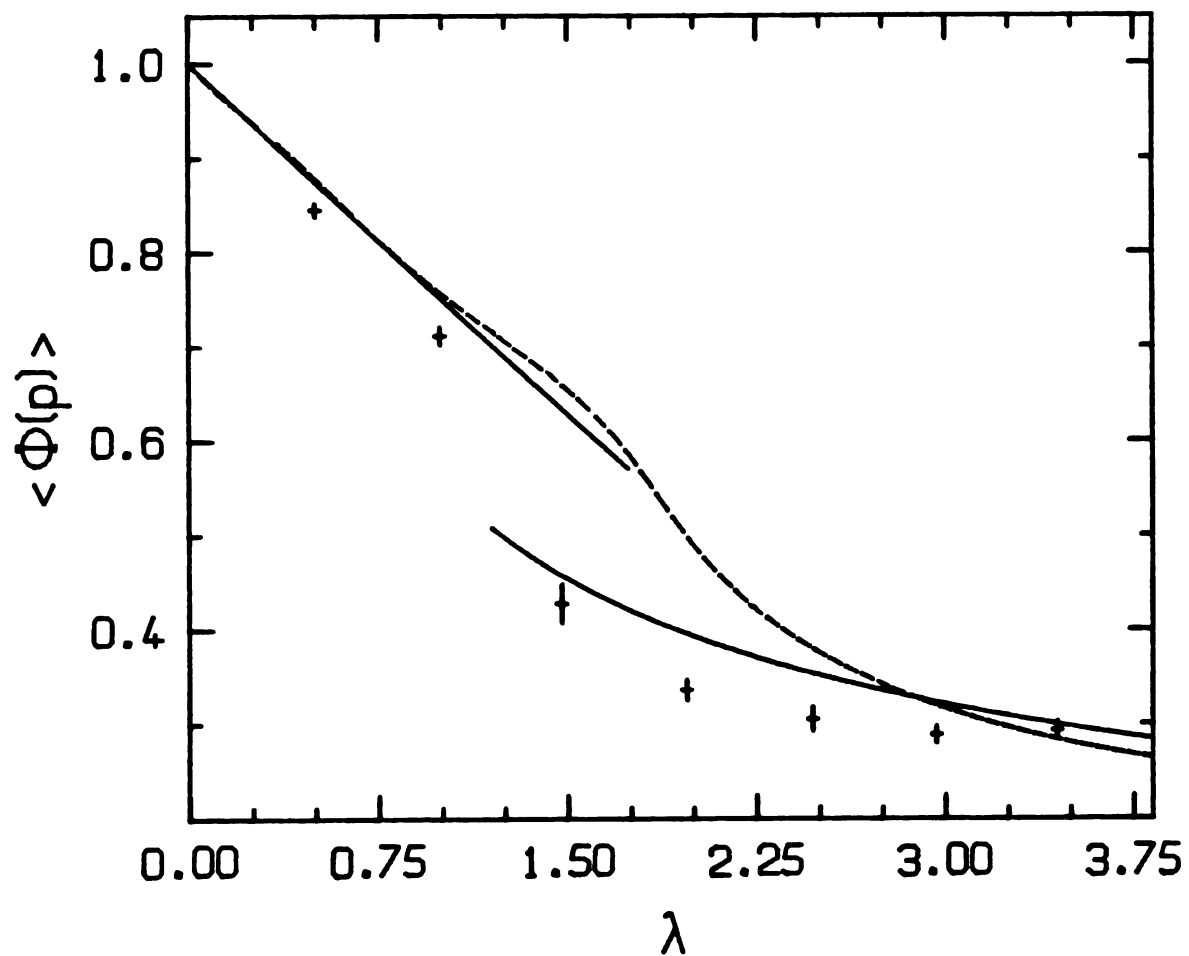


Figure 10: GPMC estimate of the mean plaquette field versus  $\lambda$  for the U(1) theory.

$\lambda \approx 1.2$  indicative of the phase transition in this model at that point. Recall that the GFMC results for this quantity are not exact and can only be trusted if they do not differ very much from the variational estimates. Thus, the lack of good agreement between the GFMC results and the large- $\lambda$  perturbation theory curve is not surprising.

As in the corresponding SU(2) results shown in Figure 5, the GFMC points at small  $\lambda$  are noticeably low; they are inconsistent with the known small  $\lambda$  behaviour given by Eq.(4.15). The comments made at the end of chapter 3 concerning this discrepancy are also valid here. However, for the point at  $\lambda \approx 0.75$  the calculation was repeated breaking each time step  $t$  into ten smaller substeps with no noticeable change in the result. Of course, this is by no means intended to be a complete study of the problem, but it does tend to cast some doubt on the explanation of the discrepancy as a failure of the small- $t$  approximation. As stated at the end of chapter 3, further investigation is clearly necessary to resolve the problem.

## CHAPTER 5

### n-space formulation of the U(1) lattice gauge theory

#### 5.1 The n-space equations

The calculations on the U(1) lattice gauge theory described in the previous chapter used a basis set in which the plaquette fields  $\Phi(p)$  are diagonal. Using such a basis the problem of how to use the gaussian wave function given in Eq.(4.22) as an importance function presents so far insurmountable difficulties and one is restricted to using the simple disordered wave function Eq.(4.11) which gives poor results at large  $\lambda$ . A different formulation of the problem is possible which allows one to use a basis in which the electric field energy is diagonal and also to use as importance functions both disordered and gaussian wave functions.

Write the wave function  $\psi[A]$  in the manifestly gauge invariant form

$$\psi[A] = \sum_{\{n\}} \exp\left[ i \sum_p n(p)B(p) \right] \phi[n] , \quad (5.1)$$

where  $n(p)$  are integer-valued plaquette variables. It is necessary to restrict  $n(p)$  in this way to ensure that the wave function  $\psi[A]$  is periodic in the gauge fields  $A(\ell)$ . Equation (5.1) resembles a Fourier series expansion in the magnetic field variables  $B(p)$ . This is not quite the case, though, because not all of the fields  $B(p)$  are independent. In fact the sum of the  $B(p)$ 's over any closed surface in the lattice must vanish in accordance with Gauss' Law.

Inserting Eq.(5.1) into the eigenvalue equation, the corresponding eigenvalue equation for the function  $\phi[n]$  may be shown to be

$$S[n]\phi[n] + \lambda \sum_{\{n'\}} K[n,n'] \phi[n'] = E\phi[n] \quad (5.2)$$

where the operator  $S[n]$ , which comes from the electric field energy, is

$$S[n] = \sum_{pp'} n(p)n(p')\Delta(p,p') , \quad (5.3)$$

$$\Delta(p,p') = \sum_{\ell} \frac{\partial B(p)}{\partial A(\ell)} \frac{\partial B(p')}{\partial A(\ell)} . \quad (5.4)$$

The operator  $K[n,n']$ , which comes from the magnetic field energy, is

$$K[n,n'] = \sum_p \{ \delta[n,n'] - \frac{1}{2}\delta[n,n'+\delta_{pp'}] - \frac{1}{2}\delta[n,n'-\delta_{pp'}] \} . \quad (5.5)$$

The function  $\delta[n,n'] = 1$  if  $n(p) = n'(p)$  for all  $p$  and is zero otherwise,  $\delta[n,n'+\delta_{pp'}] = 1$  if  $n(p) = n'(p)$  for all  $p \neq p'$  and

$n(p') = n'(p') + 1$ , and similarly for  $\delta[n, n' - \delta_{pp'}]$ .

If instead of the Hamiltonian defined in Eq.(4.6) one uses  $H_{\text{GFMC}}$  defined by

$$H_{\text{GFMC}} = H - 2N_p \lambda \quad (5.6)$$

then a slightly different equation for  $\phi[n]$  than Eq.(5.2) is obtained:

$$S[n]\phi[n] + \lambda \sum_{\{n'\}} G[n, n'] \phi[n'] = -Q^2 \phi[n] \quad (5.7)$$

where

$$G[n, n'] = K[n, n'] - 2N_p \delta[n, n'] \quad (5.8)$$

and  $Q^2$  is related to  $E_0$  the ground-state energy of  $H$  by

$$Q^2 = 2N_p \lambda - E_0 . \quad (5.9)$$

Equation (5.7) is of precisely the same form as Eq.(2.8) so the GFMC method can be used as described in chapter 2 to compute various quantities.

As in the previous two chapters we shall restrict our attention to the ground-state energy per plaquette  $E_0/N_p$  and the mean plaquette field  $\langle \phi(p) \rangle$ .

## 5.2 Variational Calculations

### 5.2.1 Disordered wave function

The simplest variational wave function to try is

$$\phi[n] = \prod_p u(n(p)) . \quad (5.10)$$

The energy

$$E_0 = E_{el} + \lambda E_{mag} , \quad (5.11)$$

where

$$E_{el} = \frac{\sum_{\{n\}} \phi^*[n] S[n] \phi[n]}{\sum_{\{n\}} |\phi[n]|^2} , \quad (5.12)$$

$$E_{mag} = \frac{\sum_{\{nn'\}} \phi^*[n] K[n,n'] \phi[n]}{\sum_{\{n\}} |\phi[n]|^2} , \quad (5.13)$$

must be minimized with respect to the choice of the single plaquette function  $u(n(p))$ . Using Eq.(5.10), the energy  $E_0$  is found to be

$$E_0/N_P = \frac{4 \sum_{\mathbb{Z}} n^2 |u(n)|^2 + \lambda \sum_{\mathbb{Z}} u^*(n) [u(n) - \frac{1}{2}u(n+1) - \frac{1}{2}u(n-1)]}{\sum_{\mathbb{Z}} |u(n)|^2} . \quad (5.14)$$

The correct functional form of  $u(n)$  may be determined by comparing this expression for the energy to the corresponding result for the quantum pendulum.

The quantum pendulum is defined by the Hamiltonian

$$H_{qp} = - \partial^2 / \partial \theta^2 + \lambda_{qp} (1 - \cos \theta) \quad (5.15)$$

where  $\theta$  is an angular variable which lies in the domain  $(0, 2\pi)$ . The wave function  $\psi_{\text{qp}}(\theta)$  may be written as a Fourier series

$$\psi_{\text{qp}}(\theta) = \sum_{\hbar} v(n) \exp(in\theta) , \quad (5.16)$$

and then the energy is easily shown to be

$$E_{\text{qp}} = \frac{\sum_{\hbar} n^2 |v(n)|^2 + \lambda_{\text{qp}} \sum_{\hbar} v^*(n) [v(n) - \frac{1}{2}v(n+1) - \frac{1}{2}v(n-1)]}{\sum_{\hbar} |v(n)|^2} . \quad (5.17)$$

Comparing this expression to Eq.(5.14) it is clear that

$$u(n) = v(n) \quad (5.18)$$

and

$$E_0(\lambda)/N_p = 4 E_{\text{qp}}(\lambda/4) \quad (5.19)$$

It is easy to show that the variational estimates of the energy per plaquette for small- and large- $\lambda$  are

$$E_0/N_p = \lambda - \lambda^2/8 + 7\lambda^4/2048 + O(\lambda^6) \quad \text{as } \lambda \rightarrow 0 , \quad (5.20)$$

$$E_0/N_p = (2\lambda)^{1/2} - 1/4 + O(\lambda^{-1/2}) \quad \text{as } \lambda \rightarrow \infty .$$

For comparison, the corresponding limits obtained from perturbation theory are (see Eq.(4.14))

$$E_0/N_p = \lambda - \lambda^2/8 + 3\lambda^4/10240 + O(\lambda^6) \quad \text{as } \lambda \rightarrow 0 , \quad (5.21)$$

$$E_0/N_p = d(n)(2\lambda)^{1/2} - d^2(n)/4 + O(\lambda^{-1/2}) \quad \text{as } \lambda \rightarrow \infty .$$

Notice that the expressions in Eqs.(5.20) and (5.21) have the same small- $\lambda$  limit but that the perturbation theory result for large  $\lambda$  is

considerably lower than the variational result. This is as expected since the magnetic field variables  $B(p)$  are disordered in the wave function in Eq.(5.1) with  $\phi[n] = \phi_1[n]$ , so that this wave function should be a good approximation of the exact ground state for small  $\lambda$ .

The optimized function  $u(n)=v(n)$  is rather too cumbersome to use for importance sampling in a GFMC calculation. Instead we shall use a simpler choice

$$u(n) = \exp(-an^2) . \quad (5.22)$$

It is a straightforward matter to minimize the energy  $E_0/N_p$  given by Eq.(5.14) with respect to  $a$  for any given  $\lambda$ . The results are almost indistinguishable from those obtained using the optimal choice over the range of  $\lambda$  considered.

### 5.2.2 Gaussian wave function

In the gaussian approximation, valid at large  $\lambda$ , the ground state wave function may be shown to be

$$\phi_2[n] = \exp[-\frac{1}{2}a \sum_{pp'} n(p) M(p,p') n(p')] \quad (5.23)$$

where

$$a = (2/\lambda)^{1/2} . \quad (5.24)$$

If the plaquette  $p$ , having corners at the sites  $\vec{x}$ ,  $\vec{x}+\vec{e}_i$ ,  $\vec{x}+\vec{e}_i+\vec{e}_j$ ,  $\vec{x}+\vec{e}_j$ , is denoted by the two indices  $\vec{x}$  and  $k$  where  $\vec{e}_i$ ,  $\vec{e}_j$ ,  $\vec{e}_k$  constitute a

right handed set of unit vectors, then the matrix  $M(p,p')$  in Eq.(5.23) is

$$M_{kk'}(\vec{x},\vec{x}') = \frac{1}{n^3} \sum_{\vec{q}} m_{kk'}(\vec{q}) \exp\left[ \frac{2\pi i}{n} \vec{q} \cdot (\vec{x} - \vec{x}') \right], \quad (5.25)$$

where

$$m_{kk'}(\vec{q}) = \frac{f^2(\vec{q})\delta_{kk'} - f_k^*(\vec{q})f_{k'}(\vec{q})}{f(\vec{q})} \quad (5.26)$$

and  $f_k(\vec{q})$ ,  $f(\vec{q})$  are given in Eqs.(4.23d) and (4.23e). Now, if instead of having  $\alpha$  fixed by Eq.(5.24), we allow it to be a free parameter then the wave function Eq.(5.23) may be used in a variational calculation, the parameter  $\alpha$  being chosen to minimize the energy  $E_0$ .

As in the earlier chapters it is necessary to use a Monte Carlo method to compute the quantities  $E_{el}$  and  $E_{mag}$ . In this case the Metropolis Monte Carlo algorithm [29] is used to generate configurations from which  $E_{el}$  and  $E_{mag}$  are computed.

### 5.2.3 Variational results

Figure 11 shows the ground-state energy per plaquette as a function of the coupling parameter  $\lambda$ . The crosses (+) are the results of the variational calculation using the wave function  $\phi_1[n]$  given in Eqs.(5.10) and (5.22). The circles (•) are computed using the wave function  $\phi_2[n]$ , Eq.(5.23). The solid and dashed lines are small- and large- $\lambda$  perturbation theory results given by Eq.(5.21). At large  $\lambda$  the

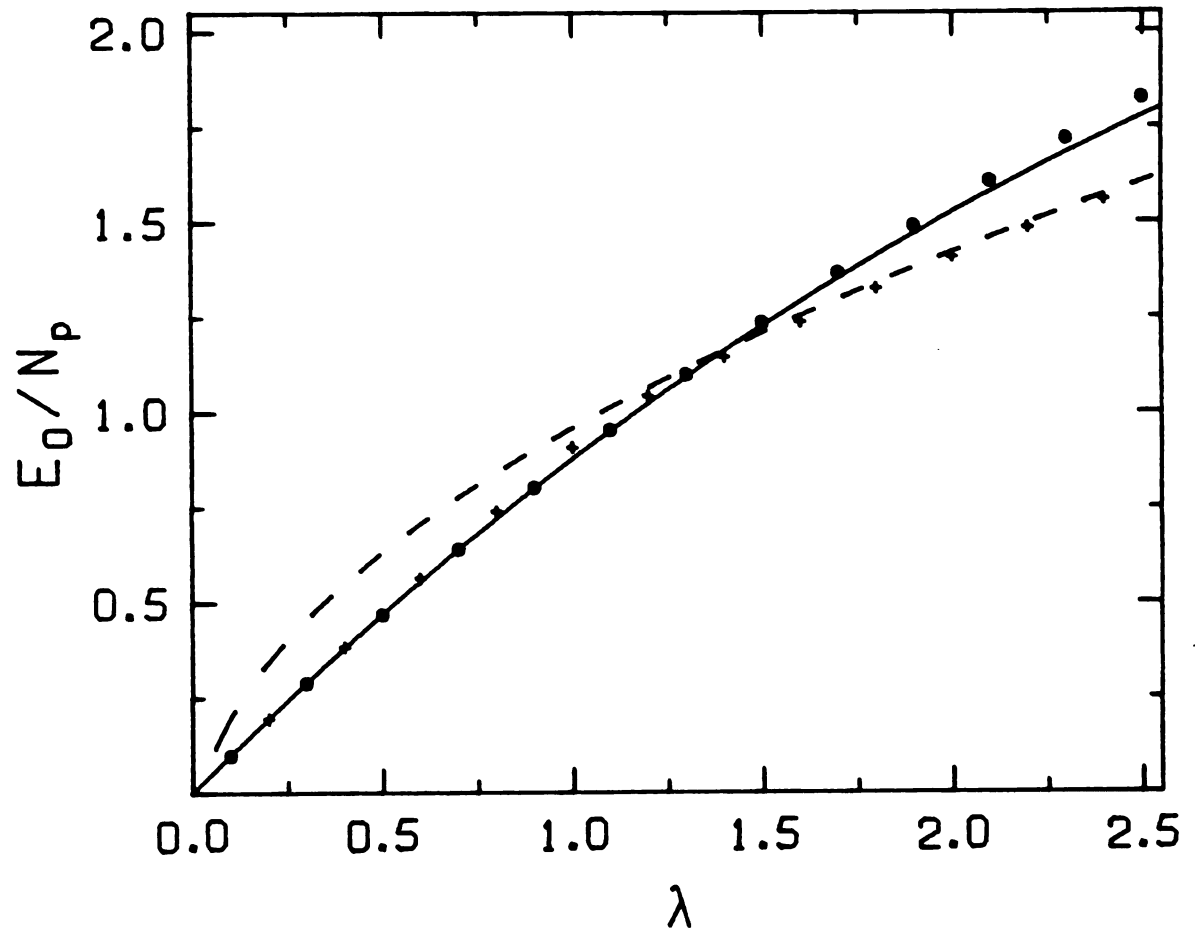


Figure 11: Variational estimates of the ground state energy per plaquette versus  $\lambda$  for the  $n$ -space formulation of the  $U(1)$  theory.

wave function  $\phi_2[n]$  is clearly the better one; this is to be expected since  $\phi_2[n]$  has built into it the explicit couplings between different plaquettes appropriate to the large  $\lambda$  limit, which are absent in  $\phi_1[n]$ . Notice, too, that for small  $\lambda$  the two variational estimates are almost identical. It is at first sight surprising that the wave function  $\phi_2[n]$ , which is constructed to be a good approximation of the ground state for large  $\lambda$ , should also be quite accurate at small  $\lambda$ . Upon further consideration, however, it is seen that if the variational parameter  $a$  is chosen to be very large then the function  $\phi_2[n]$  is sharply peaked in the region  $n(p)=0$  for all  $p$ . In terms of the magnetic field variable  $B(p)$ , the state is completely disordered, and so we see that  $\phi_2[n]$  should also be accurate at small  $\lambda$ . It is interesting to see how the variational parameter  $a$  in the wave function  $\phi_2[n]$  depends on  $\lambda$ . In Figure 12 the quantity  $a/a_h$ , where  $a_h = (2/\lambda)^{1/2}$ , is plotted as a function of  $\lambda$ . The variational parameter exhibits very striking behaviour at  $\lambda \approx 1.1$ , indicating the presence of a phase transition. Because  $\phi_2[n]$  is a good representation of the ground state at both large and small  $\lambda$ , then the fact that a phase transition is present strongly suggests that the exact ground state of the theory also must exhibit a phase transition.

The presence of a phase transition in the state described by  $\phi_2[n]$  is also evident from the variational estimate of the mean plaquette field  $\langle \phi(p) \rangle = E_{\text{mag}}/N_p$ . This is shown in Figure 13. Again the crosses (+) are variational estimates using  $\phi_1[n]$ , the circles (•) are obtained using  $\phi_2[n]$ , and the solid and dashed lines are small- and large- $\lambda$  perturbation expansions.

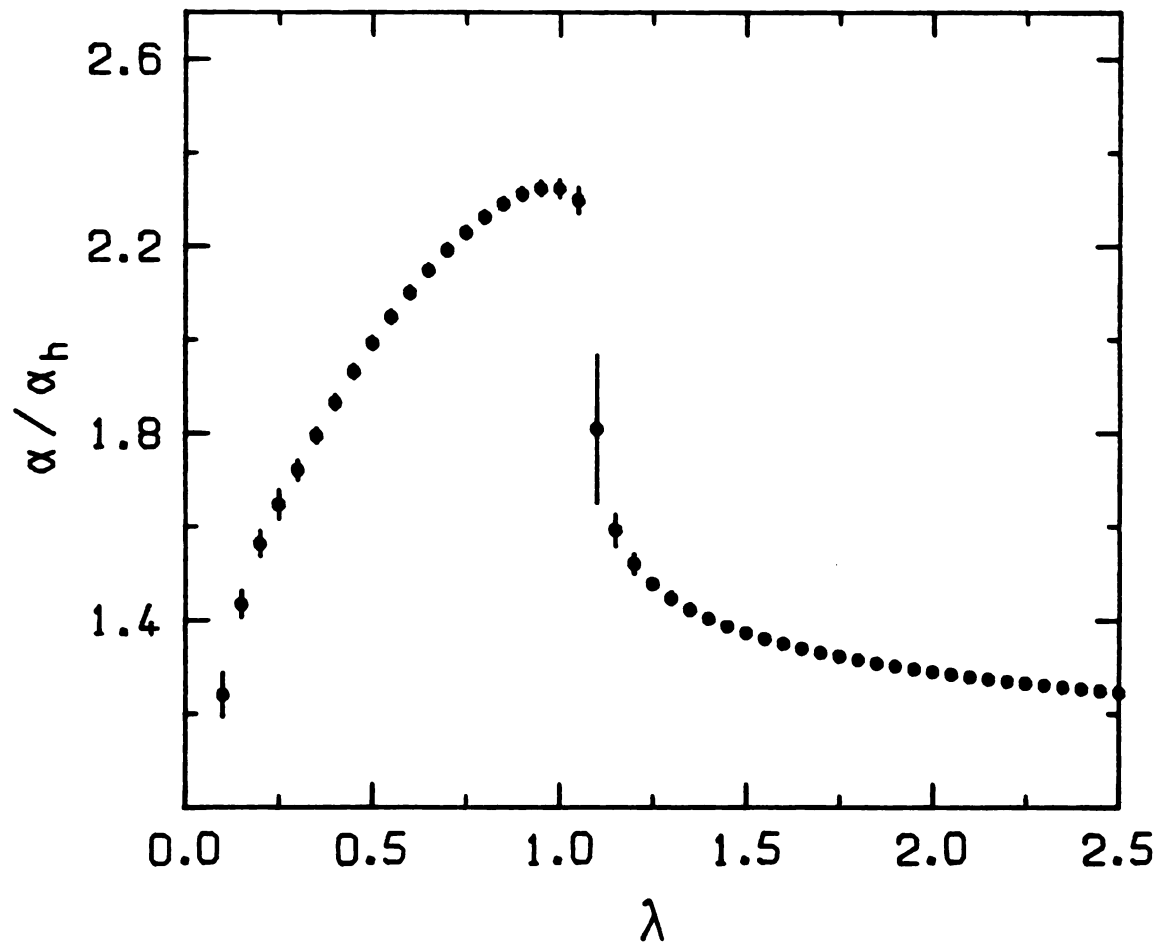


Figure 12:  $\alpha/\alpha_h$  versus  $\lambda$  for the variational wave function  $\phi_2[n]$ .

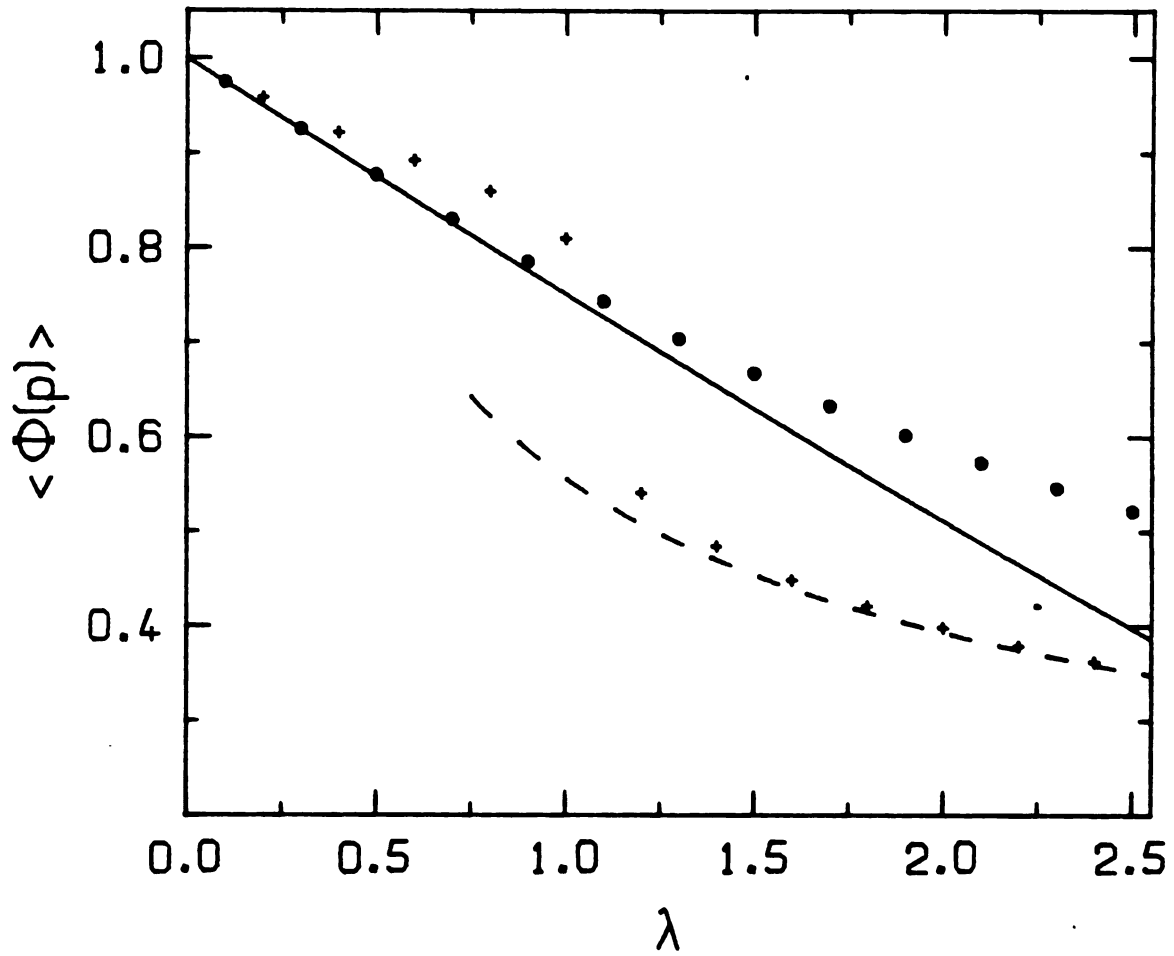


Figure 13: Variational estimates of the mean plaquette field versus  $\lambda$  for the n-space formulation of the U(1) theory.

### 5.3 GFMC calculations

The GFMC method with importance sampling may be applied precisely as described in chapter 2 to the present example. It proves most convenient to use algorithm 1 presented in Section 2.2. Due to the particular form of the function  $G[n,n']$ , which has only a small number of non-zero terms, it is possible to compute directly the normalization integral denoted by  $Z(x)$  in chapter 2 and defined in Eq.(2.20). Furthermore, again because of the special form of  $G[n,n']$ , the configurations  $n$  sampled from the kernel conditional on  $n'$  will differ from  $n'$  by at most one unit at a single plaquette, i.e.,  $n(p)=n'(p)$  for all  $p$ , or  $n(p)=n'(p)$  for all  $p \neq p_0$  and  $n(p_0)=n'(p_0) \pm 1$ . Since all the matrix elements are known, it is a simple matter to sample the kernel as a discrete probability distribution.

All the results described below were obtained on a  $3 \times 3 \times 3$  lattice and used an ensemble of approximately 100 configurations. The results are averages over 1000 GFMC iterations and required approximately 100 seconds of computation time for each value of  $Q^2$  used.

Figure 14 shows the ground state energy per plaquette  $E_0/N_p$  as a function of  $\lambda$ . The crosses (+) are GFMC estimates using the disordered wave function  $\phi_1$  for importance sampling, and the circles (●) are the results obtained using  $\phi_2$ . The solid and dashed curves are the variational bounds, obtained in the previous section, using  $\phi_1$  and  $\phi_2$  respectively. The GFMC results obtained using  $\phi_2$  for importance sampling interpolate smoothly between the known small- and large- $\lambda$

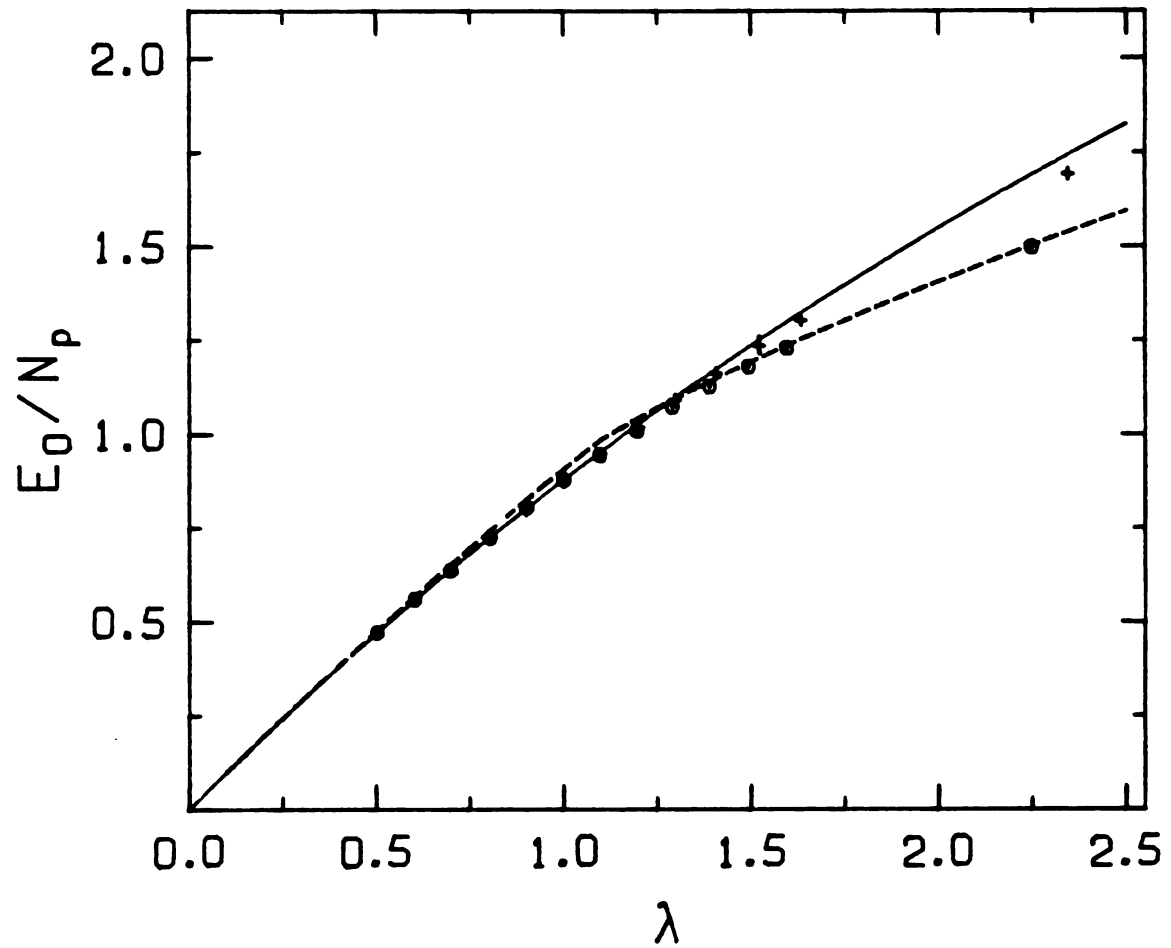


Figure 14: GFMC estimates of the ground state energy per plaquette versus  $\lambda$  for the n-space formulation of the U(1) theory.

limits. The results obtained using  $\phi_1$ , however, fail to be accurate for  $\lambda > 1.3$  and continue to lie close to the corresponding variational estimate; these GFMC estimates are not consistent with the variational bound obtained from the trial function  $\phi_2$ . It appears that the disordered state is metastable with respect to the GFMC iteration, at least for the ensemble size used here, and cannot converge to the actual ground state. This may be interpreted as evidence for a phase transition in the ground state of the theory. The trial wave function  $\phi_1$  is qualitatively different from the true ground state wave function for  $\lambda > 1.3$  where the ground state is described well by the function  $\phi_2$  with its explicit long range couplings between different plaquettes. So when this function is used for importance sampling it fails to direct the diffusion into regions of configuration space where the exact ground state wave function is greatest. Apparently, though, there is still a low energy state resembling the disordered phase which is metastable with respect to the GFMC iteration. This metastability is due to the fact that  $\phi_1$  biases the ensemble of configurations in favor of those lying in the region of configuration space dominated by this low energy state. The cross over from the disordered phase described by  $\phi_1$  to the harmonic phase described by  $\phi_2$ , the two phases being qualitatively different, is a signal for the phase transition.

This conclusion is further supported by the calculation of the mean plaquette field  $\langle\phi(p)\rangle$ . Figure 15 shows this quantity as a function of  $\lambda$  for the GFMC calculation using  $\phi_2$  for importance sampling. The crosses are GFMC estimates based on the mixed expectation value Eq.(2.62) and the circles are variational estimates based on the trial

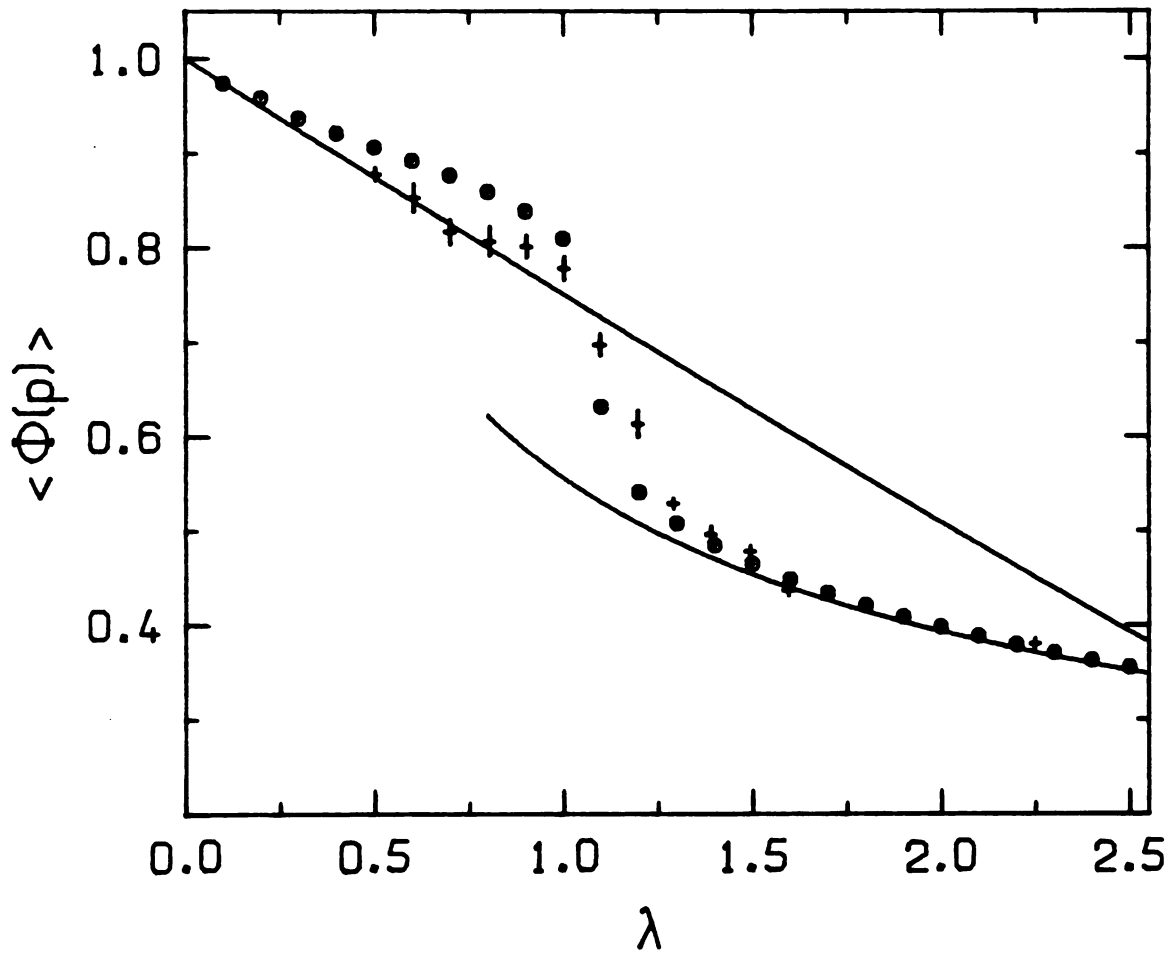


Figure 15: GFMC estimate of the mean plaquette field versus  $\lambda$  computed using the trial wave function  $\phi_2[n]$  for importance sampling.

function  $\phi_2$ . The solid curves are small- and large- $\lambda$  perturbation expansions. The variational estimate at small  $\lambda$  differs slightly from the correct small- $\lambda$  limit. The GFMC method provides a correction to the variational results which is consistent with the perturbation theory result. Notice that in the region of the phase transition,  $\lambda \approx 1.2$ , the GFMC estimates differ considerably from the variational estimates indicating that in this narrow region the function  $\phi_2$  is not a very accurate representation of the exact ground state wave function; presumably the nature of the phase transition is different in the exact ground state and the harmonic state  $\phi_2$ .

Figure 16 shows the mean plaquette field computed using  $\phi_1$  for importance sampling. The failure of this disordered wave function to accurately model the ground state of the theory and also the metastability discussed earlier are evident at large  $\lambda$ .

It is interesting to compare the results of the present chapter to those of the previous one where the calculations were performed in the space of states in which the magnetic energy is diagonal. The agreement between the two sets of results is striking. The fact that these two very different formulations of the same problem give very similar results gives us considerable confidence in the GFMC method.

Further discussion of the results of this chapter may be found in appendix B where the calculations described here are compared to similar calculations on the U(1) model in 2+1 dimensions.

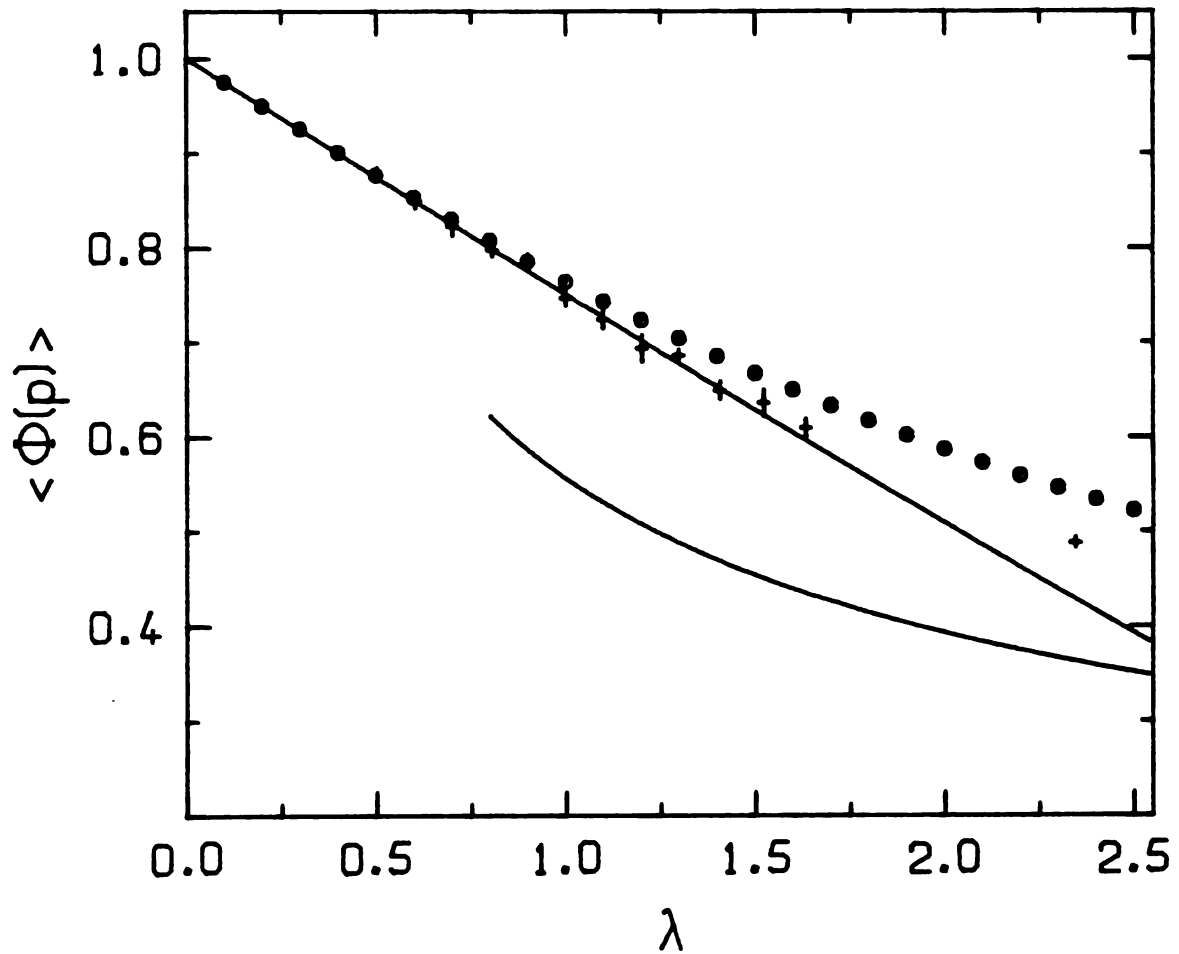


Figure 16: GPMC estimate of the mean plaquette field versus  $\lambda$  computed using the trial wave function  $\phi_1[n]$  for importance sampling.

## CHAPTER 6

### The Hamiltonian XY model

Because of the unconventional nature of the  $n$ -space formulation used in the previous chapter it would be useful to apply the same technique to study a different model. The Hamiltonian XY model admits such a treatment. The reprinted paper in this chapter describes calculations on the XY model which parallel those of the previous chapter. Again it will be found that the  $n$ -space formulation of the problem leads to a very simple implementation of the GFMC algorithm.

## Application of the Green's-function Monte Carlo method to the Hamiltonian XY model

David W. Heys and Daniel R. Stump

*Department of Physics and Astronomy, Michigan State University, East Lansing, Michigan 48824*

(Received 12 September 1983)

An application of the Green's-function Monte Carlo method to the Hamiltonian XY model is described. Importance sampling is implemented with two trial wave functions—one corresponding to a disordered state and one which incorporates the correlations derived from the spin-wave approximation of the model. Optimal trial functions are obtained from the variational principle. The Monte Carlo results are interpreted with regard to the Kosterlitz-Thouless phase transition.

### I. INTRODUCTION

The Green's-function Monte Carlo (GFMC) method is a numerical technique for studying properties of the ground state of a quantum system with many degrees of freedom. It was originally developed for application to quantum many-body problems.<sup>1,2</sup> We described an application of this method to the Kogut-Susskind Hamiltonian formulation of the compact U(1) lattice gauge theory in 2 and 3 spatial dimensions in a previous paper.<sup>3</sup> In this paper we shall describe similar calculations for the Hamiltonian formulation of the XY model.

The XY model, also called the classical planar spin model, describes classical two-dimensional spins located on a two-dimensional cubic lattice with a nearest-neighbor interaction energy proportional to  $\vec{S} \cdot \vec{S}'$ . The aim of classical statistical mechanics is to compute the partition function

$$Z = \sum_{\text{states}} \exp \left[ -\beta \sum_{\vec{r}, k} \vec{S}(\vec{r}) \cdot \vec{S}(\vec{r} + \hat{k}) \right]. \quad (1.1)$$

An important feature of this model is the Kosterlitz-Thouless phase transition,<sup>4</sup> which separates a phase in which the sum over states is dominated by spin-wave fluctuations of an ordered state, so that the spin directions are highly correlated, and a disordered phase in which the correlation between spin directions is small. This phase transition is driven by an interesting mechanism: vortices in the spin field, which are coupled in pairs at low temperatures, unbind to produce a disordered state at a critical value of  $\beta$ . Topological configurations that produce long-range disorder of the fields may also be relevant to the transition from an ordered to a disordered vacuum state in lattice gauge theories.<sup>5</sup> The XY model is important to the lattice gauge theorist as the simplest example of this mechanism. In this work we are interested in this model as a testing ground for the GFMC method.

The Metropolis Monte Carlo algorithm has been applied to the computation of the partition function (1.1).<sup>6</sup>

The Hamiltonian formulation of the XY model consists of a quantum Hamiltonian that describes a one-dimensional chain of interacting spins.<sup>7</sup> The second dimension is time. The connection between this formulation and that of Eq. (1.1) is that the partition function is a lat-

tice approximation of the Feynman path integral of the quantum system. For the sake of completeness we derive this connection in the Appendix of this paper.

It is the quantum Hamiltonian to which we apply the GFMC method.

An important, and even essential, aspect of the GFMC method is the use of importance sampling. An importance function, which should resemble the ground-state eigenfunction, is used to bias the Monte Carlo sampling in favor of regions of configuration space where the wave function is greatest. The variational principle provides a way to construct useful importance functions. In the XY-model calculations, as in the U(1)-gauge-theory calculations presented in our previous paper, we use two importance functions. The first describes a disordered state; importance sampling with this function is good at weak coupling, but becomes increasingly worse as the coupling increases. The second is derived from the spin-wave approximation of the ground state, and yields good importance sampling at both strong and weak couplings. The variational calculation that optimizes the trial function is done analytically for the disordered state, but numerically for the spin-wave state, by the Metropolis Monte Carlo method. The variational results are interesting in their own right as they give some indication of the nature of the ground state as a function of the coupling constant. Then the GFMC calculations extend the accuracy of the variational calculations.

The outline of this paper is as follows. We define the Hamiltonian XY model and explain our application of the GFMC method in Sec. II. We describe the variational calculations that yield trial functions for the GFMC importance sampling in Sec. III. We discuss the GFMC results in Sec. IV, and make some summarizing remarks in Sec. V.

### II. DEFINITION OF THE MODEL

The Hamiltonian of the XY model is<sup>7</sup>

$$H = - \sum_{i=1}^N \frac{\partial^2}{\partial \theta_i^2} - \lambda \sum_{i=1}^N [1 + \cos(\theta_i - \theta_{i+1})], \quad (2.1)$$

with the periodic boundary condition  $\theta_{N+1} = \theta_1$ . Here  $\theta_i$  is an angle variable that defines the direction of the  $i$ th

spin; thus its range is  $(-\pi, \pi)$ , and wave functions are periodic in  $\theta_i$  with period  $2\pi$ .  $H$  is defined such that the ground-state energy is negative; we let  $-Q^2$  denote this energy. In the calculations to be discussed, we formulate the eigenvalue problem in the space of variables conjugate to  $\theta_i$ ; specifically, we write the ground-state eigenfunction as

$$\psi(\vec{\theta}) = \sum_{\vec{n}} \phi(\vec{n}) \exp \left[ i \sum_{i=1}^N n_i (\theta_i - \theta_{i+1}) \right], \quad (2.2)$$

where periodicity in  $\theta_i$  requires that the variable  $n_i$  be an integer. Then the  $\vec{n}$ -space eigenfunction  $\phi(\vec{n})$  obeys the equation

$$-Q^2 \phi(\vec{n}) = S(\vec{n}) \phi(\vec{n}) - \lambda \sum_{\vec{n}'} K(\vec{n}, \vec{n}') \phi(\vec{n}'), \quad (2.3)$$

where

$$S(\vec{n}) = \sum_{i=1}^N (n_i - n_{i+1})^2 \quad (2.4)$$

and

$$K(\vec{n}, \vec{n}') = \sum_{i=1}^N [\delta(\vec{n}, \vec{n}') + \frac{1}{2} \delta(\vec{n}, \vec{n}' + \hat{\epsilon}_i) + \frac{1}{2} \delta(\vec{n}, \vec{n}' - \hat{\epsilon}_i)], \quad (2.5)$$

where  $\hat{\epsilon}_i$  is the  $N$ -component vector with  $j$ th component  $\delta_{ij}$ .

To put the eigenvalue equation into a useful form, we define

$$\chi(\vec{n}) = [Q^2 + S(\vec{n})] \phi(\vec{n}); \quad (2.6)$$

this function satisfies the equation

$$\chi(\vec{n}) = \lambda \sum_{\vec{n}'} K(\vec{n}, \vec{n}') [Q^2 + S(\vec{n}')]^{-1} \chi(\vec{n}'). \quad (2.7)$$

The GFMC method applies to an equation of this form. The method consists of simulation of a diffusion process with branching. The branching probability is proportional to  $[Q^2 + S(\vec{n}')]^{-1}$  and the diffusion is governed by  $K(\vec{n}, \vec{n}')$ . We refer to  $K(\vec{n}, \vec{n}')$  as the Green's function, although in this problem it is *not* introduced as the inverse of an operator.

The GFMC method is most powerful when combined with an importance-sampling technique.<sup>8</sup> In very large systems this technique is necessary for obtaining accurate results. We implement importance sampling by introducing a trial wave function  $\phi_T(\vec{n})$ , which should be an approximation of the actual eigenfunction. Then we define the function  $F(\vec{n})$  by

$$F(\vec{n}) = \phi_T(\vec{n}) \chi(\vec{n}). \quad (2.8)$$

This obeys the equation

$$F(\vec{n}) = \lambda \sum_{\vec{n}'} \frac{\phi_T(\vec{n})}{\phi_T(\vec{n}')} K(\vec{n}, \vec{n}') [Q^2 + S(\vec{n}')]^{-1} F(\vec{n}'), \quad (2.9)$$

which is the equation to which we apply the GFMC diffusion process. Now the diffusion is governed by the biased Green's function  $\phi_T(\vec{n}) K(\vec{n}, \vec{n}') / \phi_T(\vec{n}')$ .

The GFMC method is based on iteration of Eq. (2.9). To iterate the equation we must take  $Q^2$  to be the given quantity, and regard  $\lambda$  as the eigenvalue to be determined. Then iteration yields a sequence of functions  $F^{(0)}(\vec{n})$ ,  $F^{(1)}(\vec{n})$ , ...,  $F^{(r)}(\vec{n})$  defined by

$$F^{(r+1)}(\vec{n}) = \lambda^{(r)} \sum_{\vec{n}'} \frac{\phi_T(\vec{n})}{\phi_T(\vec{n}')} K(\vec{n}, \vec{n}') [Q^2 + S(\vec{n}')]^{-1} \times F^{(r)}(\vec{n}'), \quad (2.10)$$

where the constant  $\lambda^{(r)}$  may vary from one iteration to the next. It can be shown that  $F^{(r)}(\vec{n})$  approaches the ground-state eigenfunction with energy  $-Q^2$  as  $r \rightarrow \infty$ , independent of the initial function  $F^{(0)}(\vec{n})$ ; and that the normalization obeys the relation

$$\lim_{r \rightarrow \infty} \frac{F^{(r+1)}(\vec{n})}{F^{(r)}(\vec{n})} = \frac{\lambda^{(r)}}{\lambda}, \quad (2.11)$$

where  $\lambda$  is the coupling constant for which the ground-state energy is  $-Q^2$ . Constant normalization of the function  $F^{(r)}(\vec{n})$  (after convergence to the limit) requires  $\lambda^{(r)} = \lambda$ .

The GFMC algorithm for solving Eq. (2.9) is a simulation of a diffusion process with branching. At the  $r$ th step of the process we have an ensemble  $\mathcal{E}_r$  of field configurations

$$\mathcal{E}_r = \{ \vec{n}'_\sigma; \sigma = 1, 2, 3, \dots, N_r \};$$

let  $P_r(\vec{n})$  denote the probability distribution of  $\mathcal{E}_r$ . The next ensemble  $\mathcal{E}_{r+1}$  is obtained from  $\mathcal{E}_r$  in two steps:

(i) Each  $\vec{n}'_\sigma$  branches into  $k_\sigma$  new points, where  $k_\sigma$  is an integer picked by a random process such that the expected value of  $k_\sigma$  is

$$\lambda_0^{(r)} [Q^2 + S(\vec{n}'_\sigma)]^{-1} \sum_{\vec{n}} \frac{\phi_T(\vec{n}) K(\vec{n}, \vec{n}'_\sigma)}{\phi_T(\vec{n}'_\sigma)}. \quad (2.12)$$

The possibility  $k_\sigma = 0$  is allowed. Here  $\lambda_0^{(r)}$ , which may be thought of as a guess of the value of  $\lambda$ , can vary from one iteration to the next.

(ii) Then each of the  $k_\sigma$  points is moved from  $\vec{n}'_\sigma$  to a new configuration  $\vec{n}$  chosen from the probability distribution

$$\frac{\phi_T(\vec{n}) K(\vec{n}, \vec{n}'_\sigma) / \phi_T(\vec{n}'_\sigma)}{\sum_{\vec{n}} \phi_T(\vec{n}) K(\vec{n}, \vec{n}'_\sigma) / \phi_T(\vec{n}'_\sigma)}. \quad (2.13)$$

Note that the form of  $K(\vec{n}, \vec{n}')$  implies that  $\vec{n}$  differs from  $\vec{n}'_\sigma$  by at most one unit.

The ensemble  $\mathcal{E}_{r+1}$  is the result of processing all of the elements of  $\mathcal{E}_r$  in this way. The probability distribution of  $\mathcal{E}_{r+1}$  is

$$P_{r+1}(\bar{n}) = \lambda_0^{(r)} \frac{N_r}{N_{r+1}} \sum_{\bar{n}'} \frac{\phi_T(\bar{n})}{\phi_T(\bar{n}')} K(\bar{n}, \bar{n}') [Q^2 + S(\bar{n}')]^{-1} \times P_r(\bar{n}'). \quad (2.14)$$

That is, the evolution of  $P_r(\bar{n})$  is the same as Eq. (2.10) with

$$\lambda_0^{(r)} \frac{N_r}{N_{r+1}} = \lambda^{(r)}. \quad (2.15)$$

Therefore,  $P_r(\bar{n})$  approaches the eigenfunction  $F(\bar{n})$  as  $r \rightarrow \infty$ . Also, since  $P_r(\bar{n})$  and  $P_{r+1}(\bar{n})$  have the same normalization, specifically  $\sum_{\bar{n}} P_r(\bar{n}) = 1$  for all  $r$ , after a sufficient number of steps in the diffusion we shall have

$$\lambda_0^{(r)} \frac{N_r}{N_{r+1}} = \lambda. \quad (2.16)$$

This provides an estimate of the eigenvalue  $\lambda$  after each iteration. Note that  $\lambda_0^{(r)}$  controls the size of the ensemble; in practice we readjust the value of  $\lambda_0^{(r)}$  every few iterations so as to keep the ensemble size approximately constant. Thus the simulation yields an estimate of  $\lambda$  and a sequence of ensembles of  $\bar{n}$ -space configurations with probability distribution  $F(\bar{n})$ .

Use of the trial function  $\phi_T$  is called importance sampling. The diffusion in the space of  $\bar{n}$  configurations is controlled by the biased Green's function  $\phi_T(\bar{n})K(\bar{n}, \bar{n}')/\phi_T(\bar{n}')$ . The factor  $\phi_T(\bar{n})/\phi_T(\bar{n}')$  biases the diffusion in favor of moves  $\bar{n}' \rightarrow \bar{n}$  in directions that increase  $\phi_T(\bar{n})$ . If  $\phi_T$  is an approximation of the ground-state eigenfunction, then this bias accelerates the convergence to the ground state, and reduces fluctuations of the estimates of the eigenvalue  $\lambda$ .

The importance-sampling technique also provides a way to estimate expectation values of operators in the ground state, provided  $\phi_T$  is a good approximation of the eigenfunction  $\phi$ . If  $\phi_T$  differs from  $\phi$  by an amount of order  $\epsilon$ , then to order  $\epsilon^2$  we have

$$\frac{\langle \phi | A | \phi \rangle}{\langle \phi | \phi \rangle} = 2 \frac{\langle \phi | A | \phi_T \rangle}{\langle \phi | \phi_T \rangle} - \frac{\langle \phi_T | A | \phi_T \rangle}{\langle \phi_T | \phi_T \rangle}. \quad (2.17)$$

The left-hand side is the desired expectation value of an operator  $A$ . The second term on the right-hand side is simply the expectation value in the trial state. The first term on the right-hand side, which is called the mixed expectation value, can be estimated as

$$\frac{\langle \phi | A | \phi_T \rangle}{\langle \phi | \phi_T \rangle} = \frac{\langle A(\bar{n}) [Q^2 + S(\bar{n})]^{-1} \rangle_{\text{em}}}{\langle [Q^2 + S(\bar{n})]^{-1} \rangle_{\text{em}}}, \quad (2.18)$$

where  $\langle \rangle_{\text{em}}$  denotes the average of the enclosed quantity over the ensembles generated by the GFMC diffusion. Since Eq. (2.17) is only valid to order  $\epsilon^2$ , this estimate is not trustworthy if  $\langle A \rangle_T$  and  $\langle A \rangle$  are very different.

The trial function  $\phi_T$  is ordinarily obtained from a variational calculation. Thus the GFMC method can be

thought of as an extension of the variational principle, that improves the accuracy of numerical estimates. The GFMC determination of the eigenvalue  $\lambda$  is in principle exact, even if  $\phi_T$  is not a good approximation of  $\phi$ ; but that is only for a large enough ensemble, and in practice the calculations are not feasible if  $\phi_T$  differs from  $\phi$  too much. Expectation values computed from the mixed expectation value are valid to order  $(\phi_T - \phi)^2$ , so Eq. (2.17) gives the order- $(\phi_T - \phi)$  correction to the ordinary variational estimate. In addition, the GFMC approach can indicate whether a variational wave function is an accurate representation of the ground state by testing whether it works well as an importance-sampling function. It can be proven, for example, that fluctuations in the measurement of  $\lambda$  by Eq. (2.16) approach zero as the trial function approaches the exact eigenfunction.

In the next section we describe the two trial functions to be used for importance sampling in the GFMC calculations, and variational calculations which optimize the choice of these functions.

### III. VARIATIONAL CALCULATIONS

We shall consider two trial wave functions to approximate the ground state of the  $XY$  model. The first is defined as a function in the space of  $\theta$  configurations as

$$\psi_1(\bar{\theta}) = \prod_{i=1}^N u(\theta_i - \theta_{i+1}); \quad (3.1)$$

the energy  $\langle \psi_1 | H | \psi_1 \rangle$  is to be minimized with respect to the choice of the function  $u(\omega)$ . It can be shown that the minimum energy is obtained if  $u(\omega)$  is the ground-state eigenfunction of the Hamiltonian of a quantum pendulum,

$$h = -2 \frac{\partial^2}{\partial \omega^2} + \lambda(1 - \cos \omega), \quad (3.2)$$

where  $-\pi \leq \omega \leq \pi$ . The resulting variational bound on the energy per spin is

$$-\frac{Q^2}{N} \leq -2\lambda + e_0, \quad (3.3)$$

where  $e_0$  is the smallest eigenvalue of  $h$ . We shall present our results in terms of another energy  $E_0$ , rather than  $-Q^2$ , defined by

$$E_0 = 2\lambda N - Q^2; \quad (3.4)$$

note that  $E_0$  is the ground-state energy of

$$-\sum_{i=1}^N \frac{\partial^2}{\partial \theta_i^2} + \lambda \sum_{i=1}^N [1 - \cos(\theta_i - \theta_{i+1})]. \quad (3.5)$$

The variational estimate of  $E_0$  based on  $\psi_1$  is

$$\frac{E_0}{N} = e_0. \quad (3.6)$$

The small- and large- $\lambda$  limits of  $e_0$  are

$$e_0 \simeq \lambda - \frac{\lambda^2}{4} + \frac{7\lambda^4}{256} + O(\lambda^6) \text{ as } \lambda \rightarrow 0, \quad (3.7)$$

$$e_0 \simeq \lambda^{1/2} - \frac{1}{8} + O(\lambda^{-1/2}) \text{ as } \lambda \rightarrow \infty.$$

For comparison these limits for  $E_0/N$  are easily shown to be

$$E_0/N \simeq \lambda - \frac{\lambda^2}{4} + \frac{5\lambda^4}{768} + O(\lambda^6) \text{ as } \lambda \rightarrow 0, \quad (3.8)$$

$$E_0/N \simeq \lambda^{1/2} d(N) - \frac{1}{8} d^2(N) + O(\lambda^{-1/2}) \text{ as } \lambda \rightarrow \infty,$$

where

$$d(N) = \frac{\sqrt{2}}{N} \left[ 1 - \cos \frac{\pi}{N} \right]^{-1} \sin \frac{\pi}{N} \quad (3.9)$$

for a chain of  $N$  spins with periodic boundary conditions; the value of  $d(N)$  is approximately 0.90 for  $N$  greater than 10. Thus  $e_0$  and  $E_0/N$  have the same small- $\lambda$  limit, but  $e_0$  is greater than  $E_0/N$  for large  $\lambda$ .

The trial function  $\psi_1$  describes a disordered state of the spins. Specifically, the correlation between spins separated by a distance  $k$  is, for this wave function,

$$\langle \psi_1 | \cos(\theta_{i+k} - \theta_i) | \psi_1 \rangle = \left[ \int_{-\pi}^{\pi} d\omega u^2(\omega) \cos \omega \right]^k \quad (3.10)$$

which decreases exponentially with  $k$ . We expect  $\psi_1$  to be a good approximation of the eigenfunction for small  $\lambda$ , where the ground state is disordered in this way. But it can already be seen by comparing the limiting forms (3.7) and (3.8) that  $\psi_1$  becomes less accurate as  $\lambda$  increases.

The second trial wave function is designed to be accurate in the large- $\lambda$  limit; it turns out to be accurate at small  $\lambda$  as well. It is defined in the conjugate space of  $\vec{n}$  configurations as

$$\phi_2(\vec{n}) = \exp \left[ -\frac{1}{2} \alpha \sum_{JJ'} n_J \Delta_{JJ'} n_{J'} \right], \quad (3.11)$$

where  $\alpha$  is the variational parameter, and

$$\Delta_{JJ'} = \left[ \frac{2}{\lambda} \right]^{1/2} \frac{2}{N} \sum_{q=1}^N \exp \left[ \frac{2\pi i}{N} q(J-J') \right] \sin \frac{\pi q}{N}. \quad (3.12)$$

The motivation for this form is that with  $\alpha=1$  it duplicates the ground state of the spin-wave approximation of the model, which is known to be the eigenstate in the large- $\lambda$  limit. The spin-wave approximation consists of replacing  $1 - \cos(\Delta\theta)$  by  $\frac{1}{2}(\Delta\theta)^2$  in the Hamiltonian, and extending the range of  $\theta_i$  from  $(-\pi, \pi)$  to  $(-\infty, \infty)$ . The resulting model is solvable since its Hamiltonian is quadratic; its ground state is  $\phi_2$  with  $\alpha=1$ , but where the variables  $n_i$  take a continuum of values. We emphasize that the trial function  $\phi_2$  is not a naive harmonic approximation, because the  $n_i$  are restricted to integer values; this is necessary to preserve the periodicity of the wave function in  $\vec{\theta}$  space.

We evaluate the expectation value  $\langle \phi_2 | H | \phi_2 \rangle$  numerically, using the Metropolis Monte Carlo algorithm to generate a set of configurations  $\{\vec{n}_1, \vec{n}_2, \vec{n}_3, \dots, \vec{n}_k\}$  with

probability distribution  $\phi_2^2$ , and estimating the expectation value by the average of the operator over these configurations. This is done for many values of the variational parameter  $\alpha$ . The resulting data on the energy as a function of  $\alpha$  is then fit to a polynomial of sufficiently large degree to give a good fit. And finally we minimize the polynomial with respect to  $\alpha$ .

Figure 1 is a graph of the value of  $\alpha$  that minimizes the energy, as a function of the coupling constant  $\lambda$ . The error bars are calculated in a straightforward way from the standard errors in the polynomial coefficients found by the least-squares fit mentioned in the previous paragraph. The calculation is for a chain of 50 spins, with periodic boundary condition.

As anticipated,  $\alpha$  approaches 1, the spin-wave value, at large  $\lambda$ . As  $\lambda$  decreases,  $\alpha$  increases and so  $\phi_2$  becomes more sharply peaked at  $\vec{n}=0$ , which implies a more disordered state in  $\vec{\theta}$  space. There is a fairly dramatic variation of  $\alpha$  for  $\lambda$  near 1. A similar variational calculation for the U(1) lattice gauge theory in three dimensions, discussed in Ref. 3, has a discontinuity in the value of  $\alpha$  as a function of  $\lambda$ , indicating a phase transition in that model.

Figure 2 shows the variational bounds on  $E_0/N$  as a function of  $\lambda$ , for both trial functions  $\psi_1$  and  $\phi_2$ , along with the large- and small- $\lambda$  limits given in Eq. (3.8). Clearly the trial function  $\phi_2$  derived from the spin-wave approximation is more accurate than the disordered function  $\psi_1$  for  $\lambda \geq 1$ ; its energy approaches the correct large- $\lambda$  limit, as it must by construction. The spin-wave function is also a good approximation at small  $\lambda$ , where its energy is only slightly larger than that of the disordered state. Both functions approach the correct small- $\lambda$  limit.

The two trial functions  $\psi_1$  and  $\phi_2$  are analogs of the trial functions that we used in U(1)-lattice-gauge-theory calculations.<sup>3</sup> The analog of  $\psi_1$  is a product of single-plaquette functions, and the analog of  $\phi_2$  derives from the free-field harmonic approximation of the U(1) gauge theory.

In the next section we describe the results of GFMC calculations that use these two trial functions for importance sampling.

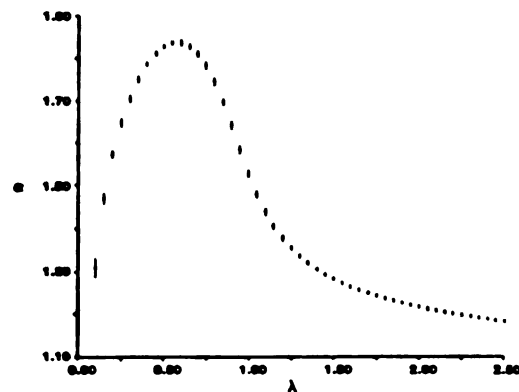


FIG. 1. Variational parameter  $\alpha$  vs coupling constant  $\lambda$ .

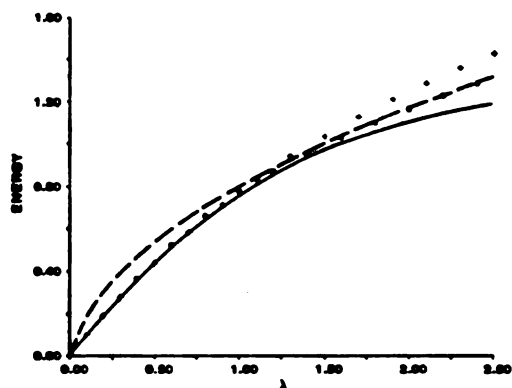


FIG. 2. Variational estimates of the ground-state energy per spin vs coupling constant  $\lambda$ . The solid and dashed curves are perturbation expansions for small and large  $\lambda$ , respectively. The crosses (+) and circles (o) are variational estimates with trial wave functions  $\psi_1$  and  $\psi_2$ , respectively. Error bars are much smaller than the size of the points.

#### IV. MONTE CARLO RESULTS

Figure 3 is a graph of  $E_0/N$ , the ground-state energy per spin of the Hamiltonian (3.5), as a function of the coupling parameter  $\lambda$ , from Green's-function Monte Carlo calculations with importance functions  $\psi_1$  and  $\psi_2$ . The curves are the variational bounds obtained in Sec. III, and the points are the GFMC results. The GFMC calculations used an ensemble of approximately 100 configurations; this ensemble size changes with each iteration. The results in Fig. 3 are averages over 800 iterations. Each GFMC point required approximately 90 sec of computation time on a CDC Cyber 750 computer at Michigan State University.

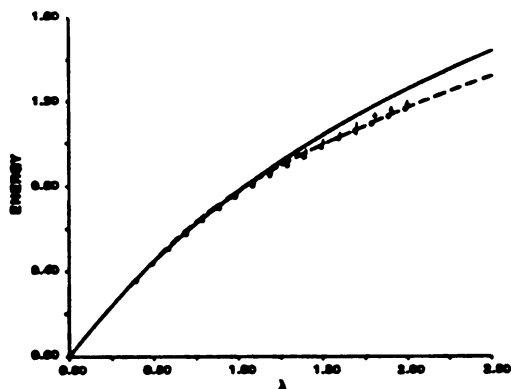


FIG. 3. Monte Carlo estimates of the ground-state energy per spin vs coupling constant  $\lambda$ . The solid and dashed curves are variational estimates with trial wave functions  $\psi_1$  and  $\psi_2$ , respectively. The crosses (+) and circles (o) are Monte Carlo results with importance functions  $\psi_1$  and  $\psi_2$ , respectively.

The results shown are for a chain of 50 spins with periodic boundary condition. As  $\lambda$  varies from 0 to  $\infty$  the energy interpolates between the small- $\lambda$  asymptotic behavior described well by the disordered wave function  $\psi_1$  and the harmonic spin-wave behavior described by  $\psi_2$ . The crossover from one form to the other occurs for  $\lambda \sim 1$ .

The two Monte Carlo estimates are almost equal, and are consistent with the variational bounds. However, there is a tendency for the GFMC estimate obtained with the disordered function  $\psi_1$  to lie higher in energy than that obtained with  $\psi_2$  in the region  $\lambda \geq 1$ . Furthermore, the former estimates have greater uncertainty, as indicated by the error bars, than the latter, for which the error bars are much smaller than the size of the point plotted. These error bars come only from the fluctuation associated with stochastic sampling. These two tendencies are not unexpected; they reflect the fact that  $\psi_1$  is not a good approximation of the ground state for  $\lambda \geq 1$ , where the spins are more correlated than in  $\psi_1$ .

It is interesting to compare these results to the analogous calculations for the U(1) lattice gauge theory in 3 and 2 spatial dimensions. In the three-dimensional model, the Monte Carlo results obtained using the disordered wave function for importance sampling are definitely different than those obtained with the harmonic wave function, in the region of large  $\lambda$ ; in fact the former results are inconsistent with the variational bound provided by the harmonic wave function. We interpret this as evidence of the phase transition of the three-dimensional U(1) gauge theory: the disordered state is metastable with respect to the GFMC diffusion process. In contrast, the Monte Carlo results are the same for the two importance functions in the two-dimensional model; this is consistent with the fact that there is no phase transition in the two-dimensional model.

Our XY model results show evidence of the Kosterlitz-Thouless phase transition, in that the disordered function does not provide effective importance sampling for  $\lambda \geq 1$ . The disordered state is not metastable, as it is in the three-dimensional U(1) gauge theory, but the energy estimate obtained with the disordered importance function is slightly larger, and has larger fluctuations, than that obtained with the spin-wave function in this region. The difference between the XY model and the U(1) gauge model is explained by the fact that the Kosterlitz-Thouless phase transition is an infinite-order transition, while the gauge-model transition is a second-order transition.

The Kosterlitz-Thouless renormalization-group calculation predicts that the phase transition of the XY model occurs at  $\lambda = 1.02$ ; this point is discussed briefly in the Appendix. That value is perfectly consistent with the interpretation of our results given above. For  $\lambda \leq 1.02$  the ground state is disordered so  $\psi_1$  acts as an effective importance function; but for  $\lambda > 1.02$  the spin directions are more correlated than in  $\psi_1$ , so this function gives weaker importance sampling.

Figures 4(a) and 4(b) show Monte Carlo estimates of the correlation function of neighboring spins

$$\mathcal{Y} = \langle 1 - \cos(\theta_i - \theta_{i+1}) \rangle. \quad (4.1)$$

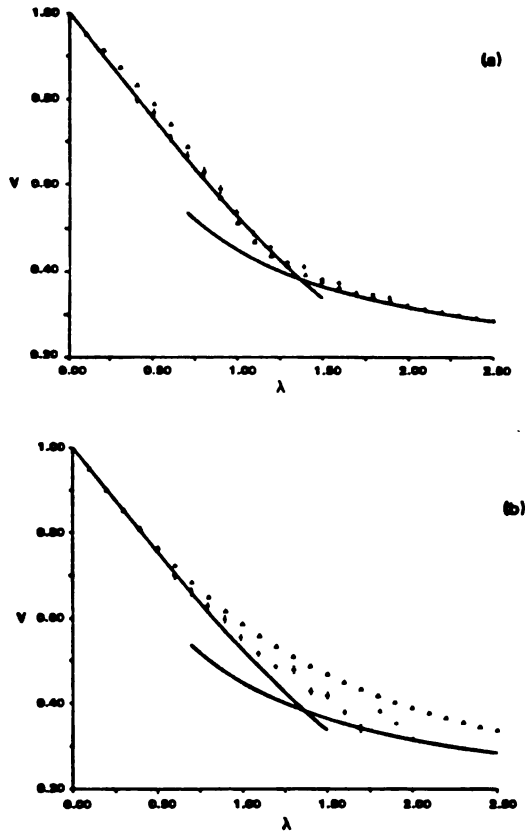


FIG. 4. The expectation value of  $1 - \cos(\theta_i - \theta_{i+1})$  vs coupling constant  $\lambda$ . The curves are perturbation expansions. The triangles ( $\Delta$ ) are simple expectation values in the variational wave functions, and the crosses (+) are Monte Carlo estimates of the mixed expectation value, Eq. (2.17). The trial functions are  $\phi_2$  for (a) and  $\phi_1$  for (b).

Note that  $\mathcal{Y}$  is related to the energy  $E_0$  by

$$\mathcal{Y} = \frac{1}{N} \frac{dE_0}{d\lambda}. \quad (4.2)$$

The Monte Carlo points in Figs. 4(a) and 4(b) are obtained from the mixed expectation value, i.e., Eq. (2.17), for the importance functions  $\phi_2$  and  $\phi_1$ , respectively. The curves on these graphs are from small- and large- $\lambda$  perturbation theory. Here there are marked differences between the Monte Carlo results. In particular, the GFMC estimates of  $\mathcal{Y}$  obtained with the disordered importance function have large uncertainty and differ significantly from the ordinary expectation value in  $\phi_1$ , in the region  $\lambda \geq 1$ . Again, this is precisely what we expect from calculations with an importance function that does not approximate the ground-state eigenfunction. It is interesting to note that the GFMC and variational estimates of  $\mathcal{Y}$  obtained with the spin-wave function  $\phi_2$  are almost equal for all  $\lambda$ , suggesting that  $\phi_2$  is quite a good representation of the eigenfunction.

## V. SUMMARY

In this paper we describe results of an application of the Green's-function Monte Carlo method to the Hamiltonian XY model. These calculations are parallel to calculations described in an earlier paper for the compact U(1) lattice gauge theory in 2 and 3 spatial dimensions.

In these models an important issue is the existence and nature of a phase transition separating a disordered phase and a phase in which the model is accurately described by its harmonic approximation. We find that the GFMC results give a good indication of such a phase transition. In particular, we can judge whether a wave function resembles the ground-state eigenfunction by its performance in reducing fluctuations when used in the importance-sampling procedure. In our calculations the disordered trial function performs poorly for values of the coupling constant for which the harmonic wave function approximates the ground state. For the three-dimensional compact U(1) gauge theory the inadequacy of the disordered trial function is obvious: it yields energy estimates that are greater than the variational bound provided by the harmonic wave function, at least for the ensemble size that we use in the GFMC diffusion. For the XY model this inadequacy is more subtle, but can be seen in the large fluctuations of energy estimates.

The GFMC method offers a second way to judge whether a trial function represents a good approximation of the ground state, based on the mixed expectation value, i.e., Eq. (2.17). If  $\phi_T$  approximates  $\phi$  then the mixed expectation value of an operator  $A$  is nearly equal to the expectation value of  $A$  in  $\phi_T$ ; if these two quantities are quite different, then  $\phi_T$  cannot be a good approximation of  $\phi$ . Thus, for example, the increasing difference between the two estimates of  $\mathcal{Y}$  as  $\lambda$  increases beyond 1 in Fig. 4(b), is another indication that the disordered wave function does not resemble the eigenfunction for  $\lambda \geq 1$ .

The Monte Carlo results imply by these considerations that the ground state of the XY model changes from a disordered state to a state better described by a harmonic wave function for  $\lambda \approx 1$ . This value is in agreement with the Kosterlitz-Thouless renormalization-group analysis, which predicts a phase transition at  $\lambda = 1.02$ .

## APPENDIX

The connection between the Hamiltonian (2.1) and the partition function (1.1) of the classical XY model derives from the Feynman path integral of the quantum problem. The path integral for the Hamiltonian  $H$  is, with imaginary time,

$$Z = \int d\theta_i(t) e^{-A}, \quad (A1)$$

where  $d\theta_i(t)$  denotes integration over paths in the space of  $\vec{\theta}$  configurations, and  $A$  is the imaginary-time action

$$A = \int dt \sum_i \left[ \frac{1}{4} \left( \frac{d\theta_i}{dt} \right)^2 + \lambda [1 - \cos(\theta_{i+1} - \theta_i)] \right]. \quad (A2)$$

We now consider a discrete approximation of the time coordinate; let  $t$  take the values

$$t_j = aj, \quad j=0,1,2,3,\dots \quad (\text{A3})$$

with interval  $a$  to be specified later. If  $a$  is small compared to the time over which  $\theta_i(t)$  varies then we may replace the integral over  $t$  by a sum over  $j$ , and the time derivative by a difference; i.e.,

$$\int dt \rightarrow a \sum_j, \quad (\text{A4})$$

$$\frac{d\theta_i}{dt} \rightarrow \frac{1}{a} [\theta(i,j+1) - \theta(i,j)],$$

where  $\theta(i,j) = \theta_i(t_j)$ . Again for small  $a$ , we may assume that  $\theta(i,j+1) - \theta(i,j)$  is small and approximate

$$[\theta(i,j+1) - \theta(i,j)]^2 \simeq 2\{1 - \cos[\theta(i,j+1) - \theta(i,j)]\}. \quad (\text{A5})$$

With these substitutions the action becomes

$$A = \sum_{i,j} \left[ \frac{1}{2a} \{1 - \cos[\theta(i,j+1) - \theta(i,j)]\} + a\lambda \{1 - \cos[\theta(i+1,j) - \theta(i,j)]\} \right]. \quad (\text{A6})$$

At this point we let the interval  $a$  be  $(1/2\lambda)^{1/2}$ ; then

$$A = \left[ \frac{\lambda}{2} \right]^{1/2} \sum_{i,j} \{2 - \cos[\theta(i,j+1) - \theta(i,j)] - \cos[\theta(i+1,j) - \theta(i,j)]\}. \quad (\text{A7})$$

The lattice "path integral" over  $\theta(i,j)$  is precisely the partition function (1.1) for classical statistical mechanics of the XY model, where the direction of the spin at  $(i,j)$  is defined by the angle  $\theta(i,j)$ , and the inverse temperature is

$$\beta = \left[ \frac{\lambda}{2} \right]^{1/2}. \quad (\text{A8})$$

This derivation of the connection between the one-dimensional quantum problem and the two-dimensional classical statistical mechanics problem is the inverse of the usual derivation,<sup>7</sup> which starts from the partition function and derives the Hamiltonian  $H$  as the transfer matrix in the limit that one of the dimensions becomes continuous.

The Kosterlitz-Thouless phase transition occurs at inverse temperature  $\beta = 2.24/\pi$ , according to a renormalization-group calculation.<sup>4</sup> Therefore, by Eq. (A8) the critical value of  $\lambda$  is 1.02. This value is perfectly consistent with the results of the GFMC calculations described in Sec. IV.

#### ACKNOWLEDGMENTS

This work was supported by the National Science Foundation under Grant No. PHY81-01520, and by a grant from Control Data Corporation.

<sup>1</sup>M. H. Kalos, Phys. Rev. **128**, 1791 (1962); Phys. Rev. A **2**, 250 (1970); M. H. Kalos, D. Levesque, and L. Verlet, *ibid.* **2**, 2178 (1974).

<sup>2</sup>D. M. Ceperley and M. H. Kalos, in *Monte Carlo Methods in Statistical Physics*, Topics in Current Physics, Vol. 7, edited by K. Binder (Springer, New York, 1979). This reference is a comprehensive review of the Green's-function Monte Carlo method.

<sup>3</sup>D. W. Heys and D. R. Stump, Phys. Rev. D **28**, 2067 (1983).

<sup>4</sup>J. M. Kosterlitz and D. J. Thouless, J. Phys. C **6**, 1181 (1973);

J. M. Kosterlitz, *ibid.* **7**, 1046 (1974).

<sup>5</sup>A. M. Polyakov, Phys. Lett. **59B**, 79 (1977); Nucl. Phys. **B120**, 429 (1977); T. Banks, R. Myerson, and J. Kogut, *ibid.* **B129**, 493 (1977); D. R. Stump, Phys. Rev. D **23**, 972 (1981).

<sup>6</sup>J. Tobochnik and G. V. Chester, Phys. Rev. B **20**, 3761 (1979).

<sup>7</sup>E. Fradkin and L. Susskind, Phys. Rev. D **17**, 2637 (1978); J. Kogut, Rev. Mod. Phys. **51**, 659 (1979).

<sup>8</sup>The importance-sampling procedure that we use is similar to that described in the paper by Kalos, Levesque, and Verlet (Ref. 1). See also Ref. 2.

## CHAPTER 7

### Summary and conclusions

The Green's function Monte Carlo (GFMC) method has been adapted for application to Hamiltonian lattice gauge theories, and has been applied to the SU(2) and U(1) theories. The results obtained so far are restricted, by the availability of computer time, to estimates of simple quantities, specifically the ground state energy per plaquette  $E_0/N_p$  and the mean plaquette field  $\langle\phi(p)\rangle$ , on a 3 x 3 x 3 lattice. This lattice is small compared to those used in path-integral Monte Carlo calculations, but the average quantities calculated here are rather insensitive to lattice size. This is indicated by perturbation theory calculations: for small  $\lambda$  the results are independent of lattice size, and for large  $\lambda$  the results are only weakly size dependent.

The GFMC calculations use a variational wave function as an importance function to bias the Monte Carlo sampling procedure in favor of regions of configuration space in which the wave function is large. Thus, if the variational wave function is a good approximation of the

exact ground state wave function, the fluctuations of GFMC estimates are greatly reduced and the rate of convergence of the estimates to their asymptotic values is increased. By comparing the GFMC results to the variational results one can obtain some indication as to how accurately the variational wave function models the exact vacuum state. Some care is necessary, however, when interpreting the results in this way. If there is considerable disagreement between the variational and GFMC results then it is clear that the variational wave function is not a good representation of the ground state. The converse is not true. If the GFMC results lie close to the variational results one cannot conclude that the variational wave function is a good representation of the ground state. Calculation of other quantities might reveal a considerable disagreement.

A good example of this kind of behaviour is provided by the SU(2) results obtained using a disordered variational wave function discussed in chapter 3. There it was found that the GFMC estimates were close to the variational results even at large  $\lambda$  where the variational wave function is known to be inaccurate from variational estimates of the string tension [9] and mass gap [10] of the theory. To conclude from the quite close agreement between the GFMC and variational results on the energy per plaquette and the mean plaquette field that the variational wave function is a good approximation of the exact ground state wave function would clearly be quite wrong.

The results on the  $U(1)$  model in the  $n$ -space formulation using a disordered trial wave function showed similar behaviour. In that case, though, the approximate agreement between the variational and GFMC results was due to metastability of the disordered state with respect to the GFMC iteration. Presumably, because of this metastability, any quantity computed by the GFMC method using the disordered importance function would give results close to the variational results. If the large  $\lambda$  limit were not known, it would be very difficult to discover such metastability. Perhaps by increasing the ensemble size to a sufficient level the metastability could be removed, but in view of the computational effort required this is probably not a good way to proceed. A better approach would be to use a different importance function to check the results, but this, of course, is not possible when one only has a single variational wave function available as is the case for the  $SU(2)$  theory.

In conclusion, the GFMC method is a potentially powerful tool for use in lattice gauge theories but it appears to be necessary to have available at least two variational wave functions, or at least to know the limiting behaviour of the theory for large and small  $\lambda$ , in order to interpret the results correctly. Future work should therefore be devoted to the development of more accurate variational wave functions for non-abelian theories, by incorporating into the wave function explicit couplings between different plaquettes. The resulting variational wave functions, although interesting in their own right, would be very useful as importance functions in the GFMC method.

## APPENDICES

## APPENDIX A

Green's function Monte Carlo calculations  
on the SU(2) and U(1) lattice gauge theories

Green's function Monte Carlo calculations on  
the SU(2) and U(1) lattice gauge theories

David W. Heys<sup>‡</sup> and Daniel R. Stump

Department of Physics and Astronomy  
Michigan State University  
East Lansing, Michigan 48824

Abstract

An application of the Green's function Monte Carlo method to the Hamiltonian formulation of the SU(2) and U(1) lattice gauge theories is described. The Green's function is that of a diffusion process in the gauge group space. A small-step approximation of the diffusion distribution is used in actual calculations. Also, a variance reduction technique is implemented, importance sampling with a disordered trial wave function optimized by the variational principle. The results of computations are reported for a  $3 \times 3 \times 3$  spatial lattice. The quantities computed are the ground-state energy and the expectation value of the magnetic energy, as a function of the gauge coupling constant. The results are compared to variational estimates and to weak-coupling perturbation theory.

---

<sup>‡</sup> Address beginning October, 1984: Department of Applied Mathematics and Theoretical Physics, University of Liverpool.

## I. Introduction

The Green's function Monte Carlo (GFMC) method is a numerical method for computation of properties of the ground state of a quantum system with many degrees of freedom. The method was originally developed for application to many-body problems in nonrelativistic quantum mechanics<sup>1,2</sup>. It is also applicable to the Hamiltonian formulation of lattice gauge theories defined by Kogut and Susskind<sup>3</sup>.

The Hamiltonian formulation is an approach to lattice gauge theories that is complementary to the Wilson path-integral formulation<sup>4</sup>. The properties of the two models are expected to be qualitatively similar. Each approach has advantages. The Hamiltonian approach is a more conventional quantum mechanics construction, in which the theory is defined in terms of field operators and a Hamiltonian operator; the basic problem is to obtain the energy eigenstates. The usual approximation methods of quantum mechanics, such as perturbation theory<sup>5</sup> and the variational principle<sup>6,7</sup>, can be used to study the eigenstates. This operator formulation provides a different kind of insight into the nature of the gauge theory than the path-integral, because it deals directly with the quantum states of the fields.

Monte Carlo methods are suited to numerical studies of systems with many degrees of freedom. Some very important results on lattice gauge theories have been obtained from Monte Carlo calculations on the path-integral formulation of the theories<sup>8,9</sup>. Therefore it is natural also to develop Monte Carlo methods for application to the Hamiltonian formulation of the theory. The GFMC method, which has already been applied successfully to quantum many-body problems, is an obvious method to try.

The first problem to solve regarding a quantum system with many degrees of freedom is to compute properties of the ground state. That is the subject of this paper, for the SU(2) and U(1) lattice gauge theories in three spatial dimensions. Specifically, we show results of GFMC computations of the ground-state energy, as

a function of the gauge coupling constant, and of the expectation value of a plaquette variable related to the magnetic field. These quantities are analogous to the mean plaquette action computed in the earliest Monte Carlo studies of path-integral lattice gauge theories<sup>9</sup>; they are interesting in that they provide an indication of the transition between the strong and weak coupling limits of the theory.

Our numerical results are limited to a small lattice, a  $3 \times 3 \times 3$  spatial lattice. This is small by the standards set by Monte Carlo calculations on the path-integral, but not small compared to other GFMC applications. The SU(2) gauge theory has 243 independent quantum variables for a  $3 \times 3 \times 3$  lattice. There is no fundamental problem in using a larger lattice; the only limitation is the availability of computer time. The quantities described in this paper are not very sensitive to lattice size, because they are averages over the entire lattice. Thus the results are already interesting for a small lattice.

We hope to use the GFMC method to study other properties of lattice gauge theories, such as the string tension or the energies of elementary excitations. We have carried out some numerical calculations of these quantities by the variational principle<sup>7,10</sup>, but it remains for the future to extend the Monte Carlo method to those calculations.

The problem presented by the Hamiltonian formulation of a lattice gauge theory is quite different than that of the path integral formulation. In the path integral, the probability distribution of the fields is given; it is  $e^{-\beta S}$  where  $S$  is the lattice action and  $\beta$  is related to the coupling constant. Then the aim of the Monte Carlo calculation is to generate a set of field configurations with this known distribution, e. g. by the Metropolis method or Creutz's heat-bath algorithm<sup>9</sup>. In the quantum problem, in contrast, the ground-state distribution of the fields is not known. What is known is only that the wave function is the lowest eigenfunction of the Hamiltonian. The aim of the GFMC method is to generate a set of field configurations with a

probability distribution related to the ground-state eigenfunction. But the GFMC algorithm does not derive from an a priori distribution; rather, it derives from the eigenvalue equation, written as an integral equation.

The integral form of the eigenvalue equation resembles a steady-state diffusion problem. The origins of the GFMC method are found in techniques of Monte Carlo solution of such diffusion problems. The idea is to simulate diffusion of an ensemble of points in the configuration space. The diffusion process is defined such that the evolution of the probability distribution of the points is identical to iteration of the eigenvalue equation. Since iteration of the equation converges to the lowest eigensolution, the GFMC ensemble of points converges to a set with probability distribution equal to the ground-state eigenfunction.

Perhaps the most interesting aspect of the GFMC method is the use of an importance sampling technique, in which a trial wave function is used to guide the diffusion to the significant region of configuration space. Importance sampling reduces the variance in the Monte Carlo estimates. But the technique is potentially more valuable than a mere computational trick. The trial function must approximate the ground-state eigenfunction to provide strong importance sampling. One may gain some insight into the structure of the eigenfunction by studying importance sampling with trial functions of different forms.

In the calculations described in this paper the wave function is a function of the gauge field, and the GFMC ensemble is an ensemble of gauge-field configurations. In the language of quantum mechanics, we are using a basis for the Hilbert space in which the gauge-field operators are diagonal. It is possible to use instead a basis in which the electric-field operators are diagonal. In fact we did use such a basis in an earlier application of the GFMC method<sup>11</sup> to the compact  $U(1)$  gauge theory<sup>12</sup> and to the XY model<sup>13</sup>. For that basis we constructed trial functions for importance sampling that approximate the eigenfunction in both the strong and weak coupling limits. For the gauge-field basis, however, we have

not succeeded in constructing a useful weak-coupling trial function. All the results reported here use a disordered trial wave function for importance sampling.

The disordered wave function is an accurate representation of the ground state in the strong-coupling limit. It is a product of independent functions of the plaquette variables; thus it is gauge invariant, and has minimal correlation between the gauge fields. Comparison of the variational estimates<sup>7</sup> based on this trial function and the GFMC results should show how well this simple wave function represents the vacuum state.

The remainder of the paper consists of Section II, on the details of our application of the GFMC method to the SU(2) and U(1) lattice gauge theories, including the implementation of importance sampling with the disordered trial wave function; Section III, on the results of computations for a  $3 \times 3 \times 3$  spatial lattice; and Section IV, a brief summary. We have also included an appendix on a technical point: the "growth estimate" fails to give an accurate measurement of the eigenvalue in our calculations.

## II. The Green's function Monte Carlo method

### A. Application to lattice gauge theories

In this section we describe an application of the Green's function Monte Carlo (GFMC) method to lattice gauge theories. The details are described for the SU(2) gauge theory; the analogous application to the U(1) gauge theory is an obvious modification.

The field variables of the SU(2) lattice gauge theory are elements of the group SU(2); an element  $U(\ell)$  is associated with each link  $\ell$  of the lattice. The group element  $U(\ell)$  may be specified in terms of a 3-component gauge field  $A_a(\ell)$  (where  $a=1,2,3$ ) or in terms of three angular variables  $(\psi(\ell), \theta(\ell), \phi(\ell))$ ; these are defined by

$$\begin{aligned} U(\ell) &= \exp\left(\frac{i}{2} \sigma_a A_a(\ell)\right) \\ &= \cos \psi(\ell) + i \sigma_a n_a(\ell) \sin \psi(\ell), \end{aligned} \quad (2.1)$$

where  $\sigma_a$  denotes the Pauli matrix and  $n_a(\ell)$  is the 3-dimensional unit vector with polar angles  $(\theta(\ell), \phi(\ell))$ . The relation between the two representations is

$$A_a(\ell) = 2 \psi(\ell) n_a(\ell). \quad (2.2)$$

Also, there is a 3-component electric field operator  $E_a(\ell)$  associated with each link, defined by the commutation relation

$$[E_a(\ell), U(\ell)] = -\frac{1}{2} \sigma_a U(\ell). \quad (2.3)$$

The operator  $E_a(\ell)$  is a differential operator acting on functions of the gauge fields  $A_a(\ell)$ , or equivalently on functions of the angles  $(\psi(\ell), \theta(\ell), \phi(\ell))$ ; in terms of  $A_a(\ell)$ ,

$$\begin{aligned} E_a &= i f(A) \frac{\partial}{\partial A_a} - \frac{1}{A^2} (f(A) - 1) A_a A_b \frac{\partial}{\partial A_b} \\ &\quad - \frac{1}{2} \epsilon_{abc} A_b \frac{\partial}{\partial A_c}, \end{aligned} \quad (2.4a)$$

where

$$A = \left( A_a A_a \right)^{1/2}, \quad f(A) = \frac{A}{2} \cot \frac{A}{2}. \quad (2.4b)$$

The Hamiltonian of the SU(2) gauge theory is<sup>3</sup>

$$H_{KS} = \frac{1}{2} g^2 \sum_{\ell} E_a^2 + \frac{4}{g^2} \sum_p \phi(p); \quad (2.5)$$

the gauge-invariant plaquette variable  $\phi(p)$  is

$$\phi(p) = 1 - \frac{1}{2} \text{Tr} U(\ell_1) U(\ell_2) U^\dagger(\ell_3) U^\dagger(\ell_4) \quad (2.6)$$

where  $(\ell_1, \ell_2, \ell_3, \ell_4)$  are the links that define the plaquette  $p$ . We use periodic boundary conditions in the definition of the plaquette field  $\phi(p)$ , to minimize finite size effects in the numerical results.

In our GFMC calculations we use a Hamiltonian  $H$  that differs from that in Eq. (2.5) by an overall scale factor, and an additive constant;  $H$  is

$$H = K - \lambda M, \quad (2.7a)$$

where

$$K = \sum_{\ell} E_a^2(\ell), \quad (2.7b)$$

$$M = \sum_p \left( 1 + \frac{1}{2} \text{Tr} U(\ell_1) U(\ell_2) U^\dagger(\ell_3) U^\dagger(\ell_4) \right). \quad (2.7c)$$

The relation between the coupling constants  $\lambda$  and  $g$  is

$$\lambda = 8/g^4. \quad (2.7d)$$

The Hamiltonians are related by

$$H_{KS} = \frac{1}{2} g^2 (H - 2 \lambda N_p) \quad (2.8)$$

where  $N_p$  is the number of plaquettes; obviously they have the same eigenstates. We write the Hamiltonian in this form because our application of the GFMC method requires that the magnetic energy be

negative.

The starting point of the GFMC method is an integral equation for the ground-state eigenfunction of  $H$ . Let  $\Psi[A_a]$  denote the eigenfunction, a function of all the link variables; it obeys the eigenvalue equation

$$H\Psi[A_a] = -Q^2 \Psi[A_a], \quad (2.9)$$

where the ground-state energy is denoted by  $-Q^2$ <sup>14</sup>. Or, Eq. (2.9) is equivalent to the integral equation

$$\Psi[A_a] = \lambda \int d\Omega' G[A_a, A_a'] M[A_a'] \Psi[A_a']; \quad (2.10)$$

the functions that appear in the integral, which are functions of the full field configuration, are defined by

$$\langle [A_a] | (K+Q^2)^{-1} | [A_a'] \rangle = G[A_a, A_a'], \quad (2.11a)$$

$$\langle [A_a] | M | [A_a'] \rangle = M[A_a] \prod_{\ell} \delta(A_a(\ell), A_a'(\ell)). \quad (2.11b)$$

The integration measure for  $SU(2)$ , which is expressed most simply in terms of the angular variables, is

$$d\Omega = \prod_{\ell} d\omega(\ell),$$

$$d\omega(\ell) = \frac{1}{2\pi^2} \sin^2\psi(\ell) \sin\theta(\ell) d\psi(\ell) d\theta(\ell) d\phi(\ell); \quad (2.12)$$

the domain of  $\psi$  and  $\theta$  is  $(0, \pi)$  and that of  $\phi$  is  $(0, 2\pi)$ . The normalization of the delta function in Eq. (2.11b) is

$$\int d\omega(\ell) \delta(A_a(\ell), A_a'(\ell)) = 1. \quad (2.13)$$

The function  $G[A_a, A_a']$  is the Green's function of the operator  $K+Q^2$ , defined by

$$(K+Q^2) G[A_a, A_a'] = \prod_{\ell} \delta(A_a(\ell), A_a'(\ell)). \quad (2.14)$$

Equation (2.10) is an eigenvalue problem, in which  $Q^2$  is the given quantity, with  $\lambda$  and  $\Psi[A_a]$  the eigenvalue and eigenfunction to be found.

The GFMC approach to the solution of Eq. (2.10) is based on iteration of the equation by simulation of diffusion. It can be shown that iteration of Eq. (2.10) converges to the ground-state eigensolution. However, it is not possible to deal directly with  $\Psi[A_a]$  because its domain is multidimensional; for the smallest lattice gauge theory, a  $3 \times 3 \times 3$  spatial lattice, there are 243 link variables. Instead, the aim of the GFMC method is to obtain a probabilistic representation of the wave function; specifically, to generate an ensemble of field configurations

$$\text{ENS} = \{ A_a^{(\sigma)}(\ell) ; \sigma = 1, 2, 3, \dots, N \} , \quad (2.15)$$

such that the probability distribution of the configurations in ENS is proportional to  $\Psi[A_a]$ <sup>15</sup>. The GFMC algorithm generates ENS by a process based on iteration of Eq. (2.10). The process is a simulation of diffusion with branching, in which:

- (i) the branching fraction  $f$  of the configuration  $A_a^{(\sigma)}(\ell)$  is proportional to  $M[A_a^{(\sigma)}]$ , and
- (ii) the diffusion creates  $f$  new configurations from  $A_a^{(\sigma)}(\ell)$ , with probability distribution  $G[A_a, A_a^{(\sigma)}]$ .

Each step in the evolution of the probability distribution of the ensemble is identical to one iteration of Eq. (2.10). The probability distribution converges to the ground-state eigenfunction.

The GFMC process described so far is incomplete, because applications of the GFMC method to systems with many degrees of freedom always require the use of an importance sampling trick, a technique also called directed diffusion. One implementation of importance sampling for lattice gauge theories is described in the next section. But before proceeding to that subject, it is useful to discuss the nature of the Green's function  $G[A_a, A_a']$ .

The crucial problem that must be solved in order to apply the GFMC method to a quantum system is to find a way to sample the Green's function as a probability distribution. The first step in this lattice gauge theory application is to separate the Green's function  $G[A_a, A'_a]$  into a product of factors, each of which acts on the fields of a single link. This is accomplished by the formula

$$\begin{aligned} \langle [A_a] | (K + Q^2)^{-1} | [A'_a] \rangle \\ = \int_0^\infty dt e^{-tQ^2} \langle [A_a] | e^{-tK} | [A'_a] \rangle. \end{aligned} \quad (2.16)$$

The left-hand side is the energy-dependent Green's function  $G[A_a, A'_a]$ ; the integrand on the right-hand side is the related time-dependent Green's function. Since  $K$  is a sum of single-link operators, the time-dependent Green's function factorizes, as

$$\langle [A_a] | e^{-tK} | [A'_a] \rangle = \prod_{\ell} \langle A_a(\ell) | e^{-t k_{\ell}} | A'_a(\ell) \rangle \quad (2.17)$$

where

$$k_{\ell} = E_a^2(\ell); \quad (2.18)$$

each factor depends only on the field variables of a single link. This representation leads to a method of sampling the distribution  $G[A_a, A'_a]$ : first select a diffusion time interval  $t$  by a random process with probability distribution

$$Q^2 e^{-t Q^2} dt; \quad (2.19)$$

then for each link select  $A_a(\ell)$  with probability distribution

$$g(t; A_a(\ell), A'_a(\ell)) = \langle A_a(\ell) | e^{-t k_{\ell}} | A'_a(\ell) \rangle. \quad (2.20)$$

Thus the problem reduces to sampling  $g(t; A_a, A'_a)$ , the diffusion Green's function for the fields of a single link. Furthermore, an important simplifying approximation can be used. In a large system, the ground-state energy  $Q^2$  is large, proportional to the number of plaquettes. Then the diffusion time interval  $t$  chosen in accord with the distribution (2.19) must be small. Thus it is only

necessary to sample the diffusion Green's function (2.20) for a small time interval. In the small- $t$  limit, this distribution describes ordinary free diffusion.

As a first step toward understanding the Green's function  $g(t; A_a, A'_a)$  it is useful to study the analogous function for a U(1) gauge theory. The group element of the U(1) gauge theory can be expressed in terms of an angle  $\theta$ , which lies in the domain  $(0, 2\pi)$ , as

$$U = e^{i\theta} ; \quad (2.21)$$

the corresponding electric-field energy is just

$$k = -\partial^2 / \partial \theta^2 . \quad (2.22)$$

The single-link diffusion function for the U(1) gauge theory is

$$\langle \theta | e^{-t k} | \theta' \rangle = \sum_{\nu=-\infty}^{\infty} (4\pi t)^{-1/2} \exp(-(\theta - \theta' + 2\pi\nu)^2 / 4t) ; \quad (2.23)$$

this is the Green's function of free diffusion on a circle. In the limit of a small diffusion time interval  $t$ , the Green's function is approximately

$$\langle \theta | e^{-t k} | \theta' \rangle \cong (4\pi t)^{-1/2} \exp(-(\theta - \theta')^2 / 4t) , \quad (2.24)$$

with the understanding that when  $\theta$  diffuses outside its domain  $(0, 2\pi)$ , it is moved back inside by a shift of  $\pm 2\pi$ . That is, diffusion on a circle may be approximated by free linear diffusion made periodic. To sample the distribution in Eq. (2.23) for a small time interval, let

$$\theta = \theta' + \epsilon \pmod{2\pi} , \quad (2.25a)$$

where  $\epsilon$  is a random variable with probability distribution

$$(4\pi t)^{-1/2} \exp(-\epsilon^2 / 4t) . \quad (2.25b)$$

The simplification in Eq. (2.25), based on the small-step approximation, extends to the SU(2) gauge theory. However, the analysis is complicated by the nontrivial geometry of the group SU(2).

To understand the nature of the Green's function  $g(t; A_a, A'_a)$  requires an insight into the geometric structure of the group SU(2), as defined by Eqs. (2.1), (2.3), and (2.12). First, an arbitrary group element U can be expressed as

$$U = x_4 + i \vec{\sigma} \cdot \vec{x} , \quad (2.26a)$$

where

$$x_4^2 + \vec{x}^2 = 1 . \quad (2.26b)$$

Thus there is a one-to-one correspondance between SU(2) group elements and points of the 3-dimensional surface of a sphere in four dimensions; we refer to this space as  $S_3$ . The angular variables  $(\psi, \theta, \phi)$  in Eq. (2.1) are simply 4-dimensional polar coordinates of a point of  $S_3$ . Second, the SU(2) integration measure  $d\omega$  is the volume element of  $S_3$ . Third, the operator  $k$  is proportional to the angular part of the d'Alembertian in four dimensions,

$$\begin{aligned} \partial_4^2 + \vec{\partial}^2 &= \frac{1}{r^3} \frac{\partial}{\partial r} \left( r^3 \frac{\partial}{\partial r} \right) - \frac{4}{r^2} k , \\ 4 k &= - \frac{1}{\sin^2 \psi} \frac{\partial}{\partial \psi} \left( \sin^2 \psi \frac{\partial}{\partial \psi} \right) \\ &\quad - \frac{1}{\sin^2 \psi} \left( \frac{1}{\sin \theta} \frac{\partial}{\partial \theta} \left( \sin \theta \frac{\partial}{\partial \theta} \right) + \frac{1}{\sin^2 \theta} \frac{\partial^2}{\partial \phi^2} \right) . \end{aligned} \quad (2.27)$$

Therefore the Green's function  $g(t; A_a, A'_a)$  is the distribution for free diffusion in  $S_3$ . In the limit of a small time interval  $t$  the diffusion distance must be small, and then the curvature of the space has a negligible effect. That is, the small- $t$  limit of the diffusion Green's function  $g(t; A_a, A'_a)$  is equal to that of free diffusion in the tangent space at  $A'_a$ .

The small- $t$  limit of the Green's function  $g(t; A_a, A_a')$  is most easily written for  $A_a$  and  $A_a'$  near zero, i. e. for the corresponding group elements  $U$  and  $U'$  near the unit element. Then the Green's function is approximately equal to that of a  $U(1) \times U(1) \times U(1)$  gauge theory, i. e.

$$g(t; A_a, A_a') \cong (\pi t)^{-3/2} \exp(-(A_a - A_a')^2/4t); \quad (2.28)$$

this is only valid near the unit element. The generalization to a small diffusion step at an arbitrary point in the group is obvious. Let  $(\psi', \theta', \phi')$  and  $(\psi, \theta, \phi)$  be the angular variables corresponding to the gauge fields  $A_a'$  and  $A_a$ ; also let the small changes in these angles be denoted by

$$\delta\psi = \psi' - \psi, \quad \delta\theta = \theta' - \theta, \quad \delta\phi = \phi' - \phi. \quad (2.29)$$

The distance between the two group elements is given by the line element of  $S_3$ ,

$$(\delta s)^2 = (\delta\psi)^2 + \sin^2\psi' \left( (\delta\theta)^2 + \sin^2\theta' (\delta\phi)^2 \right). \quad (2.30)$$

Then the generalization of Eq. (2.28) is<sup>16</sup>

$$g(t; A_a, A_a') \cong (\pi t)^{-3/2} \exp(-(\delta s)^2/t). \quad (2.31)$$

It is also useful to define a 3-vector  $\delta\vec{s}$  by

$$\delta\vec{s} = \hat{\psi}' \delta\psi + \sin\psi' \left( \hat{\theta}' \delta\theta + \sin\theta' \hat{\phi}' \delta\phi \right); \quad (2.32)$$

here  $\hat{\psi}'$ ,  $\hat{\theta}'$ , and  $\hat{\phi}'$  are the unit vectors in the  $\psi'$ ,  $\theta'$ ,  $\phi'$  directions at  $A_a'$ . The 3-vector  $\delta\vec{s}$  may be described as the diffusion move in the tangent space at  $A_a'$ , since  $\hat{\psi}'$ ,  $\hat{\theta}'$ ,  $\hat{\phi}'$  are an orthonormal basis for the tangent space. Note that the line element  $(\delta s)^2$  is equal to the length of  $\delta\vec{s}$ , i. e. the distance moved in the tangent space.

In detail, sampling the distribution  $g(t; A_a, A_a')$  in the small- $t$  limit is a 3-step procedure:

- (1) Construct the tangent space at the original point,

which corresponds to  $A'_a$ ;

- (ii) move in the tangent space according to the distribution of free diffusion, for time interval  $t$ ;
- (iii) project back into  $S_3$ , to the point that corresponds to  $A_a$ .

The algebraic realization of this geometric picture is contained in the formulas in the preceding paragraph: The tangent space is defined by the basis vectors  $(\hat{\psi}', \hat{\theta}', \hat{\phi}')$ . Diffusion in this space is a move

$$\delta \vec{s} = \delta x_1 \hat{\psi}' + \delta x_2 \hat{\theta}' + \delta x_3 \hat{\phi}' \quad (2.33)$$

with probability distribution (2.31), i. e. free diffusion. The corresponding move in the  $SU(2)$  space is obtained from the relation between the changes in the angles and the components of the move in the tangent space,

$$\delta x_1 = \delta \psi, \quad \delta x_2 = \sin \psi' \delta \theta, \quad \delta x_3 = \sin \psi' \sin \theta' \delta \phi. \quad (2.34)$$

Projection back into  $S_3$  is nontrivial if the diffusion occurs near a point at which the coordinate system  $(\psi, \theta, \phi)$  is singular, e.g. near  $\psi' = \pi$  or  $\theta' = \pi$ .

There is an analogy between the  $SU(2)$  and  $U(1)$  procedures discussed above. Step (ii) in the  $SU(2)$  case is ordinary free diffusion in the 3-dimensional Euclidean tangent space, analogous to the linear diffusion of Eq. (2.24) in the  $U(1)$  case. Step (iii) in the  $SU(2)$  case restores the point to the sphere, analogous to the use of Eq. (2.25) to put  $\theta$  back in the interval  $(0, 2\pi)$  in the  $U(1)$  case.

This discussion of the Green's function  $G[A_a, A'_a]$  is the basis of our present application of the GFMC method to lattice gauge theories. But we also use importance sampling, which leads to a more complicated sampling problem than that discussed so far. That is the subject of the next section.

## B. Importance sampling

The importance sampling trick, also referred to as biased or directed diffusion, is used to reduce the variance of the Monte Carlo estimates. This technique is a necessary part of Green's function Monte Carlo (GFMC) calculations on systems with many degrees of freedom<sup>2</sup>.

The trick is to introduce an importance function  $u[A_a(l)]$ , which approximates the ground-state eigenfunction as closely as possible, and to rewrite the integral equation (2.10) as an equation for the function<sup>17</sup>

$$F[A_a] = M[A_a] u[A_a] \Psi[A_a]. \quad (2.35)$$

The equation for  $F[A_a]$  is

$$F[A_a] = \lambda \int d\Omega' G_D[A_a, A_a'] M[A_a'] F[A_a'], \quad (2.36)$$

where

$$G_D[A_a, A_a'] = \frac{M[A_a] u[A_a]}{M[A_a'] u[A_a']} G[A_a, A_a']. \quad (2.37)$$

This has the same form as the original Eq. (2.10), and therefore the GFMC algorithm stated briefly in Sec. II A applies also to this equation. Here, however, the diffusion is governed by the function  $G_D[A_a, A_a']$ , which differs from the Green's function by a biasing factor, the ratio of the function  $M[A_a] u[A_a]$  before and after the diffusive move. This factor biases the GFMC diffusion step in favor of moves that increase the importance function  $u[A_a]$ . If  $u[A_a]$  approximates the ground-state eigenfunction, then the biasing reduces the variance of Monte Carlo estimates.

Of course introduction of the biasing factor implies that the ensemble of configurations that emerges from the GFMC iteration of Eq. (2.36) has probability distribution  $F[A_a]$ .

It is important to realize that the distribution of the configurations in the GFMC ensemble is not  $\Psi^2[A_a]$ . This is a weakness of the method, because the interesting quantities in

quantum mechanics are expectation values in the distribution  $\Psi^2[A_a]$ . However, the method does provide ways to compute certain ground-state properties. In particular, there is a formula from which the eigenvalue  $\lambda$  can be computed, in a way which is exact in the sense that the only error is statistical. Also, there is a way to estimate the ground-state expectation value of an operator, in which the trial function is used as an approximation of the ground-state eigenfunction; this approach is not exact, but has some systematic error in addition to the statistical error.

The coupling constant  $\lambda$  corresponding to the input ground-state energy  $-Q^2$  is the unknown eigenvalue in this problem, the basic quantity to be computed. It obeys the formula

$$\lambda = \int d\Omega \frac{F[A_a]}{M[A_a]} (u^{-1}[A_a] (K+Q^2) u[A_a]) / \int d\Omega F[A_a]. \quad (2.38a)$$

Since  $F[A_a]$  is the probability distribution of the configurations in the GFMC ensemble, the GFMC estimate of the coupling  $\lambda$  is

$$\lambda \cong \langle (u^{-1}[A_a] (K+Q^2) u[A_a]) / M[A_a] \rangle_{\text{ens}}, \quad (2.38b)$$

where  $\langle \rangle_{\text{ens}}$  denotes the ensemble average. In principle this estimate does not depend on whether the importance function  $u[A_a]$  is a good approximation of the eigenfunction, since Eq. (2.38a) is valid for any  $u[A_a]$ . The only error is statistical. However, the variance of the Monte Carlo estimate depends on the choice of  $u[A_a]$ . The variance is small if  $u[A_a]$  approximates the eigenfunction; in fact, if  $u[A_a]$  is equal to the eigenfunction then the right-hand side of Eq. (2.38b) is equal to  $\lambda$  for any ensemble of configurations, and so there is no variance. In practice the trial function must approximate the ground-state eigenfunction to obtain an accurate value of  $\lambda$ .

If the eigenvalue  $\lambda$  could be computed with sufficient accuracy as a function of the ground-state energy  $-Q^2$ , then certain expectation values could be deduced. For example, the ground-state expectation value of the plaquette field  $\phi(p)$  defined in Eq. (2.6)

is related to the derivative of  $Q^2$  with respect to  $\lambda$ . The form of the Hamiltonian  $H$  implies

$$\langle \Psi | \phi(p) | \Psi \rangle = 2 - \frac{1}{N_p} \frac{dQ^2}{d\lambda}, \quad (2.39)$$

where  $N_p$  is the number of plaquettes.

The GFMC method with importance sampling also yields a simple approximate estimate of the expectation value of an operator, based on the assumption that the trial function is an approximation of the ground state eigenfunction. Suppose the eigenfunction is

$$\Psi[A_a] = u[A_a] + \epsilon[A_a] \quad (2.40)$$

where  $\epsilon$  is small; then to order  $\epsilon^2$  the ground-state expectation value of a function  $C[A_a]$  of the field variables is approximated by

$$\frac{\langle \Psi | C | \Psi \rangle}{\langle \Psi | \Psi \rangle} = 2 \frac{\langle u | C | \Psi \rangle}{\langle u | \Psi \rangle} - \frac{\langle u | C | u \rangle}{\langle u | u \rangle}. \quad (2.41a)$$

The first term on the right-hand side, called the mixed expectation value, is computed from ensemble averages, by

$$\frac{\langle u | C | \Psi \rangle}{\langle u | \Psi \rangle} = \frac{\langle C[A_a] / M[A_a] \rangle_{\text{ens}}}{\langle 1 / M[A_a] \rangle_{\text{ens}}}. \quad (2.41b)$$

This Monte Carlo estimate can have some systematic error for a finite ensemble, because it involves the ratio of two ensemble averages<sup>18</sup>. The other term is the expectation value in the trial state. Since Eq. (2.41a) is only valid to order  $\epsilon^2$ , this estimate of the expectation value of  $C[A_a]$  is not trustworthy if it differs significantly from the expectation value in the trial state.

The importance function  $u[A_a]$  is normally defined to have a simple form, and optimized by the variational principle. Therefore a conservative interpretation of GFMC results is to regard them as corrections to the variational estimates of the quantities of interest. The estimate of an expectation value based on the mixed expectation value is by definition only a computation of the lowest

order correction to the variational estimate. The computation of the eigenvalue based on Eq. (2.38) is in principle exact; but since the statistical significance of the computed value is limited unless the trial function is an approximation of the eigenfunction, as a practical matter the computation of  $\lambda$  also gives the correction to the variational estimate.

In Section III we describe the results of GFMC calculations on the SU(2) and U(1) lattice gauge theories. The importance function used in those calculations is a disordered trial wave function that we described in a previous paper<sup>7</sup>. For the SU(2) gauge theory it is

$$u[A_a] = \exp(2\alpha M[A_a]) \quad (2.42)$$

where  $M[A_a]$  is the magnetic energy defined in Eq. (2.7c), and  $\alpha$  is an adjustable parameter. In Ref. 7 we described a variational estimate of the ground-state of the SU(2) gauge theory based on this trial wave function. These variational calculations are numerical; Creutz's heat-bath Monte Carlo method<sup>9</sup> is used to compute the expectation value of the energy in the state  $u[A_a]$ . In the GFMC results described in Sec. III, the value of the parameter  $\alpha$  is that determined by the variational principle.

The remainder of this section is a discussion of details of the application of the GFMC algorithm to the integral equation (2.36). It is necessary to define a diffusion process with probability distribution  $G_D[A_a, A'_a]$ . By Eq. (2.16),  $G_D[A_a, A'_a]$  can be sampled by first picking a time-interval  $t$  with distribution

$$Q^2 e^{-tQ^2} dt,$$

and then moving  $A'_a(\ell)$  to  $A_a(\ell)$  according to the distribution

$$\frac{M[A_a]}{M[A'_a]} \frac{u[A_a]}{u[A'_a]} \prod_{\ell} g(t; A_a(\ell), A'_a(\ell)). \quad (2.43)$$

But there is a complication associated with the distribution (2.43): unlike the free time-dependent Green's function, this

distribution is not normalized to unity because of the biasing factor. To take into account the normalization, it is necessary to assign a weight to each configuration in the ensemble. The weighting can be done in various ways. The most obvious way would be to use the free Green's function for diffusion, and to reweight the new configuration by the biasing factor; then the importance sampling would derive from the increase of the weight of a point that moves toward larger  $M[A_a]u[A_a]$ . However, we use a different weighting method that includes importance sampling as a part of the configuration move itself. Our approach relies on the fact that the time interval of the diffusive step is small, of order  $1/Q^2$ , i. e. of order  $1/N_p$  where  $N_p$  is the number of plaquettes.

Since the diffusion time interval  $t$  is small, the configuration move  $A'_a(\ell) \rightarrow A_a(\ell)$  is small. Let  $(\psi'(\ell), \theta'(\ell), \phi'(\ell))$  and  $(\psi(\ell), \theta(\ell), \phi(\ell))$  be the angular variables corresponding to the gauge field  $A'_a(\ell)$  and  $A_a(\ell)$ ; and let  $\delta\psi(\ell)$ ,  $\delta\theta(\ell)$ ,  $\delta\phi(\ell)$  denote the small changes of these fields, as in Eq. (2.29). Then the ratio of the trial function (2.42) before and after the move is approximately

$$\frac{u[A_a]}{u[A'_a]} \cong \prod_{\ell} \exp \left( 2\alpha \left( \delta\psi(\ell) \frac{\partial M[A'_a]}{\partial \psi'(\ell)} + \delta\theta(\ell) \frac{\partial M[A'_a]}{\partial \theta'(\ell)} + \delta\phi(\ell) \frac{\partial M[A'_a]}{\partial \phi'(\ell)} \right) \right). \quad (2.44)$$

Or, in terms of the 3-vector  $\vec{\delta s}(\ell)$  that represents the diffusion step in the tangent space at  $A'_a(\ell)$ ,

$$\frac{u[A_a]}{u[A'_a]} \cong \prod_{\ell} \exp \left( 2\alpha \vec{\delta s}(\ell) \cdot \vec{f}'(\ell) \right), \quad (2.45)$$

where

$$\vec{f}'(\ell) = \hat{\psi}' \frac{\partial M[A'_a]}{\partial \psi'(\ell)} + \frac{1}{\sin \psi'(\ell)} \left( \hat{\theta}'(\ell) \frac{\partial M[A'_a]}{\partial \theta'(\ell)} + \frac{\hat{\phi}'(\ell)}{\sin \theta'(\ell)} \frac{\partial M[A'_a]}{\partial \phi'(\ell)} \right). \quad (2.46)$$

This approximation of the ratio  $u[A_a]/u[A'_a]$  is a product of

factors, each of which acts on the fields of a single link. Thus it can be combined with the Green's function to define a distribution for the change of the fields on each link.

For a small diffusive move the Green's function is approximated by Eq. (2.31). When this is combined with the factor  $u[A_a]/u[A_a']$ , the complete distribution (2.43) can be written without approximation as

$$\begin{aligned} \frac{M[A_a]}{M[A_a']} \frac{u[A_a]}{u[A_a']} \prod_{\ell} g(t; A_a(\ell), A_a'(\ell)) & \quad (2.47) \\ = R[A_a, A_a'] \prod_{\ell} (\pi t)^{-3/2} \exp(-[\delta \vec{s}(\ell) - \alpha t \vec{f}'(\ell)]^2/t), & \end{aligned}$$

where

$$\begin{aligned} R[A_a, A_a'] = \frac{M[A_a]}{M[A_a']} \frac{u[A_a]}{u[A_a']} & \quad (2.48) \\ \times \prod_{\ell} \exp(-2\alpha \delta \vec{s}(\ell) \cdot \vec{f}'(\ell) + \alpha^2 t f'^2(\ell)). & \end{aligned}$$

Each single-link factor on the right-hand side of Eq. (2.47) is the distribution function for a process in which the link variables first make a deterministic forced move

$$\alpha t \vec{f}'(\ell),$$

and then a diffusive move

$$\delta \vec{s}(\ell)$$

for which the probability distribution is the Green's function of free diffusion in the tangent space. The other factor  $R[A_a, A_a']$  reweights the new configuration. Since  $R[A_a, A_a']$  is approximately equal to 1, the importance sampling in this approach is mainly due to the deterministic move, which forces the point in the direction of increased  $u[A_a] M[A_a]$ .

The results described in Sec. III are for calculations which use the simple small-step approximation, Eq. (2.31). It is possible to improve the approximation by subdividing the diffusion time into

smaller intervals and letting the diffusion proceed separately for each of these intervals. However, we believe that the naive small-step approximation is sufficiently accurate.

In detail, the GFMC algorithm for iteration of Eq. (2.36) is as follows. The aim is to obtain a weighted ensemble of field configurations

$$\text{ENS} = \{ A_a^{(\sigma)}(\ell), w^{(\sigma)}; \sigma = 1, 2, 3, \dots, N \}. \quad (2.49)$$

The iteration of the ensemble consists of three steps:

- (i) Branching Each configuration  $A_a^{(\sigma)}(\ell)$  in the current ensemble branches into  $f^{(\sigma)}$  new configurations, where  $f^{(\sigma)}$  is an integer chosen by a random process with expected value

$$\langle f^{(\sigma)} \rangle = \frac{1}{q} M[A_a^{(\sigma)}] w^{(\sigma)}, \quad (2.50a)$$

where

$$q = \frac{1}{N_e} \sum_{\sigma=1}^N M[A_a^{(\sigma)}] w^{(\sigma)};$$

here  $N$  is the number of configurations in the current ensemble, and  $N_e$  is a fixed number equal to the desired mean ensemble size. Each of these new configurations is assigned weight  $w'$  where

$$w' = \begin{cases} w^{(\sigma)} / f^{(\sigma)} & \text{if } \langle f^{(\sigma)} \rangle > 1, \\ q & \text{if } \langle f^{(\sigma)} \rangle < 1. \end{cases} \quad (2.50b)$$

The branching process creates an ensemble with total weight and expected distribution equal to the total weight and distribution of the current ensemble. It keeps the weights of the configurations approximately equal by splitting if  $\langle f^{(\sigma)} \rangle > 1$ , and prevents the ensemble from becoming too large by eliminating points if  $\langle f^{(\sigma)} \rangle < 1$ .

- (ii) Biased diffusion Then each field  $A_a^{(\sigma)}(\ell)$  moves to a new field  $A_a(\ell)$ , by the combined deterministic forced move plus diffusive move discussed in the previous paragraph.

(iii) Reweighting The weight assigned to this configuration in the new ensemble is

$$\frac{\lambda_0}{Q^2} R[A_a, A_a^{(\sigma)}] w'. \quad (2.50c)$$

This process ultimately converges to a weighted ensemble with probability distribution  $F[A_a]$ .

The value of the parameter  $\lambda_0$  in Eq. (2.50c) controls the size of the ensemble. For a sufficiently large ensemble, the total weight grows during this iteration if  $\lambda_0$  is larger than the eigenvalue, and decays if  $\lambda_0$  is less than the eigenvalue. In practice  $\lambda_0$  is maintained at a value such that the total weight, and therefore also the ensemble size, remains approximately constant. This property provides an estimate of the eigenvalue, which we refer to as the growth estimate. However, for a finite ensemble there is some systematic error in the growth estimate. In our lattice gauge calculations we find that the growth estimate does not yield an accurate measurement of  $\lambda$ . This point is discussed further in the Appendix.

### III. Numerical results

In this section we describe Green's function Monte Carlo (GFMC) computations of the ground-state energy and mean magnetic energy per plaquette of Hamiltonian gauge theories for a  $3 \times 3 \times 3$  lattice. The SU(2) gauge theory is defined in Sec. II. For comparison we consider also a  $U(1) \times U(1) \times U(1)$  gauge theory. The  $U(1)^3$  gauge fields are angle variables  $\theta_a(\ell)$  (with  $a=1, 2, 3$ ); the associated group element is

$$U(\ell) = \prod_{a=1}^3 \exp(i\theta_a(\ell)). \quad (3.1)$$

The  $U(1)^3$  Hamiltonian is

$$H_{Ab} = - \sum_{a,\ell} \partial^2 / \partial \theta_a^2(\ell) + \frac{\lambda}{4} \sum_{a,p} (1 - \cos B_a(p)) \quad (3.2)$$

where  $B_a(p)$  is the lattice curl at plaquette  $p$  of the gauge field  $\theta_a(\ell)$ . The Hamiltonian  $H_{Ab}$  is defined such that its harmonic, i.e. free-field limit is the same as that of  $H_{KS} / \frac{1}{2} g^2$  where  $H_{KS}$  is the SU(2) Kogut-Susskind Hamiltonian, Eq. (2.5).

Figure 1 shows the ground-state energy per plaquette as a function of the coupling constant for (a) the SU(2) gauge theory and (b) the  $U(1)^3$  gauge theory. The quantities plotted are  $E/N_p$  vs.  $\lambda$ , where  $E$  is the eigenvalue of  $H_{Ab}$  for the  $U(1)$  gauge theory, and  $E$  is the eigenvalue of  $H_{KS} / \frac{1}{2} g^2$  for the SU(2) gauge theory. In terms of  $-Q^2$ , the eigenvalue of  $H$  introduced in Eq. (2.9),  $E$  is

$$E = 2 \lambda N_p - Q^2.$$

Actually  $Q^2$  is the input, and the corresponding  $\lambda$  is the computed eigenvalue.

The dashed curves in Fig. 1 are variational bounds obtained using the disordered trial function  $u[A_a]$ . The variational calculations were described in a previous paper<sup>7</sup>. We refer to the wave function  $u[A_a]$  as disordered because the expectation value of the Wilson-loop operator obeys an area law in this state; we have calculated the corresponding string tension<sup>7</sup>. Also, this function does not explicitly couple the magnetic fields on different

plaquettes, although there is some implicit coupling because neighboring plaquettes share a common link. This disordered wave function should be a good approximation of the ground-state eigenfunction for small  $\lambda$ , so the variational bounds should be accurate estimates for small  $\lambda$ .

The solid curve is the large- $\lambda$  limit of the energy, i. e. the weak-coupling limit in terms of the original gauge coupling constant  $g$ , for the  $U(1)^3$  gauge theory. This limit is derived from the harmonic approximation of the theory. Asymptotically as  $\lambda \rightarrow \infty$ ,

$$\frac{E}{N_p} = c(n) \sqrt{2\lambda} - \frac{1}{3} c^2(n) + O(1/\sqrt{\lambda}) \quad (3.3)$$

for an  $n \times n \times n$  lattice; the constant  $c(n)$  depends weakly on  $n$ , e.g.,

$$c(3)=1.181, \quad c(\infty)=1.194. \quad (3.4)$$

In the limit  $\lambda \rightarrow \infty$ , the  $SU(2)$  gauge fields decouple into three independent  $U(1)$  fields, so the  $SU(2)$  gauge theory has the same harmonic limit as the  $U(1)^3$  gauge theory. Therefore Eq. (3.3) also gives the correct leading order contribution to the energy of the  $SU(2)$  model. However, the term constant in  $\lambda$  in Eq. (3.3) derives from four-field couplings in the weak-coupling expansion of the  $U(1)^3$  model; it would presumably be different for the  $SU(2)$  model.

The free-field limit of  $E$  lies below the variational bounds; the Monte Carlo results should converge to these lower free-field values for large  $\lambda$ .

The crosses in Fig. 1 are Monte Carlo results obtained using  $u[A_a]$  as an importance function to guide the iteration, as described in Sec. IIB. The GFMC calculation uses an ensemble of approximately 100 configurations; the ensemble size changes slightly with each iteration. The results are averages over 600 Monte Carlo iterations. The first few hundred iterations, during which convergence takes place, are discarded. In order to reduce the convergence time, the initial ensemble used in the GFMC algorithm is chosen from the distribution  $u^2[A_a]$ . Each point

required approximately 3.5 hours of computation time for the SU(2) model and 35 minutes for the U(1) model, on a CDC Cyber 750 computer at Michigan State University.

The results for the two models show quite different behaviour. The U(1) GFMC points are near the variational estimates for small  $\lambda$  but lie considerably below the variational bound for  $\lambda > 5$ , indicating that the variational wave function is not an accurate representation of the ground state for  $\lambda > 5$ . In the large- $\lambda$  range the values of  $E$  are consistent with the free-field limit. The numerical values are consistent with the results of a previous calculation<sup>12</sup>. The energy of the U(1) gauge theory changes abruptly from that of the disordered state to the free-field value. On the other hand, the SU(2) GFMC points do not show any abrupt deviation from the variational bound. This difference is easily explained; the U(1) model undergoes a phase transition from a charge confining disordered phase to a non-confining free-field phase  $\lambda \cong 4.5$ , whereas the SU(2) model does not.

Figure 2 shows the expectation value of the plaquette field  $\Phi(p)$ , defined for the two models by

$$\begin{aligned} \Phi(p) = & \quad 1 - \frac{1}{2} \text{Tr} U(\ell_1) U(\ell_2) U^+(\ell_3) U^+(\ell_4) \text{ for SU(2),} \\ & \quad 1 - \cos \left( \theta(\ell_1) + \theta(\ell_2) - \theta(\ell_3) - \theta(\ell_4) \right) \text{ for U(1).} \end{aligned} \quad (3.5)$$

Again the dashed curves are the variational estimates, and the solid curves are the large- $\lambda$  limits given by

$$\langle \Phi(p) \rangle = f c(n) / \sqrt{2 \lambda} \quad (3.6)$$

where  $f = 1$  for the SU(2) model and  $f = 4/3$  for the U(1) model. The crosses are GFMC estimates computed from the mixed expectation value, Eq. (2.41).

Again we see very different behaviour for the two models. In the U(1) model, the mean plaquette field  $\Phi(p)$  decreases abruptly in the region of the transition at  $\lambda \cong 4.5$ , from values near the variational estimate down to values near the weak-coupling limit.

In the SU(2) model, the field  $\phi(p)$  changes gradually over the range of  $\lambda$  considered, and does not differ very much from the variational estimate.

The GFMC points in Fig. 2 tend to lie below the variational curve for small  $\lambda$ . This tendency is more pronounced in the SU(2) model than in the U(1) model. Ordinarily this would be taken as evidence that the trial function  $u[A_a]$  does not adequately describe the vacuum state. In this case, however, we expect that  $u[A_a]$  does accurately describe the ground-state for small  $\lambda$  and becomes increasingly worse as  $\lambda$  increases. This is born out by the results on the energy shown in Fig. 1, where the GFMC points lie very close to the variational curve for small  $\lambda$  and begin to deviate as  $\lambda$  increases. The discrepancy may be a result of the failure of the small-time-step approximation used in calculating the matrix elements of  $e^{-tk}$ . The time step  $t$  is of order  $1/Q^2$ , which increases as  $\lambda$  decreases; thus the approximation is expected to be least valid for small  $\lambda$ . This explanation of the discrepancy could be checked by subdividing every time step into intervals smaller than  $\delta t$ , and then observing how the results change as  $\delta t$  decreases. On the other hand since the wave function is disordered for small  $\lambda$  we might expect that errors in the sampling procedure would be unimportant. The error bars in the graph are the ordinary standard deviation for 600 iterations, but we are not certain that enough iterations have been done to deduce a meaningful estimate of the uncertainty. Since the GFMC algorithm is iterative, ensembles in the sequence are not independent unless separated by a sufficient number of iterations. This convergence problem is more serious for the SU(2) model because there the diffusion takes place in a larger space, and so requires more iterations for convergence. Further investigation is clearly necessary to clarify the situation.

#### IV. Summary and conclusions

In this paper we describe an application of the Green's function Monte Carlo (GFMC) method to the SU(2) and U(1) lattice gauge theories. The numerical results obtained so far are limited, by the availability of computer time, to estimates of simple quantities, specifically the ground-state energy per plaquette  $E/N_p$  and the mean plaquette field  $\phi(p)$ , for a  $3 \times 3 \times 3$  spatial lattice.

These GFMC calculations use a disordered trial function  $u[A_a]$  as an importance function to bias the Monte Carlo sampling procedure in favour of regions of configuration space in which  $u[A_a]$  is large. By comparing the GFMC results to the variational results based on the trial function  $u[A_a]$ , we can obtain some indication as to how well  $u[A_a]$  describes the vacuum state.

For the U(1) model our results show a clear indication of the phase transition at  $\lambda \cong 4.5$  separating the charge confining phase, described well by the disordered trial function, and the non-confining free-field phase. For  $\lambda > 5$  there is a definite difference between the variational estimates and the GFMC results. The present results are in good agreement with the results of our previous Monte Carlo study of the U(1) lattice gauge theory<sup>12</sup>. There we formulated the problem in a completely different way. We wrote the wave function in the form

$$\Psi[A] = \sum_{\{n(p)\}} \exp \left( i \sum_p n(p) B(p) \right) \chi[n(p)], \quad (4.1)$$

where the variables  $n(p)$  take only integer values, and applied the GFMC method to an eigenvalue equation for  $\chi[n(p)]$ ; also we implemented importance sampling for two kinds of trial functions - a disordered wave function which accurately describes the ground state for small  $\lambda$ , and a correlated wave function derived from the harmonic limit which is accurate for large  $\lambda$ . That these two different studies of the U(1) gauge theory lead to similar results gives us considerable confidence in the GFMC method.

In one regard our earlier results on the  $U(1)$  model differ from those obtained here. In the calculations applied to the  $n(p)$ -space wave function  $\chi[n(p)]$  we found metastability behavior in the GFMC iteration for the  $U(1)$  gauge theory in three spatial dimensions. When a disordered  $n(p)$ -space trial function is used for importance sampling in the large- $\lambda$  region, the computed eigenvalue does not converge to the free-field value, but remains near the variational value. In contrast, no metastability of the GFMC iteration is seen in the  $A_a$ -space calculations. We attribute the difference to the fact that  $n(p)$  is a discrete variable, whereas  $A_a(\ell)$  is continuous valued.

For the  $SU(2)$  gauge theory our results are consistent with the nonexistence of a phase transition in that model. The trial wave function  $u[A_a]$  accurately describes the vacuum state for small  $\lambda$ . And even for large values of  $\lambda$  the variational estimates are approximately equal to the GFMC results, for the energy and mean plaquette field. The implication is that the ground state does not suddenly change as it does in the  $U(1)$  gauge theory.

When the variational and GFMC results show considerable disagreement, as in the  $U(1)$  results, then it is clear that the variational wave function is not a good representation of the vacuum state. The converse is not true. The fact that these  $SU(2)$  GFMC results are close to the variational estimates does not imply that the variational wave function is a good representation of the  $SU(2)$  vacuum state, for if we compare the results for a different quantity, e.g. the string tension, we may find considerable disagreement. In fact we know from our earlier variational calculation of the string tension<sup>7</sup> that  $u[A_a]$  does not describe the vacuum state for large  $\lambda$  with sufficient accuracy to reproduce the known asymptotic behaviour of the string tension derived from asymptotic freedom.

In view of the comments of the preceding paragraph, it would be very interesting to calculate Monte Carlo estimates of the expectation values of other quantities. Such calculations present no particular difficulty if one is willing to use estimates based

on the mixed expectation value, Eq. (2.41). But these estimates are mainly useful for revealing inadequacies in the trial function, and are not accurate when such inadequacies exist. It would be much more satisfying to compute expectation values exactly, i. e. subject only to statistical errors, rather than from the mixed expectation value, which introduces an unknown systematic error. Such a procedure does exist<sup>1,2</sup>, though it is expected to be very demanding on computer resources if any great precision is to be achieved.

It is interesting to compare the Green's-function Monte Carlo method to the projector Monte Carlo method introduced by Blankenbecler and Sugar<sup>19</sup> and recently applied to the compact U(1) lattice gauge theory in three spatial dimensions by Chin, Koonin, and Negele<sup>20</sup>. In that method  $e^{-TH}$  is used as a projection operator onto the lowest energy state of the system, where  $H = K + V$  is the Hamiltonian and  $T$  is large. The object of the projector Monte Carlo method is to obtain an ensemble of configurations with distribution  $\Psi[A_a]$ .  $T$  is divided into a large number  $N$  of small time intervals  $t = T/N$ , and the ensemble is generated by repeated action of the operator  $e^{-tH}$ . Since  $t$  is small we can write

$$e^{-tH} \cong e^{-tK} e^{-tV}, \quad (4.2)$$

correct to order  $t$ ; in the basis in which  $A_a$  is diagonal, the distribution is

$$\langle [A_a] | e^{-tH} | [A_a'] \rangle \cong \langle [A_a] | e^{-tK} | [A_a'] \rangle e^{-tV[A_a']}. \quad (4.3)$$

The technical details of a calculation with this projector method are essentially the same as those of the GFMC method. In particular, the function that governs diffusion of the configurations is  $\langle [A_a] | e^{-tK} | [A_a'] \rangle$  for both methods. Therefore, it is completely straightforward to modify our GFMC program to carry out the projector Monte Carlo calculation. This would be a useful exercise as a check on the present results.

## Appendix

Iteration of Eq. (2.36) yields a sequence of functions  $\{ F^{(r)}[A_a] \}$  defined by

$$F^{(r+1)}[A_a] = \lambda_0^{(r)} \int d\Omega' G_D[A_a, A_a'] M[A_a'] F^{(r)}[A_a'] \quad (\text{A.1})$$

where  $\lambda_0^{(r)}$  is an arbitrary parameter which may change from one iteration to the next. In the limit  $r \rightarrow \infty$ ,  $F^{(r)}[A_a]$  becomes proportional to  $F[A_a]$ , the eigensolution of Eq. (2.36); thus Eq. (A.1) can be rewritten as

$$F^{(r+1)}[A_a] = \frac{\lambda_0^{(r)}}{\lambda} F^{(r)}[A_a]. \quad (\text{A.2})$$

Integration of this equation implies that

$$\langle W^{(r+1)} \rangle = \frac{\lambda_0^{(r)}}{\lambda} \langle W^{(r)} \rangle \quad (\text{A.3})$$

where  $W^{(r)}$  is the total weight of the ensemble at step  $r$  of the iteration, and  $\langle \rangle$  denotes the expected value. Equation (A.3) provides a simple way to estimate the eigenvalue from the growth or decay of the total weight during the iteration. We refer to this as the growth estimate. In practice we adjust  $\lambda_0^{(r)}$  to maintain a constant total weight, i.e.  $W^{(r+1)} = W^{(r)}$ . In that case we may put

$$\lambda \cong \lambda_0^{(r)}. \quad (\text{A.4})$$

There is a systematic error in Eq. (A.4) caused by making the approximation

$$\frac{\langle W^{(r)} \rangle}{\langle W^{(r+1)} \rangle} \cong \frac{W^{(r)}}{W^{(r+1)}}. \quad (\text{A.5})$$

It can be shown that if this were the only source of error then  $\lambda$  would be bounded by the inequalities

$$\min(\lambda_0^{(r)}) < \lambda < \max(\lambda_0^{(r)}). \quad (\text{A.6})$$

Figure 3 shows the ground state energy per plaquette as a function of  $\lambda$  for the SU(2) gauge theory. Results for the U(1) gauge theory are similar. The crosses are GFMC results obtained from the growth estimate Eq. (A.4). The curves have the same meaning as in Fig. 1. The Monte Carlo results are clearly in error: they are systematically too high. This cannot be attributed to the systematic error in Eq. (A.5) since the inequalities (A.6) do not hold. Rather we believe that the discrepancy is due to the failure of the trial function  $u[A_g]$  to describe the eigenfunction. This is suggested by the fact that the discrepancy increases as  $\lambda$  increases, i. e. as the disordered trial state becomes a less valid approximation.

### Acknowledgements

We are pleased to thank M. Creutz, J. Hetherington, S. Koonin, and J. Negele for conversations and advice regarding this work. This research has been supported by the National Science Foundation under contract PHY-83-05722, and by a grant from Control Data Corporation.

## Footnotes

1. M. H. Kalos, Phys. Rev. 128, 1791 (1962); Phys. Rev. A 2, 250 (1970). M. H. Kalos, D. Levesque, and L. Verlet, Phys. Rev. A 9, 2178 (1974).
2. D. M. Ceperley and M. H. Kalos in Monte Carlo Methods in Statistical Physics, Topics in Current Physics, Vol. 7, ed. K. Binder (Springer-Verlag, 1979).
3. J. Kogut and L. Susskind, Phys. Rev. D 11, 395 (1975).
4. K. Wilson, Phys. Rev. D 10, 2445 (1974).
5. J. Kogut, D. K. Sinclair, and L. Susskind, Nucl. Phys. B114, 199 (1976); T. Banks, S. Raby, L. Susskind, J. Kogut, D.R.T. Jones, P. N. Scharbach, and D. K. Sinclair, Phys. Rev. D 15, 1111 (1977); C. J. Hamer, Nucl. Phys. B146, 492 (1978).
6. References on the use of the variational principle to study the U(1) gauge theory: S. D. Drell, H. R. Quinn, B. Svetitsky, and M. Weinstein, Phys. Rev. D 19, 619 (1979); D. Horn and M. Weinstein, *ibid.* 25, 3331 (1982); U. Heller, *ibid.* 23, 2357 (1981). Numerical variational calculations on the U(1) gauge theory are described in our papers Refs. 7 and 12.
7. References on the use of the variational principle to study the SU(2) gauge theory: D. Horn and M. Karliner, Nucl. Phys. B (to be published); D.W. Heys and D.R. Stump, Phys. Rev. D (to be published).
8. For a recent review article see M. Creutz, L. Jacobs, and C. Rebbi, Phys. Rep. 95, 203 (1983).
9. M. Creutz, Phys. Rev. Lett. 43, 553 (1979); Phys. Rev. D 21, 2308 (1980).
10. D.W. Heys and D.R. Stump, "A variational estimate of the energy of an elementary excitation in the SU(2) lattice gauge theory," in preparation.
11. We refer to the calculations in Refs. 12 and 13 as applications

of the Green's function, Monte Carlo method, although the diffusion operator used there is not a Green's function.

12. D.W. Heys and D.R. Stump, Phys. Rev. D 28, 2067 (1983).
13. D.W. Heys and D.R. Stump, Phys. Rev. D (to be published).
14. We have defined the Hamiltonian H in such a way that the ground-state energy is negative.
15. In quantum mechanics one ordinarily refers to  $\Psi^2$  as the probability distribution. In the GFMC method, however,  $\Psi$  itself is used as a probability distribution; this is possible because the ground-state eigenfunction is positive definite.
16. Note that the variables  $A_a$  and  $\psi$  differ by a factor of 2.
17. It can be shown that the optimal choice of  $F[A_a]$ , i.e. that minimizes the variance in the computed value of  $\lambda$ , is  $M[A_a] u[A_a] \Psi[A_a]$  where  $u[A_a]$  is the best available approximation of the ground-state eigenfunction.
18. The GFMC iteration yields a sequence of ensembles  $E_1, E_2, \dots, E_L$ . We estimate the right-hand side of Eq. (2.41b) by the average
 
$$\frac{1}{L} \sum_{i=1}^L \frac{\langle C/M \rangle_i}{\langle 1/M \rangle_i};$$
 this might make a systematic error, if the fluctuations are large, because of correlations in the values of  $\langle C/M \rangle_i$  and  $\langle 1/M \rangle_i$ .
19. R. Blankenbecler and R. L. Sugar, Phys. Rev. D 27, 1304 (1983).
20. S.A. Chin, J.W. Negele, and S.E. Koonin, Santa Barbara preprint.

## Figure captions

Figure 1. Ground-state energy per plaquette  $E/N_p$  vs. coupling constant  $\lambda$  for (a) the SU(2) gauge theory, and (b) the U(1)<sup>3</sup> gauge theory. The solid curves are the large- $\lambda$  perturbation expansion for the U(1)<sup>3</sup> model, the dashed curves are the variational bounds, and the crosses are the Monte Carlo estimates.

Figure 2. Mean plaquette field  $\phi(p)$  vs. coupling constant  $\lambda$  for (a) the SU(2) gauge theory, and (b) the U(1)<sup>3</sup> gauge theory. The solid curves are the large- $\lambda$  perturbation expansions, the dashed curves are the variational estimates, and the crosses are the Monte Carlo estimates based on the mixed expectation value.

Figure 3. Ground-state energy per plaquette  $E/N_p$  for the SU(2) gauge theory, computed from the growth estimate. The curves have the same meaning as in Fig. 1a.

FIGURE 1a

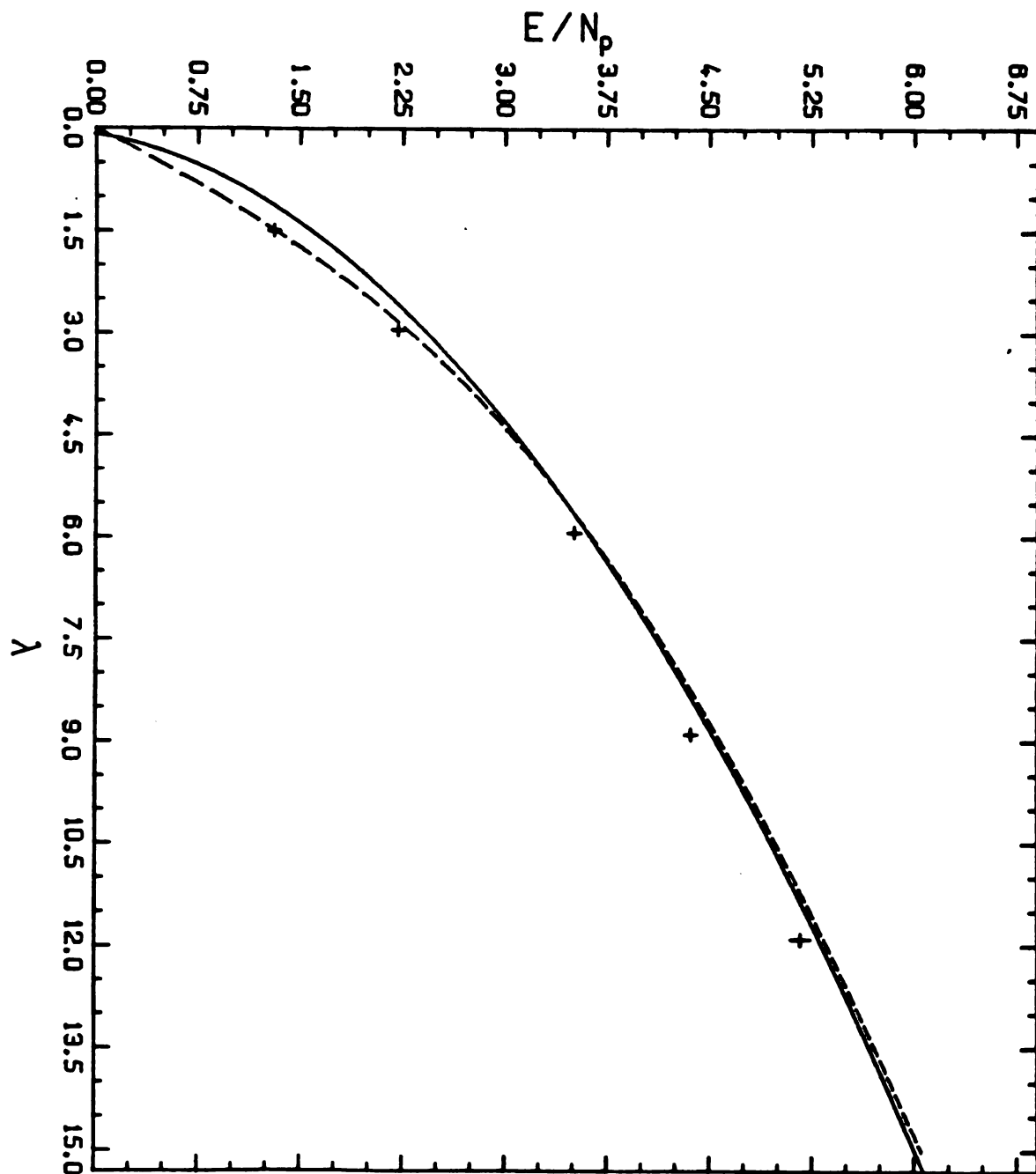


FIGURE 1b

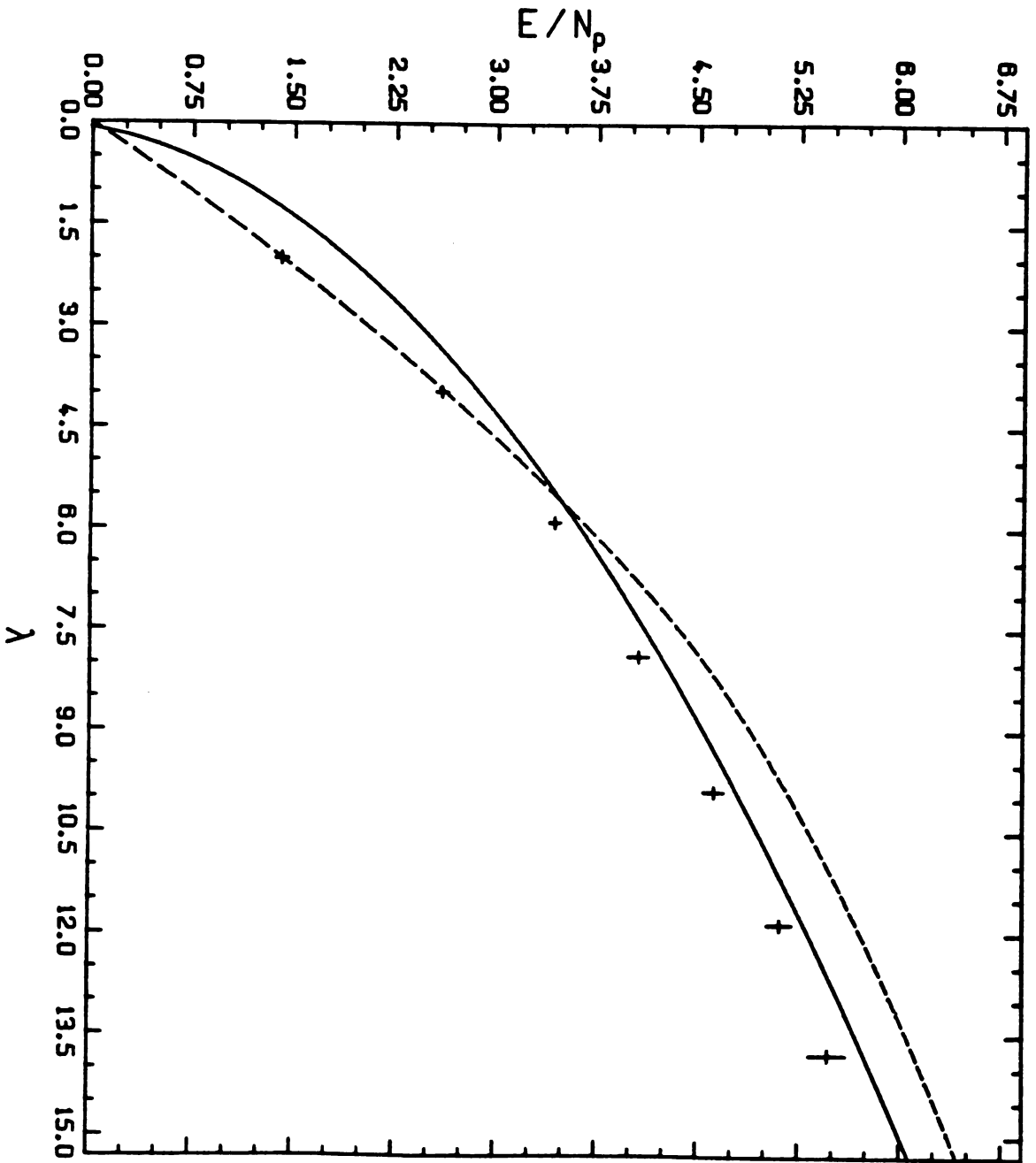


FIGURE 2a

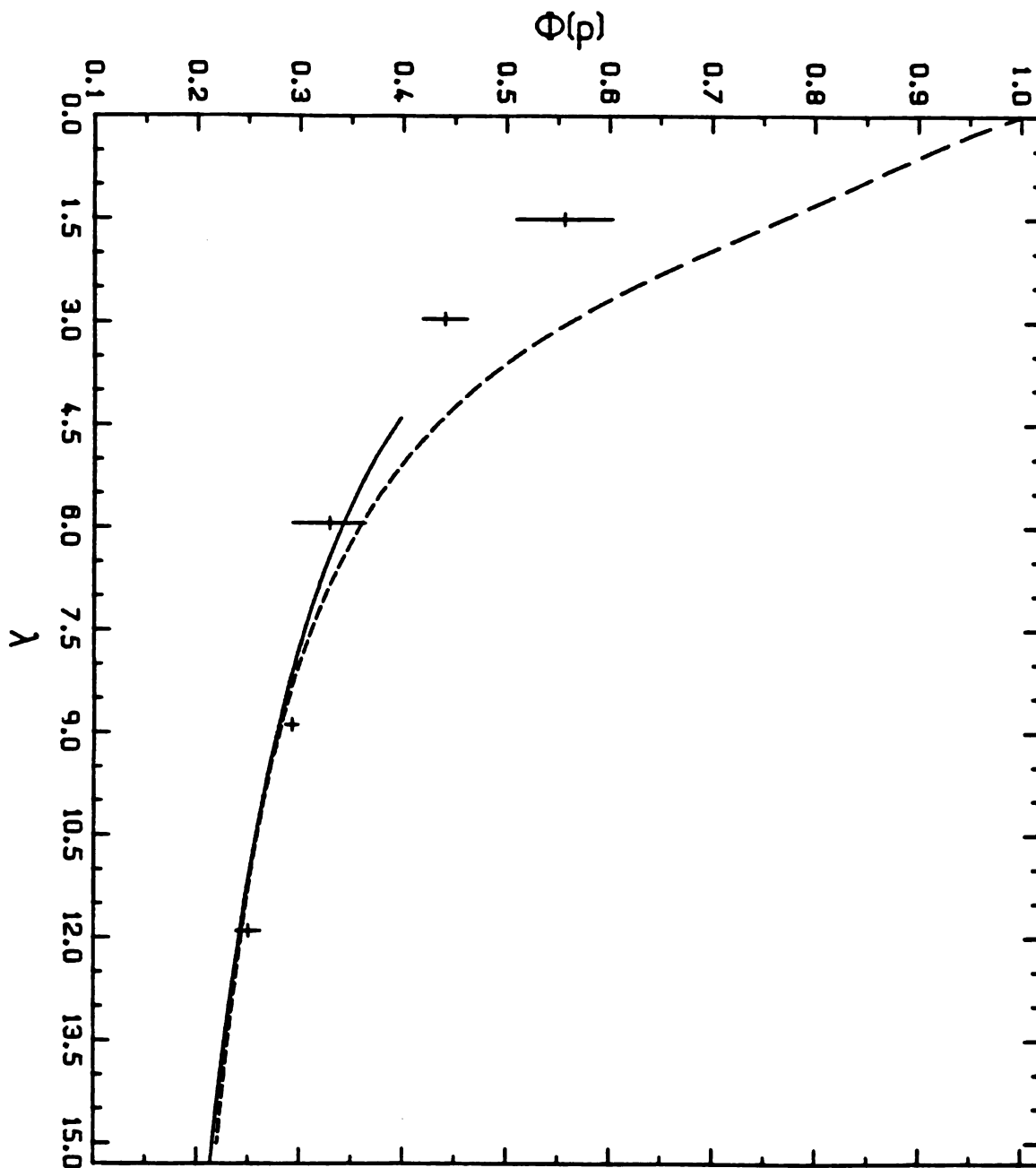


FIGURE 2b

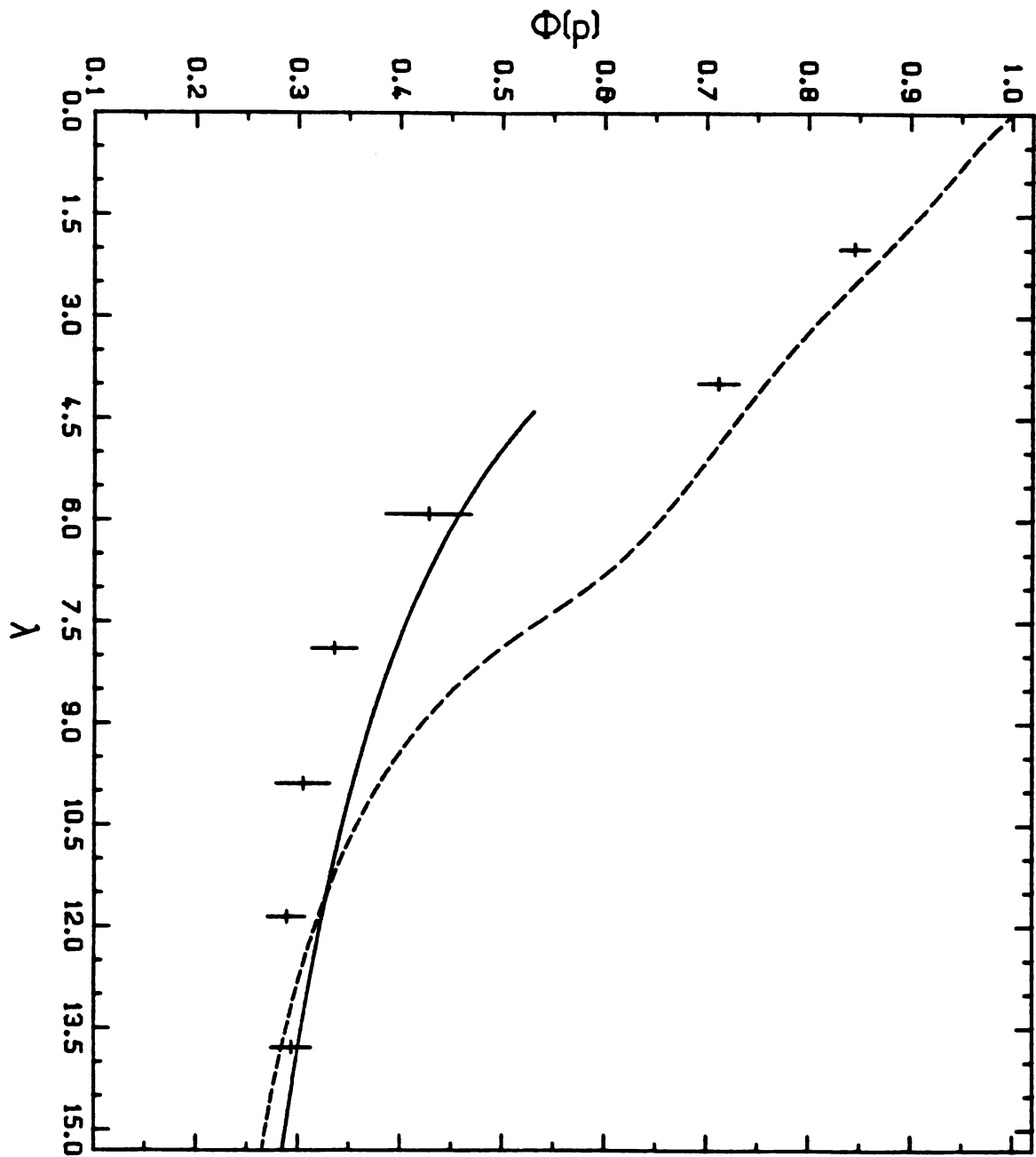
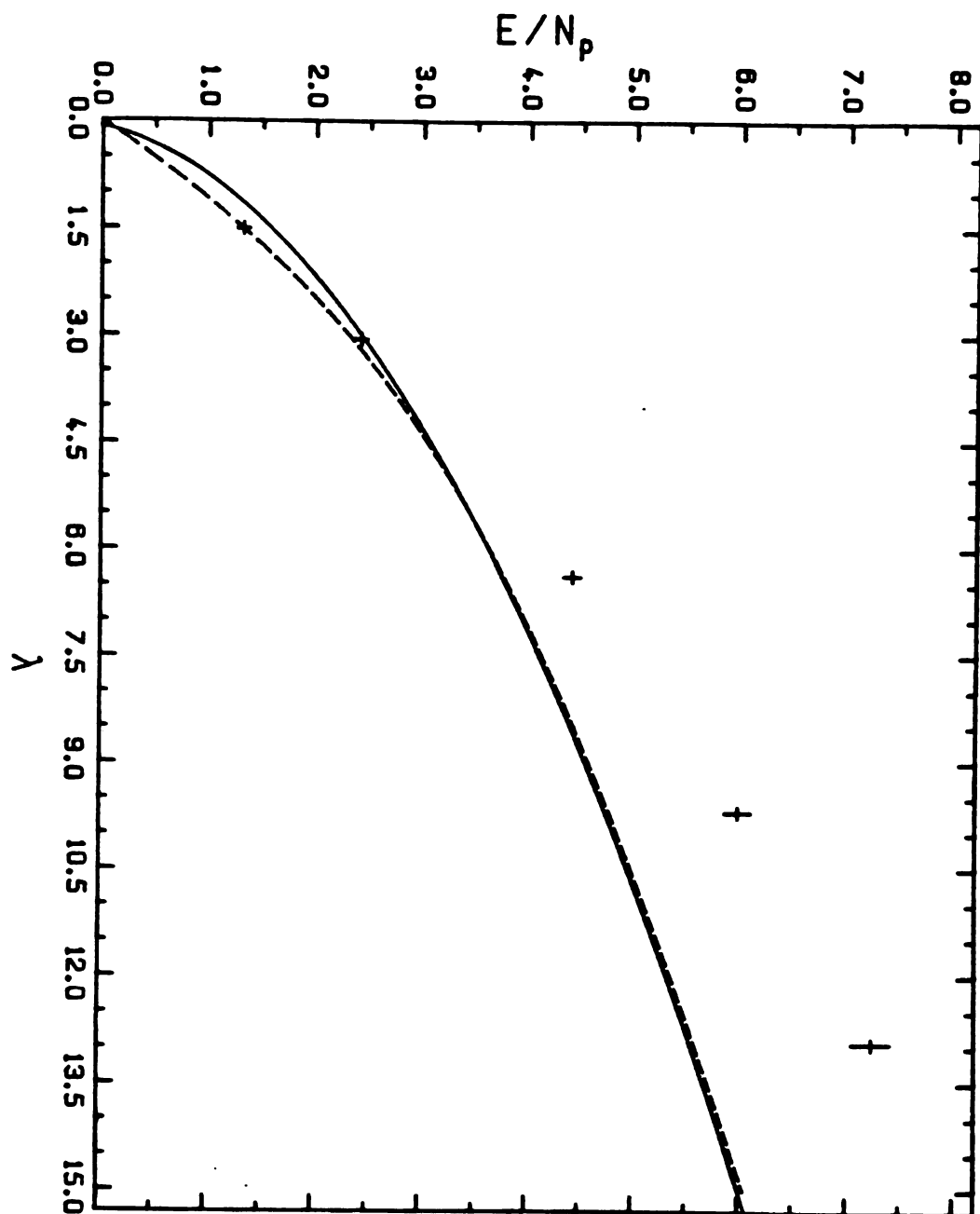


FIGURE 3



## APPENDIX B

Application of the Green's function Monte Carlo method  
to the compact Abelian lattice gauge theory

**PLEASE NOTE:**

Copyrighted materials in this document have not been filmed at the request of the author. They are available for consultation, however, in the author's university library.

These consist of pages:

Appendix B, pages 128-136

---

---

---

---

---

---

**University  
Microfilms  
International**

300 N. ZEEB RD., ANN ARBOR, MI 48106 (313) 761-4700

## Application of the Green's-function Monte Carlo method to the compact Abelian lattice gauge theory

David W. Heys and Daniel R. Stump

*Department of Physics and Astronomy, Michigan State University, East Lansing, Michigan 48824*

(Received 15 June 1983)

We have applied the Green's-function Monte Carlo (GFMC) method to the Hamiltonian formulation of the compact U(1) lattice gauge theory in three and two (space) dimensions on small lattices,  $3 \times 3 \times 3$  and  $5 \times 5$ . The GFMC method is a Monte Carlo method of finding the ground state of a quantum-mechanical system with many degrees of freedom, by iteration of an integral operator of which the ground state is an eigenstate. An interesting aspect of this method is an importance-sampling technique that makes use of a trial wave function to accelerate convergence of the Monte Carlo estimates. We used two importance functions in these calculations, which were designed to be accurate in the small- and large-coupling limits. These importance functions were optimized by the variational principle; the results of the variational calculations are interesting in their own right. Our Monte Carlo results exhibit evidence of the phase transition of the three-dimensional compact U(1) lattice gauge theory, and indicate the nonexistence of a phase transition in the two-dimensional theory.

### I. INTRODUCTION

Lattice gauge theories are used to study quark confinement and other nonperturbative aspects of gauge theories, especially those relevant to quantum chromodynamics. There are two formulations of lattice gauge theories—the path-integral formulation<sup>1</sup> in which all four dimensions are discrete and the Hamiltonian formulation<sup>2</sup> in which time remains a continuum. These theories have been investigated by a number of techniques, e.g., perturbation expansions,<sup>3</sup> mean-field theory, the variational principle,<sup>4</sup> and Monte Carlo methods.<sup>5</sup> The purpose of this paper is to describe an application of the Green's-function Monte Carlo (GFMC) method to the Hamiltonian formulation of the simplest lattice gauge theory, the compact U(1) gauge theory.

The U(1) lattice gauge theory is primarily interesting as a contrast to non-Abelian gauge theories. All lattice gauge theories exhibit the phenomenon of charge confinement in the strong-coupling limit. In non-Abelian gauge theories this phenomenon persists to weak coupling, but in the  $(3+1)$ -dimensional U(1) gauge theory there is a phase transition to a nonconfining state at a finite coupling. These statements have been amply demonstrated in investigations of the *path-integral formulation* of these lattice theories, that use the Metropolis Monte Carlo algorithm to compute the path integral.<sup>6</sup> One goal of our GFMC calculations is to try to verify these statements in the Hamiltonian formulation; the U(1) lattice-gauge-theory calculations to be described are a first step in this direction.

In U(1) lattice gauge theories the transition to a nonconfining ground state occurs in three space dimensions, but not in two dimensions. This difference can be understood in terms of the behavior of long-range topological configurations in these models. In two space dimensions there

exist vortices that maintain confinement at arbitrarily weak coupling; this was first described by Polyakov in an early instanton calculation.<sup>7</sup> Other authors argued that in three space dimensions monopoles undergo an ionization transition at a nonzero value of the coupling constant, below which the ground state is nonconfining.<sup>8</sup> These spatial configurations can be described also as time slices of spacetime configurations in the path integral of the theory.<sup>9</sup> The results of path-integral Monte Carlo calculations have shown that the U(1) gauge theory does have a phase transition in three space dimensions, but not in two dimensions.<sup>10</sup> Our Green's-function Monte Carlo calculations also demonstrate this fact.

The GFMC method is a Monte Carlo method that reveals properties of the ground state of a system with many degrees of freedom. It was developed to solve quantum many-body problems, and has been applied to a number of examples of these.<sup>11,12</sup> We have applied this method to several lattice field theories, including the U(1) lattice gauge theory, and the XY- and Z<sub>2</sub>-gauge models. In our experience it is not difficult to put a lattice field theory into a form to which the GFMC method can be applied; in fact this can usually be done in more than one way, and one has the problem of deciding which one to try.

The simplest quantity to calculate in the GFMC method is the ground-state energy as a function of coupling constant. This quantity is analogous to the average action per plaquette calculated in Monte Carlo studies of the path-integral lattice field theories. In principle the GFMC method can be extended to calculation of other quantities, e.g., the expectation value of a Wilson loop operator; but in practice we have not yet carried out any such calculations on the U(1) gauge theory.

Perhaps the most interesting aspect of the GFMC method is an *importance-sampling technique*.<sup>12</sup> This technique, which is an essential part of the method, makes use

of an approximation of the ground-state wave function, called the importance function, to bias the Monte Carlo diffusion process; this reduces the scale of fluctuations associated with stochastic sampling, and so accelerates the convergence of Monte Carlo estimates to an accurate value of the computed quantity. In principle the results do not depend on the importance function but in practice it should be similar to the ground-state eigenfunction. Normally the importance function is obtained from a variational calculation. One can judge whether a wave function does resemble the eigenfunction by determining whether it performs adequately as an importance function in reducing statistical fluctuations. Thus this approach can be combined with the variational principle in a potentially powerful way: two variational wave functions with about the same energy expectation value can be distinguished on the basis of their performance as importance functions.

The results of our calculations on the U(1) lattice gauge theory show a rather clear signal of the phase transition of this theory in three (space) dimensions. The same signal is not seen in calculations on the two- (space) dimensional theory, as expected since this theory is not supposed to have a phase transition separating confining and nonconfining ground states. Also, the transition in the three-dimensional theory is not a first-order transition. Our calculations have been restricted to small lattices; the results to be described are for  $3 \times 3 \times 3$  and  $5 \times 5$  lattices (remember that the fourth dimension is a continuum). We believe that the quantities that we have calculated are meaningful on such small lattices, and that the only effect of a larger lattice would be to make a sharper transition between strong- and weak-coupling behaviors. Of course this would not be true of *all* quantities.

The paper is organized as follows. Section II is a sketch of the GFMC method, with importance sampling, in general terms. Section III A defines the U(1) lattice gauge theory and our approach to the application of the GFMC method to this model; Sec. III B describes the variational wave functions that we use for importance sampling. These variational calculations are interesting in their own right. Section IV discusses the Monte Carlo results. Section V lists some conclusions.

## II. THE NUMERICAL METHOD

### A. The Green's-function Monte Carlo method

The Green's-function Monte Carlo (GFMC) method was developed as a numerical method for finding the ground state of a Hamiltonian with many degrees of freedom.<sup>13</sup> Let  $H$  be of the form

$$H = H_1 - \lambda H_2, \quad (2.1)$$

where  $H_1$  and  $H_2$  are positive operators and  $\lambda$  is a coupling parameter. Let  $-K^2$  denote the lowest eigenvalue of  $H$ , assumed to be negative. The eigenvalue equation

$$H\psi = -K^2\psi \quad (2.2)$$

can be written as an integral equation, as

$$\psi = \lambda(H_1 + K^2)^{-1}H_2\psi. \quad (2.3)$$

The starting point for the GFMC method is to regard Eq. (2.3) as an equation for  $\psi$  and  $\lambda$  with  $K^2$  given. Next, introduce a complete set of basis states  $|\bar{\mu}\rangle$  for which  $H_2$  is diagonal, i.e.,

$$\langle \bar{\mu} | H_2 | \bar{\mu}' \rangle = V(\bar{\mu}') \delta(\bar{\mu}, \bar{\mu}'). \quad (2.4)$$

The multidimensional quantity  $\bar{\mu}$  that labels one of these states is a configuration of the quantum variables of the model, e.g., a field configuration in a lattice field theory. In what follows we use a notation appropriate for a problem in which  $\bar{\mu}$  has discrete values, but the method applies equally to continuous-valued variables. If  $\psi(\bar{\mu}) = \langle \bar{\mu} | \psi \rangle$  then

$$\psi(\bar{\mu}) = \lambda \sum_{\bar{\mu}'} G(K^2; \bar{\mu}, \bar{\mu}') V(\bar{\mu}') \psi(\bar{\mu}'), \quad (2.5)$$

where

$$G(K^2; \bar{\mu}, \bar{\mu}') = \langle \bar{\mu} | (H_1 + K^2)^{-1} | \bar{\mu}' \rangle. \quad (2.6)$$

The GFMC method applies to integral equations of the form of Eq. (2.5).<sup>14</sup> In applications to quantum many-body problems,  $V$  is a potential and  $G$  a Green's function. In our applications of the GFMC method to lattice field theories we begin also with an equation of the form of Eq. (2.5), but not always one in which  $G$  is introduced as an inverse operator. In particular, for the U(1) lattice-gauge-theory calculations to be described,  $G$  is simply one of the operators in the Hamiltonian.

The GFMC method is a Monte Carlo algorithm for solving Eq. (2.5) by iteration. Let  $\mathcal{E}' = \{\bar{\mu}'_\sigma; \sigma = 1, 2, 3, \dots, N'\}$  be an ensemble of configurations with probability distribution  $\psi_i(\bar{\mu}')$ . One iteration of the equation yields a new ensemble  $\mathcal{E} = \{\bar{\mu}_\sigma; \sigma = 1, 2, 3, \dots, N\}$  where the configurations  $\bar{\mu}_\sigma$  are obtained from the  $\bar{\mu}'_\sigma$  by a process that consists of two steps, branching and diffusion:

(i) Each  $\bar{\mu}'_\sigma$  branches into  $n_\sigma$  new points, where  $n_\sigma$  is an integer picked by a random process such that the expected value of  $n_\sigma$  is  $\lambda_0 V(\bar{\mu}'_\sigma)$ . The possibility  $n_\sigma = 0$  is allowed. Here  $\lambda_0$  is thought of as an approximation of the eigenvalue  $\lambda$ .

(ii) Then each of the  $n_\sigma$  points is moved from  $\bar{\mu}'_\sigma$  to a new configuration  $\bar{\mu}$  chosen from the probability distribution  $P(\bar{\mu}, \bar{\mu}'_\sigma)$  defined by

$$P(\bar{\mu}, \bar{\mu}'_\sigma) = G(\bar{\mu}, \bar{\mu}'_\sigma) / \sum_{\bar{\mu}} G(\bar{\mu}, \bar{\mu}'_\sigma). \quad (2.7)$$

In the lattice field theories to which we have applied this method the denominator of Eq. (2.7) is a constant, independent of  $\bar{\mu}'_\sigma$ . This will be assumed below. Note that the processes (i) and (ii) require that  $V(\bar{\mu})$  and  $G(\bar{\mu}, \bar{\mu}')$  be positive; it may be necessary to add a constant to the Hamiltonian to meet this requirement. The probability distribution  $\psi_f(\bar{\mu})$  of points in the new ensemble  $\mathcal{E}$  is

$$\psi_f(\bar{\mu}) = \frac{1}{N} \sum_{\sigma} P(\bar{\mu}, \bar{\mu}'_\sigma) \lambda_0 V(\bar{\mu}'_\sigma); \quad (2.8)$$

or, in terms of  $\psi_i(\bar{\mu})$ ,

$$\psi_f(\bar{\mu}) = \frac{N'}{N} \sum_{\bar{\mu}'} P(\bar{\mu}, \bar{\mu}') \lambda_0 V(\bar{\mu}') \psi_i(\bar{\mu}') . \quad (2.9)$$

It can be shown that the sequence of ensembles generated by iterating the process just described converges to an ensemble for which the probability distribution is  $\psi(\bar{\mu})$ , the solution of Eq. (2.5). The parameter  $\lambda_0$  determines how the ensemble size changes on further iteration: after the process has converged, so that  $\psi_i = \psi_f = \psi$  in Eq. (2.9), we shall have on average

$$\frac{N}{N'} = \frac{\lambda_0}{\lambda} \left[ \sum_{\bar{\mu}} G(\bar{\mu}, \bar{\mu}') \right]^{-1} , \quad (2.10)$$

where it should be remembered that the factor  $\sum_{\bar{\mu}} G(\bar{\mu}, \bar{\mu}')$  is independent of  $\bar{\mu}'$ . This provides a way to determine the eigenvalue  $\lambda$ , which in the problem defined by Eq. (2.1) is the value of coupling constant for which the ground-state energy is  $-K^2$ .

In practice, one readjusts the value of  $\lambda_0$  every  $n$  iterations so as to keep the ensemble size approximately constant. The adjusted value of  $\lambda_0$  converges to  $\lambda$  times  $\sum_{\bar{\mu}} G(\bar{\mu}, \bar{\mu}')$ .

The method described here yields a numerical determination of the eigenvalue  $\lambda$ , and a sequence of ensembles of configurations with probability distribution  $\psi(\bar{\mu})$  (after convergence). It is also possible to invent ways to extend the method to calculations of other quantities, e.g., expectation values of operators, but in practice these require a large increase in computation time.

### B. Importance sampling

For problems with many degrees of freedom it is advantageous, and as a practical matter even necessary, to modify the GFMC method by use of an importance sampling technique.<sup>12,13</sup> A wave function  $\psi_T(\bar{\mu})$ , which should resemble the ground-state eigenfunction  $\psi(\bar{\mu})$  as closely as possible, is introduced by rewriting the integral equation, Eq. (2.5), in terms of a new function:

$$F(\bar{\mu}) = \psi_T(\bar{\mu}) \psi(\bar{\mu}) \quad (2.11)$$

as

$$F(\bar{\mu}) = \lambda \sum_{\bar{\mu}'} \frac{\psi_T(\bar{\mu}')}{\psi_T(\bar{\mu})} G(\bar{\mu}, \bar{\mu}') V(\bar{\mu}') F(\bar{\mu}') . \quad (2.12)$$

Now one regards  $F(\bar{\mu})$  and  $\lambda$  as the unknown eigenfunction and eigenvalue.

The iterative diffusion process described in Sec. II A is used again to generate ensembles with probability distribution  $F(\bar{\mu})$ . The diffusion process is changed in two ways by the presence of the importance function  $\psi_T(\bar{\mu})$ . First, the probability distribution that governs diffusion of the particles is now

$$\frac{\psi_T(\bar{\mu}) G(\bar{\mu}, \bar{\mu}') [\psi_T(\bar{\mu}')]^{-1}}{\sum_{\bar{\mu}'} \psi_T(\bar{\mu}') G(\bar{\mu}, \bar{\mu}') [\psi_T(\bar{\mu}')]^{-1}} . \quad (2.13)$$

The effect of this change is that the diffusion process is biased in favor of moves  $\bar{\mu}' \rightarrow \bar{\mu}$  for which  $\bar{\mu}$  is in the region of configuration space where  $\psi_T(\bar{\mu})$  is large. If  $\psi_T(\bar{\mu})$  is at least qualitatively similar to the eigenfunction  $\psi(\bar{\mu})$ , this biasing reduces the fluctuations due to stochastic sampling, and so speeds up the convergence to accurate numerical estimates.

The second change in the diffusion process is a normalization effect in the selection of  $n_o$ , the number of new points generated from the point  $\bar{\mu}'_o$ . The expected value of  $n_o$  should now be

$$\langle n_o \rangle = \lambda_0 V(\bar{\mu}'_o) \sum_{\bar{\mu}} \psi_T(\bar{\mu}) G(\bar{\mu}, \bar{\mu}'_o) [\psi_T(\bar{\mu}'_o)]^{-1} . \quad (2.14)$$

For  $\psi_T(\bar{\mu}) = 1$ , i.e., without importance sampling, the normalizing sum is independent of  $\bar{\mu}'_o$  in the lattice field theories we have considered, so this factor would not be needed. But for a nontrivial  $\psi_T(\bar{\mu})$ , the computation of the normalizing sum may be the trickiest part of the program.<sup>15</sup>

Again it can be shown that the iteration converges to ensembles with probability distribution  $F(\bar{\mu})$ , the solution of Eq. (2.12). Also, after convergence the expected change in ensemble size for one iteration is given by

$$\frac{N}{N'} = \frac{\lambda_0}{\lambda} . \quad (2.15)$$

Importance sampling reduces the fluctuation of ensemble size, so that Eq. (2.15) converges more rapidly to an accurate estimate of  $\lambda$ . The optimal choice of  $\psi_T(\bar{\mu})$  can be derived, and turns out to be simply related to the exact eigenfunction  $\psi(\bar{\mu})$ ; this choice would actually reduce fluctuations to zero.

The importance-sampling technique provides a way to estimate ground-state expectation values that requires little additional computation. Suppose the eigenfunction  $\psi(\bar{\mu})$  differs from the trial function  $\psi_T(\bar{\mu})$  by a small amount of order  $\epsilon$ ; then to order  $\epsilon^2$  we have

$$\frac{\langle \psi | A | \psi \rangle}{\langle \psi | \psi \rangle} = 2 \frac{\langle \psi | A | \psi_T \rangle}{\langle \psi | \psi_T \rangle} - \frac{\langle \psi_T | A | \psi_T \rangle}{\langle \psi_T | \psi_T \rangle} . \quad (2.16)$$

Here the left-hand side is the desired expectation value of an operator  $A$ ; the first term on the right is twice the average of  $A$  in the ensembles generated by the GFMC iteration of Eq. (2.12), and the other term is simply evaluated for  $\psi_T$ . The estimate (2.16), called the mixed expectation value, has statistical error from the fact that it involves stochastic sampling, plus systematic error from the fact that it is valid to order  $\epsilon^2$  only. It is trustworthy only if  $\langle \psi | A | \psi \rangle$  and  $\langle \psi_T | A | \psi_T \rangle$  are not too different.

In summary, the importance-sampling method outlined above is obviously most useful when an accurate approximation of  $\psi(\bar{\mu})$  is known, e.g., from a variational calculation. Then the GFMC approach calculates the corrections to that approximation exactly (up to statistical errors due to sampling fluctuations). But even if  $\psi_T(\bar{\mu})$  is not partic-

ularly accurate it may still perform the function of importance sampling in reduction of fluctuations, provided the diffusion by Eq. (2.13) is biased in a qualitatively correct way.

### III. THE LATTICE GAUGE THEORY

#### A. Compact U(1) lattice gauge theory

The Hamiltonian of the U(1) lattice gauge theory is<sup>16</sup>

$$H = \frac{1}{2}g^2 \sum_l E^2(l) - \frac{1}{g^2} \sum_p [1 + \cos B(p)], \quad (3.1)$$

where  $E(l)$  is the electric field on lattice link  $l$  and  $B(p)$  is the magnetic field on lattice plaquette  $p$ . If  $p$  is the plaquette associated with site  $\bar{x}$  and directions  $ij$  then

$$B(p) = A(\bar{x} + \hat{i}, j) - A(\bar{x}, j) - A(\bar{x} + \hat{j}, i) + A(\bar{x}, i), \quad (3.2)$$

where  $A(\bar{x}, i)$  is the gauge field on the link  $l$  associated with site  $\bar{x}$  and direction  $i$ . The fundamental commutation relation is

$$[E(l), A(l')] = -i\delta(l, l'). \quad (3.3)$$

The variables  $A(l)$  or  $B(p)$  are restricted to lie in the range  $(-\pi, \pi)$ .

In our application of the GFMC method to the U(1) lattice gauge theory we arrived at the basic integral Eq. (2.5) by a somewhat different path than that described in Sec. II A. By a special choice of basis states we avoided the use of an inverse operator, i.e., a Green's function, in constructing our form of Eq. (2.5). Still, since the ultimate equation does have that form the GFMC method applies.

We shall consider a basis in which the *electric field energy* is diagonal. Specifically, let the ground-state eigenfunction be written in the gauge-invariant form

$$\psi = \sum_{\{n(p)\}} \exp \left[ i \sum_p n(p) B(p) \right] \phi[n(p)], \quad (3.4)$$

where  $n(p)$  are *integer-valued* plaquette variables. Let  $-g^2 Q^2/2$  denote the vacuum energy. Then the eigenvalue equation

$$H\psi = -\frac{1}{2}g^2 Q^2 \psi \quad (3.5)$$

becomes, in terms of the  $n(p)$ -space wave function,

$$\begin{aligned} -\frac{1}{2}g^2 Q^2 \phi[n(p)] &= \frac{1}{2}g^2 S[n(p)] \phi[n(p)] \\ &\quad - \frac{1}{g^2} \sum_{\{n'(p)\}} G[n(p), n'(p)] \phi[n'(p)]. \end{aligned} \quad (3.6)$$

Here the diagonal operator  $S[n(p)]$ , which comes from the electric field energy, is

$$S[n(p)] = \sum_{p, p'} n(p) n(p') \Delta(p, p'), \quad (3.7a)$$

$$\Delta(p, p') = \sum_l \frac{\partial B(p)}{\partial A(l)} \frac{\partial B(p')}{\partial A(l)}. \quad (3.7b)$$

The nondiagonal operator  $G[n, n']$ , which comes from the magnetic field energy, is

$$\begin{aligned} G[n(p), n'(p)] &= \sum_{p_0} \{ \delta[n(p), n'(p)] \\ &\quad + \frac{1}{2} \delta[n(p), n'(p) + \delta_{p_0}] \\ &\quad + \frac{1}{2} \delta[n(p), n'(p) - \delta_{p_0}] \}. \end{aligned} \quad (3.8)$$

$G[n, n']$  will play the role of the Green's function in the GFMC iteration, i.e., of the function that controls diffusion of the points in the space of  $n(p)$ -configurations; but note that  $G[n, n']$  is not the *inverse* of either operator in the original Hamiltonian.

To put the equation in the form of Eq. (2.5), define a new wave function

$$\chi[n(p)] = \frac{1}{2}g^2 \{ Q^2 + S[n(p)] \} \phi[n(p)]. \quad (3.9)$$

Then the equation obeyed by  $\chi[n(p)]$  is

$$\chi[n(p)] = \lambda \sum_{\{n'(p)\}} G[n(p), n'(p)] V[n'(p)] \chi[n'(p)], \quad (3.10)$$

where

$$\lambda = 2/g^4 \quad (3.11)$$

and

$$V[n(p)] = (Q^2 + S[n(p)])^{-1}. \quad (3.12)$$

We have applied the GFMC method to Eq. (3.10). The diffusion step in the GFMC iteration involves moving a point in  $n(p)$ -space from  $n'(p)$  to  $n(p)$  by the function  $G[n, n']$ ; the definition of  $G[n, n']$ , Eq. (3.8), implies that  $n(p)$  and  $n'(p)$  differ at most by one unit on one plaquette.

We have obtained Monte Carlo results only for the smallest lattice in three dimensions, of size  $3 \times 3 \times 3$ . (It should be remembered that "time" is a fourth continuous dimension in the Hamiltonian formulation.) Although this is a small lattice size compared to those used in studies of the path-integral formulation of lattice gauge theories by the Metropolis Monte Carlo algorithm, it is not small compared to other applications of the GFMC method; it has 81 independent quantum variables in the original Hamiltonian. With these many variables it is essential to use importance sampling in the GFMC program. The importance-sampling functions that we used were obtained from variational calculations, described next.

#### B. Variational calculations

The first variational wave function is

$$\psi_1 = \prod_p u[B(p)]; \quad (3.13)$$

the energy  $\langle \psi_1 | H | \psi_1 \rangle$  is to be minimized with respect to the choice of the single-plaquette function  $u(B)$ .<sup>17</sup> The minimum occurs if  $u(B)$  is the ground-state eigenfunction of the operator

$$h = -4 \frac{\partial^2}{\partial B^2} + \lambda(1 - \cos B), \quad (3.14)$$

where  $-\pi \leq B \leq \pi$ . This is the Hamiltonian of a quantum pendulum. The resulting variational estimate of the vacuum energy per lattice plaquette is

$$-\frac{1}{2}g^2 Q^2/N_p = -\frac{1}{2}g^2(2\lambda - e_0), \quad (3.15)$$

where  $e_0$  is the smallest eigenvalue of  $h$ . The energy  $-Q^2$  is not really the natural energy to use in describing our results; instead we shall use  $E_0$ , defined by the relation

$$-\frac{1}{2}g^2 Q^2 = -\frac{1}{2}g^2(2\lambda N_p - E_0). \quad (3.16)$$

Note that  $E_0$  is the smallest eigenvalue of

$$\sum_l E^2(l) + \lambda \sum_p [1 - \cos B(p)], \quad (3.17)$$

where  $\lambda = 2/g^4$ . The first variational estimate of  $E_0$  is

$$E_0/N_p = e_0. \quad (3.18)$$

It can easily be shown that the small- and large- $\lambda$  limits of  $e_0$  are

$$\begin{aligned} e_0 &\simeq \lambda - \frac{\lambda^2}{8} + \frac{7\lambda^4}{2048} + O(\lambda^6) \text{ as } \lambda \rightarrow 0, \\ e_0 &\simeq \sqrt{2\lambda} - \frac{1}{4} + O(\lambda^{-1/2}) \text{ as } \lambda \rightarrow \infty. \end{aligned} \quad (3.19)$$

For comparison these limits of  $E_0/N_p$  are, for an  $n \times n \times n$  lattice,

$$\begin{aligned} E_0/N_p &\simeq \lambda - \frac{\lambda^2}{8} + \frac{3\lambda^4}{10240} + O(\lambda^6) \text{ as } \lambda \rightarrow 0, \\ E_0/N_p &\simeq \sqrt{2\lambda} c(n) - \frac{1}{4}c^2(n) + O(\lambda^{-1/2}) \text{ as } \lambda \rightarrow \infty, \end{aligned} \quad (3.20)$$

where  $c(n)$  is a dimensionless number, e.g.,

$$c(3) = 0.787, \quad c(5) = 0.795, \quad c(\infty) = 0.796. \quad (3.21)$$

Note that  $e_0$  and  $E_0/N_p$  have the same small- $\lambda$  limit, but that  $E_0/N_p$  is smaller than  $e_0$  in the large- $\lambda$  limit.

In the trial wave function  $\psi_1$  the magnetic fields on different plaquettes are uncorrelated;  $\psi_1$  describes a disordered state in  $B(p)$ -space. In particular, the expectation value of a Wilson loop operator in the state  $\psi_1$  decreases exponentially with the loop area,

$$\left\langle \psi_1 \left| \prod_{p \in L} e^{iB(p)} \right| \psi_1 \right\rangle = \exp \left[ - \sum_{p \in L} \gamma \right], \quad (3.22)$$

where

$$\gamma = -\ln \int_{-\pi}^{\pi} dB |u(B)|^2 e^{iB}. \quad (3.23)$$

Since the vacuum state of the three-dimensional U(1) lattice gauge theory is, for weak coupling, an ordered state in which the expectation value of the Wilson loop operator

decreases exponentially with the loop perimeter, the state  $\psi_1$  should not be a good approximation of the eigenstate  $\psi$  for weak coupling, i.e., for large  $\lambda = 2/g^4$ . This may already be seen in the difference between  $E_0/N_p$  and  $e_0$  in the large- $\lambda$  limit.

The second variational wave function is written as a probability amplitude in  $n(p)$ -space, as

$$\phi_2 = \exp \left[ -\frac{1}{2}\alpha \sum_{p,p'} n(p)M(p,p')n(p') \right]. \quad (3.24)$$

Here  $\alpha$  is the variational parameter and  $M(p,p')$  is the matrix that reproduces the ground state of  $H$  in a noncompact harmonic approximation of the U(1) lattice gauge theory. This approximation consists of two parts: replacement of  $1 - \cos B$  by  $B^2/2$ , and extension of the range of  $B$  from  $(-\pi, \pi)$  to  $(-\infty, \infty)$ . The resulting model is solvable since its Hamiltonian is quadratic; the ground-state wave function is Eq. (3.24) with  $\alpha = 1$ , but where the plaquette variables  $n(p)$  take a continuum of values. It should be emphasized that  $\phi_2$  is not the wave function of a noncompact harmonic approximation in our calculations, because the variables  $n(p)$  are restricted to integer values; the function in  $A(l)$ -space, defined by Eq. (3.4), is periodic in  $A(l)$ . The matrix  $M(p,p')$  is, for an  $n \times n \times n$  lattice,

$$\begin{aligned} M(p,p') &= \frac{g^2}{n^3} \sum_{\vec{v}} \exp \left[ \frac{2\pi i}{n} \vec{v} \cdot (\vec{x} - \vec{x}') \right] (f^2 \delta_{kk'} - f_k^2 f_{k'}) / f, \\ f_k &= 1 - \exp(2\pi i v_k / n), \quad f = (f_k^2 f_{k'})^{1/2}; \end{aligned} \quad (3.25)$$

here  $p, p'$  are the plaquettes  $(\vec{x}, k)$  and  $(\vec{x}', k')$  with normal directions  $k, k'$ , and the sums over  $v_i$  run from 1 to  $n$ .

The harmonic wave function described in the previous paragraph is equivalent to the variational wave function considered by Horn and Weinstein,<sup>4</sup> although it is written in a somewhat different form. Our calculations use the reciprocal space of field configurations  $n(p)$  conjugate to the plaquette variable  $B(p)$ . Horn and Weinstein work in the space of configurations of the lattice variable  $A(l)$ , and maintain gauge invariance by a projection technique involving functional integration. In spite of the formal differences, we believe that the two approaches are equivalent.

We were unable to calculate analytically the expectation value of  $H$  in the state  $\phi_2$  (Ref. 18); instead we evaluated  $\langle \phi_2 | H | \phi_2 \rangle$  using the Metropolis Monte Carlo algorithm to generate a set of configurations with probability distribution  $\phi_2^2$ . The result is shown in Fig. 1, graphs of the value of the variational parameter  $\alpha$  that minimize  $\langle \phi_2 | H | \phi_2 \rangle$  vs coupling parameter  $\lambda = 2/g^4$ . Figure 1(a) is for a three-dimensional lattice of size  $3 \times 3 \times 3$ ; values of  $\alpha$  for lattice size  $5 \times 5 \times 5$  differ very little from those for  $3 \times 3 \times 3$ . Figure 1(b) is for a two-dimensional lattice of size  $5 \times 5$ . At weak coupling, i.e., large  $\lambda$ ,  $\alpha$  approaches 1, the value that corresponds to the harmonic approximation. At strong coupling the wave function is sharply peaked at small  $n(p)$ , corresponding to a disordered state in the space of magnetic field configurations. The rapid variation of  $\alpha$  for  $\lambda$  near 1 in the three-dimensional case is presumably a reflection of the phase transition of the U(1)

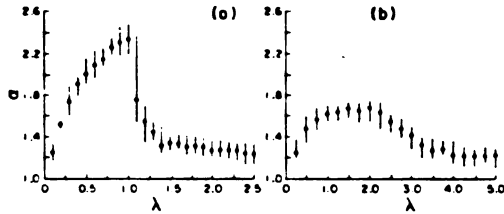


FIG. 1. Variational parameter  $\alpha$  vs coupling constant  $\lambda$  for (a) three dimensions and (b) two dimensions. Error bars include systematic error.

lattice gauge theory. The character of the transition seen in the variational calculation is consistent with a second-order transition<sup>19</sup>: within the accuracy of our Monte Carlo determination of  $\langle \phi_2 | H | \phi_2 \rangle$  there is only one minimum for any  $\lambda$ , the position of which varies continuously as shown in Fig. 1. For a first-order transition, in contrast, one might expect to have two *local* minima at different values of  $\alpha$  such that the position of the absolute minimum changes discontinuously from one to the other at some transition point  $\lambda_c$ .

Figure 2 shows variational estimates of  $E_0/N_p$  for different values of  $\lambda$  for both of the trial wave functions  $\psi_1$  and  $\phi_2$ , along with the large- and small- $\lambda$  limits of  $E_0/N_p$  given for three-dimensions in Eq. (3.20). Again Fig. 2(a) is for a  $3 \times 3 \times 3$  lattice and Fig. 2(b) is for a  $5 \times 5$  lattice.

Note that in the weak-coupling region, i.e.,  $\lambda > 1$ , the second variational estimate is the better one; this is as anticipated since the construction of  $\phi_2$  incorporates the correlations between magnetic fields on different plaquettes appropriate to the weak-coupling limit (with  $\alpha = 1$ ). Note too that the two variational estimates are almost the same in the strong-coupling region.

The variational calculations show an interesting difference between the two- and three-dimensional theories: the transition between small- and large- $\lambda$  behavior is much sharper in the three-dimensional theory. This agrees with the conjecture that there is no phase transition to a non-confining phase in the two-dimensional theory. On the other hand, the variational estimate based on the harmonic wave function  $\phi_2$  is better at large  $\lambda$ , even in the two-dimensional theory; evidently the vacuum state is not as simple as one with no correlations between the  $B$  fields on different plaquettes. This is consistent with the speculation that it is the influence of long-range topological defects, two-dimensional vortices, that maintains disorder in the two-dimensional theory at large  $\lambda$  (Ref. 7); the vortices live on top of an essentially harmonic wave function.

#### IV. MONTE CARLO RESULTS

In this section we shall describe the results of GFMC calculations for the compact U(1) lattice gauge theory. The basic equation that defines our GFMC algorithm is Eq. (3.10). A brief recapitulation of the method is as follows: Each complete Monte Carlo iteration of Eq. (3.10) replaces an ensemble  $\mathcal{E}' = \{n'_\sigma(p); \sigma = 1, 2, \dots, N'\}$  of  $N'$  configurations of the integer-valued plaquette variables

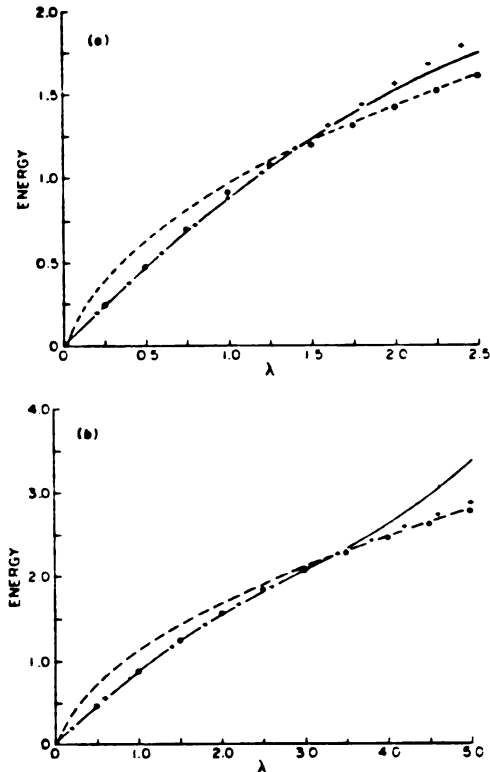


FIG. 2. (a) Variational estimates of the vacuum energy per plaquette vs coupling constant  $\lambda$  for the three-dimensional theory. The solid and dashed curves are from perturbation expansions at small and large  $\lambda$ , respectively. The crosses (+) and circles (○) are variational estimates with trial wave functions  $\psi_1$  and  $\phi_2$ , respectively. (b) Variational estimates of the vacuum energy per plaquette for the two-dimensional theory. The curves and points have the same meaning as in (a).

$n(p)$  by a new ensemble  $\mathcal{E} = \{n_\sigma(p); \sigma = 1, 2, \dots, N\}$ . This replacement is a two-step process involving branching, which is governed by  $V[n'_\sigma(p)]$ , and diffusion, which is governed by  $G[n(p), n'_\sigma(p)]$ . The change in ensemble size  $N' \rightarrow N$  provides a measurement of the eigenvalue  $\lambda$ . Importance sampling is provided by the trial wave functions  $\psi_1$  and  $\phi_2$  defined in Sec. III B.

Figure 3 shows Monte Carlo estimates of the energy per plaquette  $E_0/N_p$ , i.e., the quantity defined in Eqs. (3.16) and (3.17), for three and two (space) dimensions; the lattice sizes are  $3 \times 3 \times 3$  and  $5 \times 5$ . The two sets of points on this graph are the results obtained with the two importance functions. The curves are the ordinary variational estimates, of which individual points were shown in Fig. 2. These curves are *not* perturbation theory curves; however, the trial wave function  $\psi_1$  is known to be an accurate approximation of the eigenfunction at small  $\lambda$ , and  $\phi_2$  is accurate at large  $\lambda$ . By the variational principle these curves are rigorously upper bounds on the energy  $E_0$ .

We shall describe the results as estimates of  $E_0/N_p$  vs  $\lambda$ , but it should be recalled that  $E_0$  is the input quantity

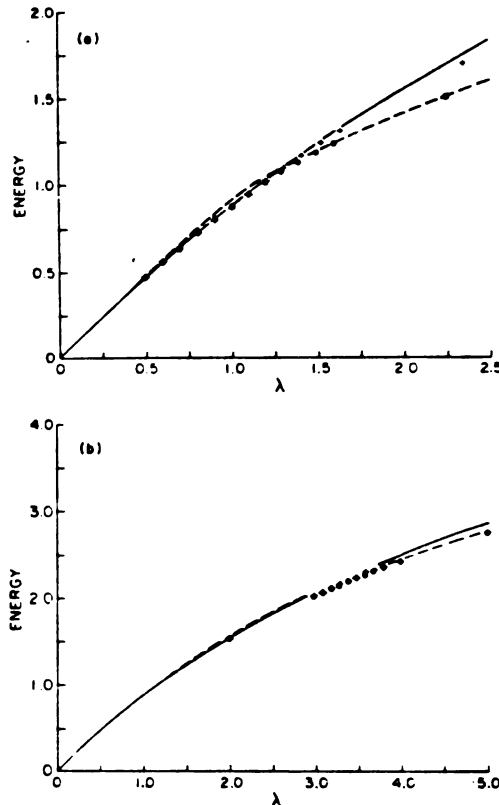


FIG. 3. (a) Monte Carlo estimates of the vacuum energy per plaquette vs coupling constant  $\lambda$  for the three-dimensional theory. The solid and dashed curves are variational estimates with trial function  $\psi_1$  and  $\psi_2$ , respectively. The crosses (+) and circles (o) are Monte Carlo results with importance functions  $\psi_1$  and  $\psi_2$ , respectively. (b) Monte Carlo estimates of the vacuum energy per plaquette for the two-dimensional theory. The curves and points have the same meaning as in (a).

and  $\lambda$  the unknown eigenvalue that is output by the GFMC calculation.

These calculations used ensembles of approximately 100 configurations; this size fluctuates with each iteration. We also checked some results with larger ensembles. Typically 1000 iterations were used to obtain the estimate of  $E_0/N_p$  shown. Each computation took roughly 1.5 min on a CDC Cyber 750 computer. To be sure of convergence we checked that the final estimate is independent of the starting ensemble; e.g., that an initial ensemble with all values of  $n(p)$  equal to zero gives the same final value as one with randomly generated values of  $n(p)$ .

The Monte Carlo results obtained with importance function  $\psi_2$  lie on a continuous curve that interpolates between the known small- $\lambda$  and large- $\lambda$  dependences. These results can be thought of as a calculation of the correction to the variational energy. The correction is very small except when  $\lambda \sim 1$  because the variational estimate with trial function  $\psi_2$  accurately describes the ground state in both the small- and large- $\lambda$  limits. The Monte Carlo correction

for  $\lambda \sim 1$  is just enough to push the energy below the variational bound provided by the other trial function  $\psi_1$ .

In contrast, the Monte Carlo results with importance function  $\psi_1$  show an interesting failure: for  $\lambda \geq 1.3$  these estimates are not consistent with the variational bound due to  $\psi_2$ . We interpret this as the strongest evidence in our calculations of the existence of a phase transition in the three-dimensional U(1) gauge theory. This conclusion is based on the following argument: The trial wave function  $\psi_1$ , which has no correlation between the magnetic field values on different plaquettes, is qualitatively different than the ground-state eigenfunction if  $\lambda \geq 1.3$ , which instead has the long-range correlations associated with the matrix  $M(p, p')$  that defines the harmonic wave function  $\psi_2$  in Eq. (3.24). Therefore the importance function  $\psi_1$  fails to direct the diffusion process to the region of the space of configurations where the most significant ground-state configurations are located. Furthermore, the disordered phase of the system should still exist as a low-energy state concentrated in the same region of configuration space as the uncorrelated importance function  $\psi_1$ . Apparently this uncorrelated state is metastable with respect to the GFMC iteration; for a finite-ensemble size and iteration time it cannot converge to the actual ground state  $\psi$ . Similar metastable states are exhibited as hysteresis loops in Monte Carlo studies of the path-integral formulation of lattice gauge theories. So, for  $\lambda \geq 1.3$  there are two qualitatively different low-energy states: the actual ground state described well by the harmonic wave function  $\psi_2$ , and the uncorrelated state which is metastable with respect to GFMC iteration with the uncorrelated importance function  $\psi_1$ .

The results of the GFMC calculations on the two-dimensional theory are quite different. These are shown in Fig. 3(b). The Monte Carlo results obtained with the two different importance functions agree with one another over the entire range of  $\lambda$ , and are consistent with both variational bounds. There is no sign of a metastable state. We take this as the best evidence of the nonexistence of a phase transition in the two-dimensional U(1) lattice gauge theory. In particular, it seems that either of the trial wave functions  $\psi_1$  and  $\psi_2$  resembles the eigenfunction closely enough to be used successfully as an importance function for any  $\lambda$ .

The crossover from small- $\lambda$  to large- $\lambda$  behavior in the three-dimensional theory occurs continuously as a function of  $\lambda$ . Thus the phase transition appears not to be a first-order transition. We have also investigated a model with a first-order phase transition, the  $Z_2$ -gauge theory in three (space) dimensions, by the GFMC method. There, in contrast to the U(1) theory, the slope of the curve of energy vs  $\lambda$  changes discontinuously at  $\lambda = 1$ , the self-duality point, even in a lattice as small as  $3 \times 3 \times 3$ . There also we find metastable states by using as an importance function a wave function with the order or disorder suited to the other phase.

Another quantity that we have computed is the expectation value of the  $B$  field; more precisely the quantity

$$\mathcal{B} = \langle \psi | 1 - \cos B(p) | \psi \rangle. \quad (4.1)$$

Note that  $W$  is not independent of the energy per plaquette  $E_0/N_p$ , since

$$W = \frac{\partial}{\partial \lambda} \left[ \frac{E_0}{N_p} \right]. \quad (4.2)$$

However, we calculate  $W$  directly from Eq. (4.1), not by using Eq. (4.2). The computed values of  $W$  are shown as a function of coupling constant  $\lambda$  in Fig. 4, for the three-dimensional theory. There the curves show the perturbation expansions of the expectation value of  $1 - \cos B(p)$  for large and small  $\lambda$ . The points are variational and Monte Carlo estimates; the Monte Carlo points are computed from the mixed expectation value, i.e., Eq. (2.16), for the two importance functions.

Figure 4(a) is for the harmonic trial function  $\phi_2$ . Note that the ordinary expectation value in the variational state  $\phi_2$  agrees with the large- $\lambda$  perturbation curve, but differs from the small- $\lambda$  curve, as expected. The GFMC method computes the correction to the variational estimate; at

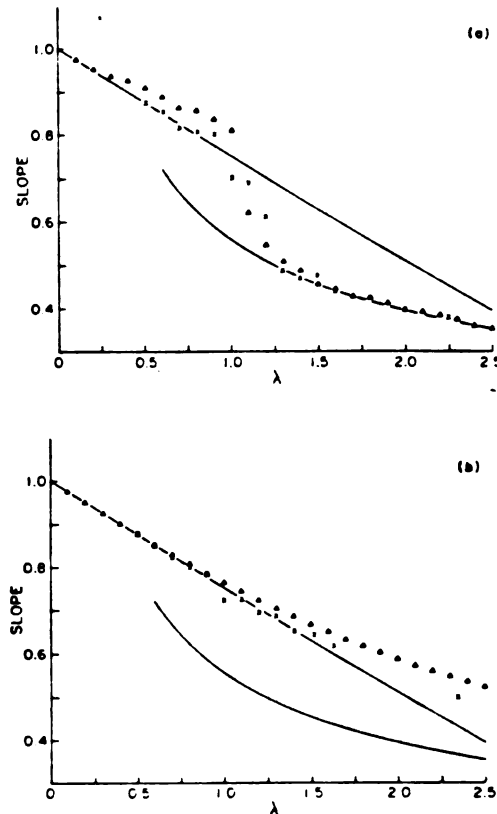


FIG. 4. (a) The expectation value of  $1 - \cos B$  for the three-dimensional theory, calculated from the trial function  $\phi_2$ . The curves are perturbation expansions. The triangles ( $\Delta$ ) are for the simple expectation value in  $\phi_2$ ; the crosses ( $\times$ ) are Monte Carlo calculations of the mixed expectation value, Eq. (2.16). (b) The expectation value of  $1 - \cos B$  calculated from the trial function  $\phi_1$ . The curves and points have the same meaning as in (a).

small  $\lambda$ , say,  $\lambda \leq 1.0$ , the corrected values are consistent with small- $\lambda$  perturbation theory.

Figure 4(b) is for the uncorrelated trial function  $\phi_1$ . Here the expectation value in  $\phi_1$  agrees with the small- $\lambda$  perturbation expansion, but deviates from the large- $\lambda$  expansion. In this case the correction computed by the GFMC method is not large enough to bring the result into agreement with the perturbation expansion at large  $\lambda$ . As before we interpret this failure as a consequence of the metastability of the uncorrelated state with respect to the GFMC iteration, and claim it as evidence of the phase transition.

We have not included error bars on the points on these graphs. These results involve averages over 1000 iterations for ensembles of approximately 100 configurations. In all graphs except Figs. 4(a) and 4(b) the standard deviation is small compared to the size of the point plotted on the graph. To check whether the standard deviation is a reasonable measure of the error, we verified that averaging over half as many measurements increased the standard deviation by about  $\sqrt{2}$ . In Figs. 4(a) and 4(b) the standard deviations were somewhat larger, but still comparable to the size of the point plotted on the graph.

## V. SUMMARY

We have applied the Green's-function Monte Carlo (GMFC) method to the compact U(1) lattice gauge theory in three and two dimensions on small lattices,  $3 \times 3 \times 3$  and  $5 \times 5$ . The GFMC importance-sampling technique was implemented with two trial wave functions: the uncorrelated trial function  $\psi_1$ , which resembles the strong-coupling eigenfunction; and the harmonic wave function  $\phi_2$ , which derives from the weak-coupling eigenfunction but is also quite accurate at strong coupling as well.

In the three-dimensional theory the vacuum energy per plaquette varies continuously with  $\lambda$ , but undergoes a rather sharp crossover from small- $\lambda$  dependence to large- $\lambda$  dependence, around  $\lambda \sim 1.3$ . In the small- $\lambda$  region, where there is little correlation between  $B$  fields on different plaquettes, the two importance functions yield approximately equal values of the energy. But in the large- $\lambda$  region, where there are long-range correlations between plaquettes as described by the trial function  $\phi_2$ , the uncorrelated importance function  $\psi_1$  yields values inconsistent with the variational bound placed by  $\phi_2$ . We interpret this as metastability of the disordered state, and as evidence of the phase transition of the U(1) lattice gauge theory.

In the two-dimensional theory, in contrast, the vacuum energy per plaquette varies slowly with  $\lambda$ , and the two importance functions yield equal energies for all values of  $\lambda$ . We interpret this as an indication that there is no phase transition in the two-dimensional theory.

We have used the term "metastable" to describe the false ground state found by the Monte Carlo calculation when using an importance function appropriate to the disordered phase in a region of coupling constant where the true ground state has correlations described by the harmonic wave function. This choice of words may be misleading in that the false state may never converge to the true state if the ensemble size is too small; the false

state is then actually stable. This property is also seen in quantum many-body problems with phase transitions, such as solid to liquid helium. We have not attempted to study the convergence of the metastable state by increasing the ensemble size. It is possible that the minimum size necessary to allow the convergence to occur is so large that the calculations are not feasible. All that can be said theoretically is that the iteration is stable only for the true ground state if the ensemble is large enough. Of course this is only an issue in systems with a phase transition, for which there are two qualitatively different low-energy states.

Our calculations were restricted to small lattices. Calculations for larger lattices are certainly feasible; the only limitation is computer time. GFMC calculations have been done with several hundred quantum variables; for comparison, a  $3 \times 3 \times 3$  lattice gauge theory has 81 link variables. We believe that the results of calculations on larger lattices would be very similar to those described above. In particular the vacuum energy per plaquette does not depend very much on the lattice size. We have seen two indications of this. First, the perturbation expansions

are independent of lattice size for small  $\lambda$ , and only very weakly dependent for large  $\lambda$ , as indicated by (3.21). Second, we carried out the ordinary variational calculations for lattices of different sizes, and found only a very small lattice-size dependence.

These U(1) lattice-gauge-theory calculations were done in a special way, by formulating the problem in the space of configurations of the plaquette variable  $n(p)$  defined in Eq. (3.4). That formulation leads to an equation that is especially simple to iterate by the GFMC method. It is our impression that there does not exist a similar special formulation of the SU(2) lattice gauge theory. Therefore we intend to apply the GFMC method to that theory by an approach more along the lines described in Sec. II A.

#### ACKNOWLEDGMENTS

We are pleased to thank the following people for discussions about this research: M. Creutz, T. DeGrand, J. Negele, S. Koonin, J. D. Stack, M. H. Kalos, and D. Ceperley. This research has been supported by the National Science Foundation and Michigan State University.

- 
- <sup>1</sup>K. G. Wilson, *Phys. Rev. D* **10**, 2445 (1974).  
<sup>2</sup>J. Kogut and L. Susskind, *Phys. Rev. D* **11**, 395 (1975).  
<sup>3</sup>J. Kogut, D. K. Sinclair, and L. Susskind, *Nucl. Phys.* **B114**, 199 (1976); T. Banks, J. Kogut, and L. Susskind, *Phys. Rev. D* **13**, 1043 (1976); A. Carroll, J. Kogut, D. K. Sinclair, and L. Susskind, *ibid.* **13**, 2270 (1976).  
<sup>4</sup>S. D. Drell, H. R. Quinn, B. Svetitsky, and M. Weinstein, *Phys. Rev. D* **19**, 619 (1979); D. Horn and M. Weinstein, *ibid.* **25**, 3331 (1982).  
<sup>5</sup>M. Creutz, L. Jacobs, and C. Rebbi, *Phys. Rev. Lett.* **42**, 1390 (1979).  
<sup>6</sup>M. Creutz, *Phys. Rev. Lett.* **43**, 553 (1979); *Phys. Rev. D* **21**, 2308 (1980).  
<sup>7</sup>A. M. Polyakov, *Phys. Lett.* **59B**, 79 (1977); *Nucl. Phys.* **B120**, 429 (1977).  
<sup>8</sup>T. Banks, R. Myerson, and J. Kogut, *Nucl. Phys.* **B129**, 493 (1977). See also A. Guth, *Phys. Rev. D* **21**, 2291 (1980); M. Gopfert and G. Mack, *Commun. Math. Phys.* **82**, 545 (1982).  
<sup>9</sup>D. R. Stump, *Phys. Rev. D* **23**, 972 (1981).  
<sup>10</sup>M. Creutz and G. Bhanot, *Phys. Rev. D* **21**, 2892 (1980); B. Lautrup and M. Nauenberg, *Phys. Lett.* **95B**, 63 (1980).  
<sup>11</sup>M. H. Kalos, *Phys. Rev.* **128**, 1791 (1962); *Phys. Rev. A* **2**, 250 (1970).  
<sup>12</sup>M. H. Kalos, D. Levesque, and L. Verlet, *Phys. Rev. A* **9**, 2178 (1974); D. M. Ceperley, G. V. Chester, and M. H. Kalos, *Phys. Rev. B* **17**, 1070 (1978); P. A. Whitlock, D. M. Ceperley, G. V. Chester, and M. H. Kalos, *ibid.* **19**, 5598 (1979); P. A. Whitlock and M. H. Kalos, *J. Comp. Phys.* **30**, 361 (1979).  
<sup>13</sup>D. M. Ceperley and M. H. Kalos, in *Topics in Current Physics*, edited by K. Binder (Springer, Berlin, 1979), Vol. 7. This reference is a comprehensive review of applications of the Monte Carlo method to quantum systems.  
<sup>14</sup>Our approach is patterned after the early GFMC method described in Ref. 11, but with importance sampling.  
<sup>15</sup>In the calculations described in this paper this normalization constant was recalculated exactly after each Monte Carlo iteration. By contrast, in some calculations, e.g., those of Ref. 12, the normalization is taken into account only in an approximate way.  
<sup>16</sup>J. Kogut, *Rev. Mod. Phys.* **51**, 659 (1979).  
<sup>17</sup>U. Heller, *Phys. Rev. D* **23**, 2357 (1981). In this paper a variational wave function of the form of Eq. (3.13) is used in a study of the two-(space) dimensional U(1) gauge theory.  
<sup>18</sup>We later learned of the remarkable advances made by Horn and Weinstein (the second reference of footnote 4) for analytic evaluation of this quantity. Our variational Monte Carlo calculation, the results of which are shown in Fig. 1, amounts to a numerical evaluation of the energy expectation value, which in their approach is computed by introduction of a "partition function" with a sum over states that projects onto the gauge-invariant space. Because we use a function of the plaquette variable  $n(p)$ , this projection is not explicitly used by us, although it may be implicit.  
<sup>19</sup>That the phase transition of the U(1) gauge model in three dimensions is of second order was first suggested by the calculations of B. Lautrup and M. Nauenberg, Ref. 10.

In the preceding reprinted article graphs of the quantity  $\langle 1 - \cos B(p) \rangle$  versus  $\lambda$  were not given for the two dimensional theory. For the sake of completeness, these are shown in Figures B1 and B2.

Figure B1 is for the harmonic trial function  $\phi_2$  and Figure B2 is for the uncorrelated trial function  $\psi_1$ . The circles ( $\bullet$ ) are variational estimates and the crosses ( $+$ ) are GFMC results. The solid curves are perturbation expansions. Notice that although the variational estimates using the two wave functions are quite different at large  $\lambda$ , the two sets of GFMC results are reasonably consistent with each other. This is in contrast to the three dimensional theory where the wave function  $\psi_1$  acted very poorly as an importance function for large  $\lambda$ . This difference is due to the fact that there is a phase transition in the three dimensional theory whereas in two dimensions there is no phase transition.

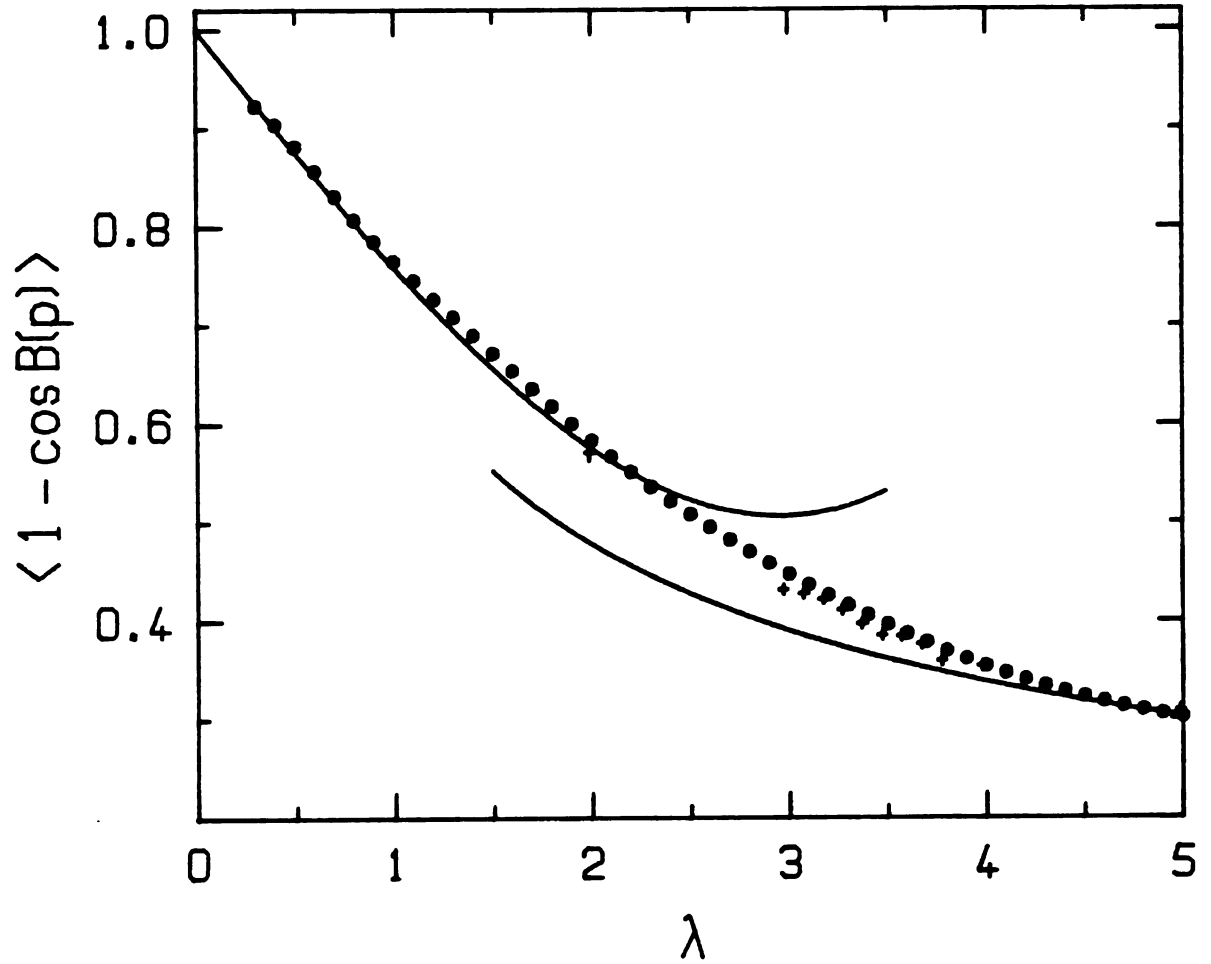


Figure B1: GFMC estimate of the expectation value of  $1 - \cos B(p)$  for the two dimensional  $U(1)$  theory using the harmonic wave function  $\phi_2$  for importance sampling.

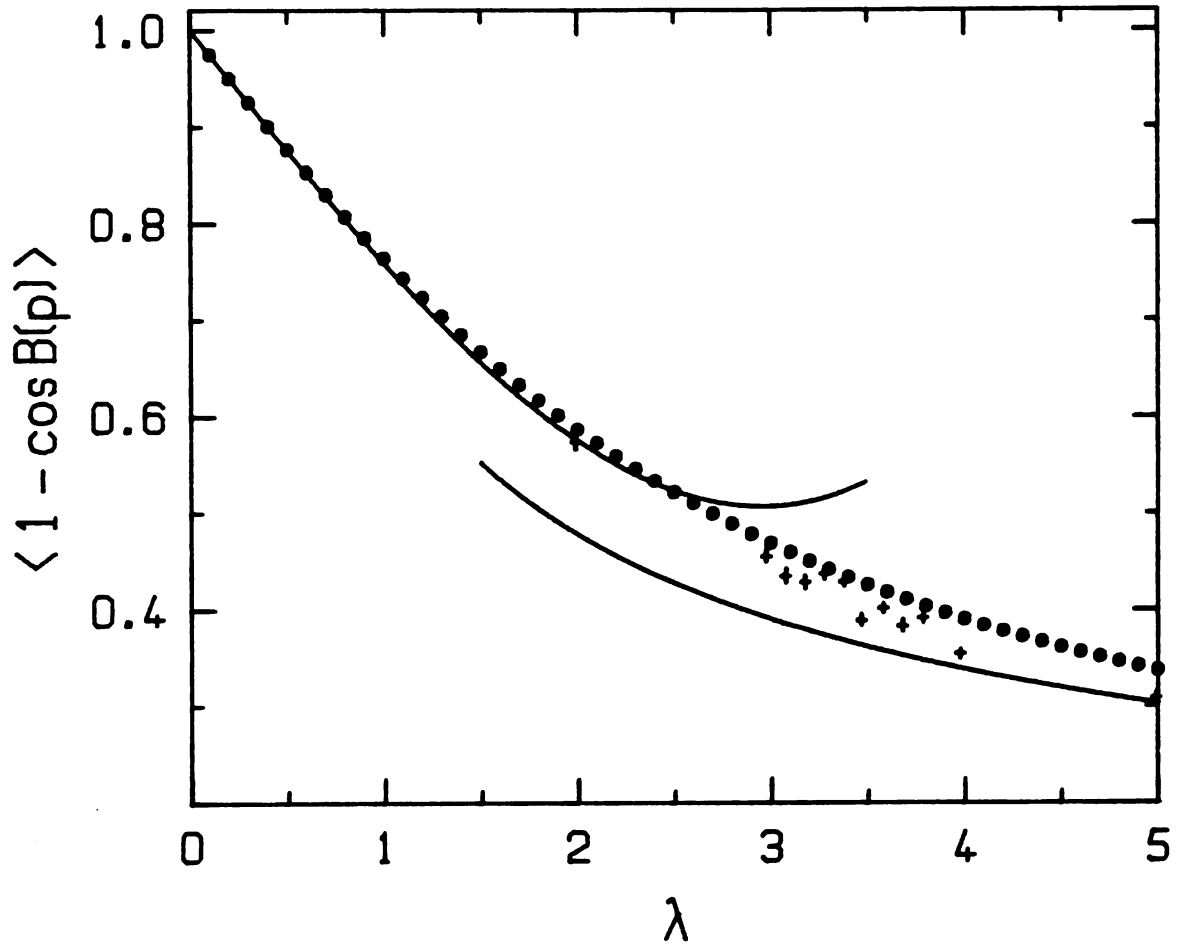


Figure B2: GFMC estimate of the expectation value of  $1 - \cos B(p)$  for the two dimensional  $U(1)$  theory using the uncorrelated wave function  $\psi_1$  for importance sampling.

**LIST OF REFERENCES**

## LIST OF REFERENCES

- [1] D.J. Gross and F. Wilczek, Phys. Rev. Lett. 30, 1343 (1973);  
H.D. Politzer, Phys. Rev. Lett. 30, 1346 (1973).
- [2] K.G. Wilson, Phys. Rev. D 10, 2445 (1974).
- [3] J. Kogut and L. Susskind, Phys. Rev. D 11, 395 (1975).
- [4] M. Creutz, Phys. Rev. D 15, 1128 (1977).
- [5] J. Kogut, D.K. Sinclair, and L. Susskind, Nucl. Phys. B114, 199 (1976);  
T. Banks, S. Raby, L. Susskind, J. Kogut, D.R.T. Jones, P.N. Scharbach, and D.K. Sinclair, Phys. Rev. D 15, 1111 (1977);  
C.J. Hamer, Nucl. Phys. B146, 492 (1978).
- [6] H.W. Hamber, Phys. Rev. D 24, 941 (1981).
- [7] R. Balian, J.M. Drouffe, and C. Itzykson, Phys. Rev. D 10, 3376 (1974).
- [8] S.D. Drell, H.R. Quinn, B. Svetitsky, and M. Weinstein, Phys. Rev. D 19, 619 (1979);  
D. Horn and M. Weinstein, Phys. Rev. D 25, 3331 (1982);  
U. Heller, Phys. Rev. D 23, 2357 (1981);  
D. Horn and M. Karliner, Nucl. Phys. B235 [FS11], 135 (1984).
- [9] D.W. Heys and D.R. Stump, Phys. Rev. D 29, 1791 (1984).
- [10] D.W. Heys and D.R. Stump, "A Variational Estimate of the Energy of an Elementary Excitation of the SU(2) Lattice Gauge Theory", Michigan State University preprint.
- [11] M. Creutz, L. Jacobs, and C. Rebbi, Phys. Rep. 95, 203 (1983).
- [12] J. Kogut, Rev. Mod. Phys. 55, 775 (1983).

- [13] J. Kogut, Rev. Mod. Phys. 51, 659 (1979).
- [14] L.P. Kadanoff, Rev. Mod. Phys. 49, 267 (1977).
- [15] M. Creutz, Phys. Rev. D 21, 2308 (1980).
- [16] M. Creutz, Phys. Rev. Lett. 45, 313 (1980).
- [17] E. Pietarinen, Nucl. Phys. B190 [FS3], 349 (1981).
- [18] H. Hamber and G. Parisi, Phys. Rev. Lett. 47, 1792 (1981);  
E. Marinari, G. Parisi, and C. Rebbi, Phys. Rev. Lett. 47, 1795 (1981).
- [19] J. Kogut, M. Stone, H.W. Wyld, J. Shigemitsu, S.H. Shenker, and D.K. Sinclair, Phys. Rev. Lett. 48, 1140 (1982).
- [20] L.D. McLerran and B. Svetitsky, Phys.Lett. 98B, 195 (1981);  
J. Kuti, J. Polonyi, and K. Szlachanyi, Phys. Lett. 98B, 199 (1981);  
J. Engels, F. Karsch, H. Satz, and I. Montvay, Phys. Lett. 101B, 89 (1981).
- [21] B. Berg, A. Billoire, and C. Rebbi, Ann. Phys. 142, 185 (1982);  
M. Falcioni, E. Marinari, M.I. Paciello, G. Parisi, F. Rapuano, B. Taglienti, and Z. Yi-Cheng, Phys. Lett. 110B, 295 (1982);  
B. Berg and A. Billoire, Phys. Lett. 113B, 65 (1982);  
K. Ishikawa, M. Teper, and G. Schierholz, Phys. Lett. 116B, 429 (1982).
- [22] H. Hamber, E. Marinari, G. Parisi, and C. Rebbi, Phys. Lett. 108B, 314 (1982);  
D. Weingarten, Phys. Lett. 109B, 57 (1982);  
D. Weingarten and D. Petcher, Phys. Lett. 99B, 33 (1981);  
F. Fucito, G. Martinelli, C. Omero, G. Parisi, R. Petronzio, and R. Rapuano, Nucl. Phys. B210 [FS6], 407 (1982).
- [23] M.H. Kalos, Phys. Rev. 128, 1791 (1962).
- [24] M.H. Kalos, Phys. Rev. A 2, 250 (1970);  
M.H. Kalos, D. Levesque, and L. Verlet, Phys. Rev. A 9, 218 (1974);

- P.A. Whitlock, D.M. Ceperley, G.V. Chester, and M.H. Kalos, Phys. Rev. B 19, 5598 (1979).
- [25] D.M. Ceperley and M.H. Kalos, in Topics in Current Physics, edited by K. Binder (Springer, Berlin, 1979), Vol 7.
- [26] N. Hamermesh, Group Theory (Addison-Wesley, Reading, Mass., 1964).
- [27] R. Balian, J.M. Drouffe, and C. Itzykson, Phys. Rev. D 11, 2104 (1975); Phys. Rev. D 19, 2514 (1979).
- [28] B. Lautrup and M. Nauenberg, Phys. Lett. 95B, 63 (1980).
- [29] N. Metropolis, A.W. Rosenbluth, M.N. Rosenbluth, A.H. Teller, and E. Teller, J. Chem. Phys. 21, 1087 (1953).

MICHIGAN STATE UNIVERSITY LIBRARIES



3 1293 03085 2200